Università degli Studi di Roma Tre

Roma Tre

Dipartimento di Ingegneria Industriale, Elettronica e Meccanica

Dottorato di Ricerca in Ingegneria Meccanica e Industriale

XXXVIII Ciclo

Design, Development, and Fabrication of Cost-Effective Biodegradable Single-Use Plastic Products

PhD Tutor

Prof. Massimiliano Barletta

PhD Candidate

Annalisa Genovesi

PhD Coordinator

Prof.ssa Ornella Chiavola

Anno Accademico 2024 - 2025

Summary

Index of Figures V

Index of Tables XIII

Abbreviations XVII

Abstract 2

Introduction 3

1 Plastic Packaging: Background and Literature Review 5

1.1 Traditional Plastic Packaging 5

1.2 Packaging based on Polylactic acid 6

1.3 Packaging containing copolyesters of Succinic Acid 15

1.4 Colored solutions 23

1.5 Home compostable solutions 35

1.6 Recycling of bioplastics 43

1.7 Multilayer thermoformed trays with high thermal stability 47

1.8 Aim of the research 53

2 Materials 58

2.1 Bioplastics 58

2.1.1 Poly (Lactic Acid) – PLA 60

2.1.2 Poly (Butylene Succinate) – PBS 63

2.1.3 Poly (Butylene Adipate – co – Terephthalate) – PBAT 67

2.1.4 Polyhydroxyalkanoates – PHAs 69
2.2 Chain Extenders 74
2.3 Antioxidants 76
2.4 Mineral Filler 79
2.5 Slip and Anti-block Agents 80
2.6 Definition of the formulations 81
3 Plastic Processing Technology 83
3.1 Twin – screw extrusion 83
3.1.1 Types of twin screw extruders 84
3.1.2 Screw design 86
3.1.3 Feeding systems 90
3.1.4 Compounding of the defined blends 91
3.2 Cast extrusion 96
3.2.1 Single screw extruders 96
3.2.2 Cast extrusion dies 98
3.2.3 Production of the sheets via cast extrusion 100
3.3 Thermoforming 103
3.3.1 Thermoforming process 104
3.3.2 Production of the thermoformed trays 107
4 Experimental Methods 111
4.1 Rheological Characterization 111

4.1.1 Melt Flow Rate – MFR 111
4.1.2 Capillary Rheometer 112
4.2 Mechanical Characterization 114
4.2.1 Tensile Test 114
4.2.2 Compression Test 115
4.3 Fourier Transform Infrared Spectroscopy – FTIR 116
4.4 X-Ray Diffractometry – XRD 116
4.5 Thermal Characterization 116
4.5.1 Differential Scanning Calorimetry – DSC 116
4.5.2 Functional Heat Resistance Tests 116
5 Results and Discussion 118
5.1 Rheological properties 118
5.1.1 MFR Analysis 118
5.1.2 Capillary Rheometer 119
5.2 Mechanical properties 126
5.2.1 Tensile properties of the cast extruded films 126
5.2.2 Compression of the thermoformed trays 130
5.3 FTIR Analysis 133
5.4 X-ray Diffraction 137
5.5 Thermal characterization 138
5.5.1 DSC Analysis 138

5.5.2 Thermal resistance 142

5.6 Product cost evaluation 144

6 Conclusions and future developments 150

References 153

Index of Figures

Figure 1.1 Schematic representation of a PLA-based blend [3] 7

Figure 1.2 Natural Bibo – Biodegradable and compostable items produced by Bibo Italia S.p.A. 7

Figure 1.3 Appearance of the pellets of the PLA-based formulations 12

Figure 1.4 a) Cast extrusion process of the compound designed for the thermoforming process; b) Production of izod samples using the compound designed for the Injection Molding process. 12

Figure 1.5 Thermoformed trays obtained using the PLA-based formulation 13

Figure 1.6 Izod samples produced via Injection molding using the SI LA3CL2 formulation 14

Figure 1.7 Injection molded spoons in SI LA3CL2 14

Figure 1.8 Temperature profiles adopted during the compounding process of PLA/PBS formulations 19

Figure 1.9 Appearance of the produced PLA/PBS pellets: a) Series L; b) Series LS; c) Series S. 21

Figure 1.10 Cast extrusion of the formulations based on PLA/PBS 22

Figure 1.11 Details of the thermoformed trays based on PLA and PBS. 23

Figure 1.12 Colored masterbatches 25

Figure 1.13 Appearance of the pellets of the yellow compound 29

Figure 1.14 Appearance of the pellets of the pink compound 29

Figure 1.15 Appearance of the pellets of the light blue compound 29

Figure 1.16 Appearance of the pellets of the green compound 30

Figure 1.17 Cast extrusion process of the colored sheets 32

Figure 1.18 Aspect of the colored sheets after the extrusion process 32

Figure 1.19 Phases of the thermoforming process 33

Figure 1.20 Heating power adopted during the thermoforming process of the colored sheets 33

Figure 1.21 Top view of the colored thermoformed trays 34

Figure 1.22 Bottom view of the colored thermoformed trays 34

Figure 1.23 Aspect of the produced home compostable granules. Left: B-TPS-1; right: B-PHBH-1. 37

Figure 1.24 B-TPS1 cast extruded sheet. Left: defects related to humidity; right: sheet after the parameters optimization 39

Figure 1.25 Cast extrusion of B-TPS1 sheets with thickness below 120 μm 40

Figure 1.26 Cast extrusion process of B-PHBH1 41

Figure 1.27 Material accumulation at the die during the extrusion of B-PHBH1 41

Figure 1.28 B-TPS1 home compostable trays 43

Figure 1.29 B-PHBH1 home compostable trays 43

Figure 1.30 PLA/PBS recycling study: schemes of the extrusion process [10] 46

Figure 1.31 Results of the rheological characterization performed on the PLA/PBS aged compounds [10] 47

Figure 1.32 Process scheme [11] 50

Figure 1.33 Food trays thermoformed from F_T1 sheet (left) and F_T2 sheet (right) [11] 51

Figure 2.1 Classification of bioplastics [57] 58

Figure 2.2 "OK biobased" and "DIN geprüft biobased" labels 59

Figure 2.3 “OK industrial compost label” and “Seedling” labels..... 59

Figure 2.4 Poly(lactic acid) structure [60] 60

Figure 2.5 L-LA and D-LA molecular structure [61] 61

Figure 2.6 Natureworks Ingeo products [64] 63

Figure 2.7 Total Corbion Luminy products [65] 63

Figure 2.8 Chemical structure of PBS [66]..... 64

Figure 2.9 Production process of PBS [67] 64

Figure 2.10 BioPBS commercialized by PTT MCC Biochem Co., Ltd. [70] 66

Figure 2.11 Properties of PBS TH803S [71] 66

Figure 2.12 Typical properties of PBS KingFa A200 series 67

Figure 2.13 Synthesis of PBAT [73] 68

Figure 2.14 General structure of Polyhydroxyalkanoates [82]..... 70

Figure 2.15 Classification of PHAs based on number of carbon atoms of the monomeric units and based on their structure [87]..... 71

Figure 2.16 Chemical Structure of PHB [94] 72

Figure 2.17 Chemical structure of PHBH [97] 73

Figure 2.18 Chemical structure of a generic Joncryl ADR chain extender [104]..... 75

Figure 2.19 Schematic mechanism of the reaction of an epoxy chain extender with a degraded polymer [104]..... 75

Figure 2.20 Structure of commercial primary antioxidants [106] 76

Figure 2.21 Structure of commercially available secondary antioxidants [109] 77

Figure 2.22 Auto-oxidation reaction of a polymeric compounds and effect of primary/secondary antioxidants [110] 78

Figure 2.23 Technical data sheet of ADK STAB A611 78

Figure 3.1 Production process routes for polymeric compounds [117] 83

Figure 3.2 Screw parameters of a twin screw extruder [118] 84

Figure 3.3 Differences between co-rotating and counter-rotating twin screw extruders [119] 85

Figure 3.4 Compenetrating screw types [119] 85

Figure 3.5 Co-rotating Twin-Screw Extruder: Examples of Barrel and Screw Element Modularity [120] 86

Figure 3.6 Design of the screw in the feeding section [121] 87

Figure 3.7 Screw design to melt the polymer [121] 88

Figure 3.8 Conveying elements [121] 89

Figure 3.9 Example of kneading blocks (lesunscrew.com) 89

Figure 3.10 Effect of the kneading block geometry on the polymer melt [121] 89

Figure 3.11 Representation of the Movacolor gravimetric feeders 91

Figure 3.12 Scheme of the COMAC 26 extruder 92

Figure 3.13 Screw profile of the COMAC 26 extruder 92

Figure 3.14 COMAC 26 extrusion system 93

Figure 3.15 Compounding process of PLA-PHBH blends: a) strands exiting the die of the extruder, b) strands entering the pelletizer system, and c) pellets after the cut. 94

Figure 3.16 Strands at the exit of the extrusion die: a) T733, and b) T734. 95

Figure 3.17 Scheme of the cast extrusion process [124] 96

Figure 3.18 Elements of a single screw extruder [125] 97

Figure 3.19 Functional zones of a single screw extruder [125] 98

Figure 3.20 Geometric parameters of the screw of a single screw extruder [125] 98

Figure 3.21 Variation of the velocity profile within the polymer melt at the exit of a die [126] 99

Figure 3.22 Manifold die [127] 99

Figure 3.23 Coathanger die [127] 100

Figure 3.24 Fishtail die [127] 100

Figure 3.25 Eurexma Minicast 20 extrusion system 101

Figure 3.26 Cast extrusion process: a) Sheet after the calanders; b) Sheet before drawing. 102

Figure 3.27 Cast extrusion process: a) overview of the extruder, b) sheet of T733 after the calender, and c) sheet of T734 after the calender. 103

Figure 3.28 Schematic representation of thermoforming cycle time [130] 104

Figure 3.29 Typical thermoforming processes: a) Male mold drape and b) Female mold drape. [129] 105

Figure 3.30 Example of thermal history of a part during a thermoforming cycle [130] 106

Figure 3.31 Vacuum forming: a) Male mold and b) Female mold [126]. 106

Figure 3.32 Pressure forming [126]. 107

Figure 3.33 Defects observed during thermoforming: a) insufficient heating time and poor detail fidelity; b) excessive heating time causing wrinkles on the bottom of the tray; c) presence of humidity during the cast extrusion of the sheets. 108

Figure 3.34 Final aspect of the trays after manual trimming: a) PLA-PHBH 82, b) PLA-PHBH 55, c) PLA-PHBH 28. 109

Figure 3.35 Aspect of the trays at the end of the thermoforming cycle: a) T733 and b) 734. 110

Figure 4.1 Schematic representation of a Melt Flow Rate tester[131] 111

Figure 4.2 Schematic representation of a die in a capillary rheometer [133] 113

Figure 4.3 Schematic diagram for different kinds of time-independent fluids [135] ... 114

Figure 4.4 Shimadzu AGS-X Tensile tester 115

Figure 5.1 Apparent viscosity vs shear rate curves at different temperatures – PLA-PHBH 28 119

Figure 5.2 Apparent viscosity vs shear rate curves at different temperatures – PLA-PHBH 55 120

Figure 5.3 Apparent viscosity vs shear rate curves at different temperatures – PLA-PHBH 82 120

Figure 5.4 Carrau-Yasuda fitting for PLA-PHBH 28 121

Figure 5.5 Carrau-Yasuda fitting for PLA-PHBH 55 121

Figure 5.6 Carrau-Yasuda fitting for PLA-PHBH 82 122

Figure 5.7 Apparent viscosity vs shear rate curves at different temperatures – T733 .. 123

Figure 5.8 Apparent viscosity vs shear rate curves at different temperatures – T734 .. 124

Figure 5.9 Carrau-Yasuda fitting for T733 125

Figure 5.10 Carrau-Yasuda fitting for T734 125

Figure 5.11 Stress – strain curves obtained for PLA - PHBH – Talc Cast extruded films a) in MD (Machine Direction) and b) in TD (Transverse Direction) 127

Figure 5.12 Stress – strain curves obtained for PBAT – PBS – Talc Cast extruded films in MD (Machine Direction) and in TD (Transverse Direction)..... 129

Figure 5.13 Force – displacement curve obtained during the compression of PLA-PHBH 82 thermoformed trays..... 130

Figure 5.14 Force – displacement curve obtained during the compression of PLA-PHBH 55 thermoformed trays..... 131

Figure 5.15 Force – displacement curve obtained during the compression of PLA-PHBH 28 thermoformed trays..... 131

Figure 5.16 Force – displacement curve obtained during the compression of T733 thermoformed trays..... 132

Figure 5.17 Force – displacement curve obtained during the compression of T734 thermoformed trays..... 133

Figure 5.18 FTIR analysis of the PLA-PHBH blends. a) FTIR Spectra of the pellets; b) FTIR Spectra of the films; c) FTIR Spectra of the trays. 134

Figure 5.19 FTIR spectra of PBAT-PBS based a) pellets, and b) films and trays. 136

Figure 5.20 FTIR spectra in the 1350 – 1200 cm^{-1} region for pellets, films, and trays. a) T733 and b) T734. 136

Figure 5.21 XRD Spectra of the PLA-PHBH films..... 137

Figure 5.22 XRD Spectra of PBAT – PBS based compounds 138

Figure 5.23 DSC thermograms of the PLA-PHBH compounds: a) First Heating; b) Second Heating; c) Cooling. 139

Figure 5.24 DSC thermograms: a) First heating, b) Cooling and c) Second Heating .. 141

Figure 5.25 Thermal resistance test of PLA-PHBH 82 trays. From left to right: before, during and after the test. 143

Figure 5.26 Thermal resistance test of PLA-PHBH 55 trays. From left to right: before, during and after the test. 143

Figure 5.27 Thermal resistance test of PLA-PHBH 28 trays. From left to right: before, during and after the test. 143

Figure 5.28 Thermal resistance test of T733 trays. From left to right: before, during and after the test. 144

Figure 5.29 Thermal resistance test of T734 trays. From left to right: before, during and after the test. 144

Figure 5.30 Global production capacities of bioplastics 2024 (market segments by polymers) [189] 145

Figure 5.31 Cost per kg related to the production of 13 g - trays 147

Figure 5.32 Cost per kg related to the production of 15 g - trays 147

Figure 5.33 Cost per kg related to the production of 20 g - trays 148

Figure 5.34 Material cost per 1000 trays 148

Index of Tables

Table 1.1 PLA-based formulation designed for thermoforming. H: >40%; M: 5-40%; L: <5%. 8

Table 1.2 PLA-based formulation designed for Injection Molding. H: >40%; M: 5-40%; L: <5%. 10

Table 1.3 Processing parameters adopted for the PLA-based formulations for thermoforming 11

Table 1.4 Processing parameters adopted for the PLA-based formulations for injection molding 11

Table 1.5 Processing parameters adopted during cast extrusion of the thermoforming compound..... 12

Table 1.6 Formulations based on PLA and PBS. H: >40%; M: 5-40%; L: <5%. 17

Table 1.7 Processing parameters set and recorded during the compounding process of the PLA/PBS blends 20

Table 1.8 Temperature profile adopted during cast extrusion of PLA/PBS compounds 21

Table 1.9 Processing parameters adopted during cast extrusion of PLA/PBS compounds 22

Table 1.10 Colored formulations. H: >40%; M: 5-40%; L: <5%. 26

Table 1.11 High-intensity color formulations. H: >40%; M: 5-40%; L: <5%. 27

Table 1.12 Processing parameters adopted during the extrusion of the yellow compound 28

Table 1.13 Processing parameters adopted during the extrusion of the pink compound 28

Table 1.14 Processing parameters adopted during the extrusion of the light blue compound..... 28

Table 1.15 Processing parameters adopted during the extrusion of the green compound 28

Table 1.16 Processing parameters adopted to produce the yellow sheets with different thickness values 30

Table 1.17 Processing parameters adopted to produce the pink sheets with different thickness values 31

Table 1.18 Processing parameters adopted to produce the light blue sheets with different thickness values 31

Table 1.19 Processing parameters adopted to produce the green sheets with different thickness values 31

Table 1.20 Definition of home-compostable formulations (B-TPS1) 37

Table 1.21 Definition of home-compostable formulations (B-PHBH 1) 37

Table 1.22 Processing parameters adopted during the extrusion process of home compostable formulations 38

Table 1.23 PLA/PBS recycling study: definition of the formulations [10] 45

Table 1.24 Processing parameters adopted during twin screw extrusion [10] 46

Table 1.25 Processing parameters adopted during cast extrusion [10] 47

Table 1.26 First set of formulations studied for multilayer thermoformed trays [11] 48

Table 1.27 Optimized formulations studied for multilayer thermoformed trays [11] 48

Table 1.28 Temperature profile and processing parameters for INN inner layer material extrusion [11] 49

Table 1.29 Temperature profile and processing parameters for OUT_T1p [11] 49

Table 1.30 Temperature profile and processing parameters for OUT_T2p [11] 49

Table 1.31 Temperature profile and processing parameters for cast extrusion of F_T1 and F_T2 [11] 50

Table 1.32 Results of the mechanical characterization of the cast extruded sheets [11] 51

Table 1.33 DSC analysis for INN, OUT_T1 and OUT_T2 [11] 52

Table 2.1 General properties of PLA [62] 61

Table 2.2 General properties of PBS [68] 65

Table 2.3 Properties of PBAT (Adapted from [72]) 68

Table 2.4 Major commercially available PBAT grades [76] 69

Table 2.5 Properties of PHB 72

Table 2.6 Properties of melt processed PHBH. 73

Table 2.7 Typical properties of Joncryl ADR chain extender [104] 75

Table 2.8 PLA – PHBH based formulations 82

Table 2.9 PBAT – PBS based formulations 82

Table 3.1 Processing parameters adopted for the twin screw extrusion 94

Table 3.2 Temperature profiles adopted during twin screw extrusion 95

Table 3.3 Processing parameters adopted and recorded during twin screw extrusion ... 95

Table 3.4 Processing parameters adopted for the cast extrusion process 101

Table 3.5 Processing parameters adopted during cast extrusion of T733 102

Table 3.6 Processing parameters adopted during cast extrusion of T734 102

Table 3.7 Processing parameters adopted during thermoforming of PLA-PHBH based sheets 108

Table 3.8 Processing parameters adopted during thermoforming of PBAT-PBS based sheets 109

Table 4.1 MFR Range used in specific Polymer Processes [132] 112

Table 5.1 MFR values of the PLA – PHBH blends 118

Table 5.2 MFR values of the PBAT – PBS blends 118

Table 5.3 Carreau-Yasuda fitting paramters for PLA-PHBH compounds 122

Table 5.4 Carreau-Yasuda fitting paramters for PBAT-PBS compounds 126

Table 5.5 Results of the mechanical characterization of the PLA - PHBH – Talc Cast extruded films in MD (Machine Direction) 127

Table 5.6 Results of the mechanical characterization of the PLA - PHBH – Talc Cast extruded films in TD (Machine Direction) 128

Table 5.7 Results of the mechanical characterization of the PBAT – PBS – Talc Cast extruded films in MD (Machine Direction) and in TD (Transverse Direction) 129

Table 5.8 Results of the compression test for PLA - PHBH based thermoformed trays 132

Table 5.9 Results of the compression test for PBAT – PBS based thermoformed trays 133

Table 5.10 Results of the DSC Analysis of the PLA-PHBH compounds 140

Table 5.11 Results of the DSC Analysis 142

Table 5.12 Cost of the defined materials per kg 146

Table 5.13 Cost of cast extruded sheets per kg 146

Abbreviations

AO	Antioxidant
BDO	1,4-butanediol
CE	Chain extender
DSC	Differential Scanning Calorimetry
FTIR	Fourier Transform Infrared Spectroscopy
HDT	Heat Deflection Temperature
LA	Lactic Acid
LCA	Life Cycle Assessment
LDPE	Low Density Polyethylene
LIW	Loss-in-weight
MD	Machine Direction
MFI	Melt Flow Index
MFR	Melt Flow Rate
PBAT	Poly(butylene adipate - co terephthalate)
PBS	Poly(butylene succinate)
PBSA	Poly(butylene succinate - co - adipate)
PDLA	Poly(D-lactide)
PE	Polyethylene
PHA	Polyhydroxyalkanoate
PHBH	Poly(3-hydroxybutyrate-co-3-hydroxyhexanoate)
PLA	Poly(lactic acid)
PLC	Polycaprolactone
PLLA	Poly(L-lactide)
PP	Polypropylene
PS	Polystyrene
SA	Succinic Acid
TD	Transverse Direction
VST	Vicat Softening Temperature
XRD	X-Ray Diffractometry

Abstract

Single-use food trays are widely employed in take-away and delivery services, contributing substantially to landfill accumulation. Although bioplastic alternatives have been developed, their limited processability and high production costs have hindered large-scale adoption. To address this challenge, in this work two different sets of compounds were evaluated. Fist, compatibilized blends of polylactic acid (PLA), poly(3-hydroxybutyrate-co-3-hydroxyhexanoate) (PHBH), and 20 wt% talc were studied. The presence of PHBH, a biopolymer obtained by bacterial fermentation and marine biodegradable allows to reduce the environmental footprint of the compound. Due to the susceptibility of PHBH to degradation during extrusion as a result of shear stress, talc was incorporated at a concentration of 20 wt%. Additionally, a second series of compatibilized blends comprising Poly(butylene adipate-co-terephthalate) (PBAT) and Poly(butylene succinate) (PBS) with talc concentrations of 30 and 40 wt% was assessed. These formulations are distinguished by a significantly reduced cost, attributable to the recent decline in PBAT prices and the feasibility of incorporating substantial quantities of talc. The blends were compounded via twin-screw extrusion and used to produce thermoformed trays. Mechanical, thermal and morphological properties of the compounds and semi-finished products were evaluated. The incorporation of a reactive chain extender improves the strength of the compounds, counteracting the stiffening effect of talc. Blends with higher PLA content exhibited superior mechanical performance, with a maximum stress of 40 MPa and an elastic modulus of 1.1 GPa. Blends based on PBAT and PBS presented an elastic modulus of around 300 MPa and a tensile strength of around 25 MPa. The introduction of 40 wt% leads to a drastic drop in ductility in transverse direction. Trays with PBAT/PBS polymeric phase did not fracture during compression tests. With reference to PLA/PHBH trays, only the trays with PLA as the main polymeric phase did not fracture in compression up to deformations greater than 80%. The formulations examined in this study present an optimal balance among cost, stiffness, and environmental sustainability. The PLA/PHBH formulations emerge as the most suitable option when prioritizing a reduced environmental impact, although with a higher production cost. In contrast, formulations based on PBAT/PBS are ideal candidates when minimizing cost is a primary consideration.

Introduction

In recent years, the food service industry has experienced significant transformation, with the rise of take-away and delivery orders leading to a marked increase in the use of disposable plastic tableware. Food packaging waste constitutes approximately 30% of residential waste in the United States and significantly contributes to the expansion of landfills. Polystyrene (PS) is one of the most prevalent materials employed for disposable packaging and fast-food containers. In response to the pressing need for reform in plastic waste management, the European Commission implemented Directive (EU) 2019/904 on Single-Use Plastics (SUP), which bans the use of synthetic plastics in disposable products, effective from July 2021. In Italy, this Directive has been formally incorporated into national legislation through the Decreto Legislativo 8 novembre 2021, n.16, in alignment with the broader European Union strategy to reduce plastic pollution. Within this framework, there is a necessity to design a new class of materials that meet market demands. Manufacturers have primarily concentrated on developing new materials with properties and processability similar to those traditionally utilized. This strategy enables the adoption of new production lines with minimal alterations to existing processes and manufacturing facilities. The ultimate objective of this developmental trajectory, as addressed in the present thesis, is the creation of cost-effective solutions. These solutions must be comparable not only in terms of processability and functionality but also in economic viability and sustainability.

The first chapter of this thesis provides a thorough overview of the solutions developed in recent years in response to Directive (EU) 2019/904 on Single-Use Plastics (SUP). It specifically emphasizes the research strategies employed by the Technology and Processing Systems group within the Department of Industrial, Electronics, and Mechanical Engineering at Roma Tre University, where this research was conducted. Chapter Two outlines the materials used in this study, detailing the design criteria for formulating the mixtures. Chapter Three explains the production technologies applied and describes the experimental development of the compounds under investigation. Chapter Four details the experimental methodologies used to characterize the compounds and the manufactured articles, while Chapter Five presents the results, contextualized within the

existing body of literature. Chapter Six articulates the conclusions and suggests developments for future research.

1 Plastic Packaging: Background and Literature Review

1.1 Traditional Plastic Packaging

In recent years, bioplastics have attracted considerable attention in the realm of single-use plastic packaging, prompting manufacturers to invest heavily in dedicated scientific research. This commitment has led to the development of well-established production technologies and the commercialization of a wide array of material grades. This heightened focus stems from the substantial environmental challenges posed by the disposal of fossil-based plastic waste. In response to the urgent need for reform in plastic waste management, the European Commission enacted Directive (EU) 2019/904 on Single-Use Plastics (SUP), which prohibits the use of synthetic plastics in disposable products, effective July 2021. The directive aims to promote circular approaches and prioritize non-toxic and reusable products. This necessity arises from the increasing amount of marine litter, which is constituted by single – use plastic items for over 50%. The focus of the directive is on single – use plastic products, which are intended to be used only once or for a very short period of time before being disposed of: fast food containers or meals, sandwiches, wraps, salad boxes with cold or hot food, or food containers of fresh or processed food that do not need further preparation, such as fruits, vegetables, or desserts fall into this definition [1].

In Italy, the Directive has been formally transposed into national law by means of the Decreto Legislativo 8 novembre 2021, n.16, aligning with the broader European Union strategy to mitigate plastic pollution. Italy's implementation reflects the SUP Directive's objectives through specific legislative measures, including restrictions on single-use plastic products and enhanced waste management protocols. The main points of the Decreto Legislativo are the reduction of plastic use (Art. 4), the limitation of the placing on the market of certain products (Art. 5), the introduction of marks on the products, indicating the presence of plastics (Art. 7), and the Extended Producer Responsibility (EPR) (Art. 8).[2]

In this context, a new class of materials needs to be designed to meet market requirements. These compounds must meet one or more specific technological and functional requirements, such as:

1. Compostability according to the EN1342 standard, which relates to industrial composting.
2. Compostability in a domestic environment (Home Composting).
3. Good processability in relation to conventional plastic processing technologies (e.g., compounding extrusion, cast extrusion, and thermoforming).
4. Being economically competitive.
5. The raw material supply chain must be reliable and fit to meet demand.
6. The thermo – mechanical properties of the new products must be similar to those of the old ones or, at least, suitable for the specific application.

In this regard, different strategies have been adopted to meet all the demands, and the study performed in the present thesis aims to continue this work.

1.2 Packaging based on Polylactic acid

One of the first biopolymers to be widely used in single – use plastic packaging industry is Polylactic acid (Section 2.1.1). Polylactic acid (PLA) is a semicrystalline polyester derived from lactic acid synthesized entirely from renewable resources such as corn, sugar beet, and wheat. This biopolymer exhibits compostability, high rigidity, and favorable mechanical strength owing to its elevated elastic modulus, positioning it as a viable substitute for conventional petroleum-based plastics. However, PLA is inherently brittle under mechanical stress and has limited thermomechanical properties, which restricts its suitability for certain industrial applications. To enhance the properties of PLA, the production of binary blends in which PLA is the main polymeric phase is one of the most widely used strategies. Most bioplastics are immiscible; therefore, they form different microstructures with different properties depending on their composition, as shown in Figure 1.1. The two main types of microstructures are co-continuous and dispersed structures. Dispersed structures are formed when one of the polymers in the binary blend is present in a high percentage in the compound (> 60 wt.%). In this case, the polymer present at lower concentrations formed a droplet-like dispersion in the matrix of the main polymer. The properties of the resulting compound were similar to those of

the main polymer. In co-continuous structures, both polymers are continuous, and the properties of the resulting compound are limited by the weaker polymer.

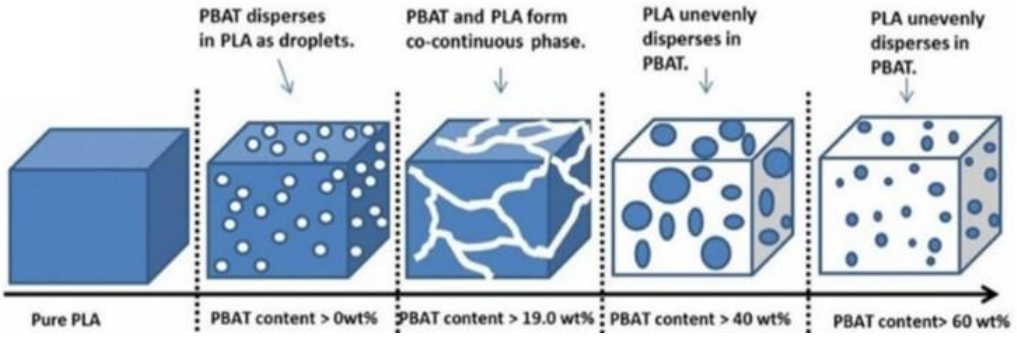

Figure 1.1 Schematic representation of a PLA-based blend [3]

The research team first developed PLA-based formulations in collaboration with Bibo Italia S.p.A., an Italian company that produces single-use plastic plates, cups, and cutlery. The company is based in Settimo Torinese (TO) and has great expertise in both thermoformed and injection – molded items. The company currently produces a line of bioplastic items called "Natural Bibo", which are both biodegradable and compostable (Figure 1.2). The PLA-based formulation for thermoforming is presented in Table 1.1.

Figure 1.2 Natural Bibo – Biodegradable and compostable items produced by Bibo Italia S.p.A.

In the initial formulation, the research team selected polylactic acid (PLA) as the primary polymer phase and polycaprolactone (PCL) as the secondary polymer phase. The specific

The PLA grade employed was Luminy L175 (Total Corbion), chosen for its high molecular weight, which resulted in a reduced melt flow index (MFI) suitable for flat-die extrusion and thermoforming processes. Luminy L175 presents a lower concentration of the L-stereoisomer than other PLA grades (for example, Luminy L175X). Poly (L-lactide) (PLLA) exhibits a spatial configuration (L-configuration) that differs from that of the bulk material (D-configuration), preventing efficient molecular packing with adjacent chains. This structural mismatch reduces the fraction of the material available for crystallization, thereby lowering the maximum achievable crystallinity upon system cooling. Furthermore, the non-crystallizable chains remain tightly intercalated with chemically identical but stereochemically opposed chains, kinetically hindering crystal formation despite their thermodynamic feasibility. The selection of Luminy L175 (with a lower L-stereoisomer content than L175X) promotes the development of a more extensive crystalline phase in the final product, with faster crystallization kinetics. This crystalline phase is essential for endowing the material with high-temperature mechanical resistance, a critical requirement for applications such as food packaging, where PLA's inherently low glass transition temperature (T_g) would otherwise limit its performance.

Table 1.1 PLA-based formulation designed for thermoforming. H: >40%; M: 5-40%; L: <5%.

	TF LA3CL2
Material	**wt.%**
PLA Luminy L175	H
PCL CAPA 6800	M
PLA Luminy D070	L
Epoxy chain extender	L
Talc	M
Ethylene bis stearamide	L
Melt Strength Enhancer	L
Titanium dioxide bio masterbatch	L

Polycaprolactone is a class of polymers distinguished by its rapid biodegradation under industrial composting conditions, as certified by the OK Compost label. However, these materials are derived from fossil feedstocks and have several limitations, including low melting temperatures (<70 °C), high production costs, and limited market availability. Polycaprolactone (PCL) is a semi-crystalline polymer with a melting point ranging

between 59 °C and 64 °C and a glass transition temperature of -60 °C. It is highly hygroscopic and has been extensively studied in the literature because of its notable biodegradability. Chemically, PCL's structure imparts properties analogous to polyolefins, while its aliphatic ester linkages render it susceptible to enzymatic degradation. This characteristic makes PCL a suitable candidate for blending with PLA to accelerate its degradation. The selected commercial grade of PCL was Capa 6800, as it presented a lower MFR, making it suitable for the intended processing method. As PLA is the main polymeric phase, the resulting compound possesses suitable mechanical and thermal resistance. Luminy D070 PDLA (Total Corbion) was incorporated to promote the formation of PDLA/PLLA stereocomplexes, which act as nucleating agents. The presence of these stereocomplexes enhances the crystallization kinetics and thermal stability of the PLA matrix while simultaneously improving its mechanical properties. Talc was used as a mineral filler because it guarantees low gas permeability, good thermal resistance, and enhanced mechanical properties. Ethylene Bis Stearamide (EBS), an organic wax, was used as an internal lubricant and dispersing agent for the mineral phase (lamellar talc). EBS was chosen because of its dual functionality as an internal lubricant and dispersant, in addition to its nucleating capability. Improving the dispersion of talc enhances both its reinforcing and nucleating functions, as a greater interfacial surface area is exposed to the polymer matrix. This contributes to improving the processability of the compound and amplifying the effectiveness of other implemented strategies. A melt-strength-enhancing additive was used to improve the processability of the compound via cast extrusion. Thermo-hydrolytic degradation phenomena were compensated for using an epoxy chain extender. Finally, to obtain a white compound, a small percentage of the white bio-masterbatch was incorporated. This coloring additive contains PLA and titanium dioxide, the latter of which also contributes to enhanced thermal resistance.

The same strategies were also applied by the research team to define a PLA-based formulation designed specifically for Injection Molding. The main difference is the polymer grades used. In fact, a high viscosity is required for thermoforming because cast extrusion and thermoforming technologies require good melt stability. In Injection Molding, better processability is obtained using low-viscosity grades, as it eases the process of filling the mold cavity. The designed formulation for injection molding is presented in Table 1.2. PLA L105 is a PLA produced by Total Corbion, characterized by

a lower molecular weight and, therefore, a higher Melt Flow Index. CAPA 6500 is a low-viscosity commercial PCL grade polymer.

In this case, no coloring agents, such as masterbatches, were added, as the Research Team deemed the talc content sufficient to impart the desired coloration to the formulation. Titanium dioxide is particularly suited for applications involving thermoforming processes; however, in injection molding, it excessively stiffens the polymer melt, potentially hindering its processability.

Table 1.2 PLA-based formulation designed for Injection Molding. H: >40%; M: 5-40%; L: <5%.

	SI LA3CL2
Material	**wt.%**
PLA Luminy L105	H
PCL CAPA 6500	M
PLA Luminy D070	L
Epoxy chain extender	L
Talc	M
Ethylene bis stearamide	L
Melt Strength Enhancer	L
Sukano PLA MRS533	L

An additional modification introduced into the formulation involved incorporating the additive Sukano PLA MRS533. This additive primarily facilitates a more efficient mixing of PLA with PCL and the mineral phase (talc), but its most critical role is functioning as a mold release agent, easing the demolding process. The improved dispersion of the components contributed to the reduction in the material viscosity at the processing temperatures. Moreover, the demolding phase of cutlery production is particularly delicate, necessitating additives that can simplify this step and prevent issues that might otherwise extend the cycle time and increase the production cost of the molded item.

The designed formulations were produced via twin-screw extrusion. The extrusion procedure was conducted iteratively for all target formulations following a systematic preparation protocol. Prior to manual feeding into the extruder, each constituent was precisely weighed and pre-mixed separately. This premixing requirement originated from the use of two distinct feeder systems: a gravimetric feeder for powdered components and

a volumetric feeder for discontinuous pelletized materials. The powdered additives were mechanically blended using a planetary mixer to achieve a homogeneous distribution while minimizing airborne particulate dispersion in the work environment. The bulk pelletized materials were manually mixed to ensure adequate distribution. The processing parameters adopted and recorded during the extrusion process are presented in Table 1.3 and in Table 1.4, respectively, for the thermoforming and injection molding formulations. The produced pellets are shown in Figure 1.3. Recipe constituents were extruded via a co-rotating twin-screw system without preliminary drying, whereas the resulting compound pellets underwent mandatory dehumidification before subsequent flat-die extrusion or injection molding. This critical drying step prevents hydrolytic degradation during subsequent thermoforming processes, which could compromise material properties owing to atmospheric moisture absorption. The measured melt flow rate (MFR) values aligned closely with those of the constituent materials, providing empirical confirmation of the absence of significant degradation phenomena during processing. This consistency in rheological behavior indicates the successful preservation of molecular weight characteristics throughout the compounding and extrusion processes.

Table 1.3 Processing parameters adopted for the PLA-based formulations for thermoforming

Extruder speed (rpm):	500			Melt temperature (°C):						~ 170
Side-feeder speed (rpm):	256			Melt pressure (bar):						~ 25
Cutting blade speed (%):	40			Extruder torque (%):						~ 30
Machine flow rate (kg/h):	40			Measured machine flow rate (kg/h):						n.a.
Temperature profile (°C):	T1	T2	T3	T4	T5	T6	T7	T8	T9	HEAD
	175	180	185	175	170	170	160	160	155	170

Table 1.4 Processing parameters adopted for the PLA-based formulations for injection molding

Steady-state machine parameters										
Extruder speed (rpm):	600			***Melt temperature (°C):***						~ 160
Sidefeeder speed (rpm):	256			***Melt pressure (bar):***						~ 20
Cutting blade speed (%):	35			***Extruder torque (%):***						~ 30
Machine throughput (kg/h):	55			***Measured machine throughput (kg/h):***						n.d.
Thermal profile (°C):	***T1***	***T2***	***T3***	***T4***	***T5***	***T6***	***T7***	***T8***	***T9***	***HEAD***
	170	175	180	175	170	160	155	150	145	165

Figure 1.3 Appearance of the pellets of the PLA-based formulations

The processability of the injection-molding formulation was evaluated using a vertical press to manufacture standardized Izod and dog-bone specimens (ISO 527). Concurrently, the thermoforming-grade formulation was processed via cast extrusion to produce sheet stock, which was subsequently formed into trays using a laboratory-scale thermoforming equipment.

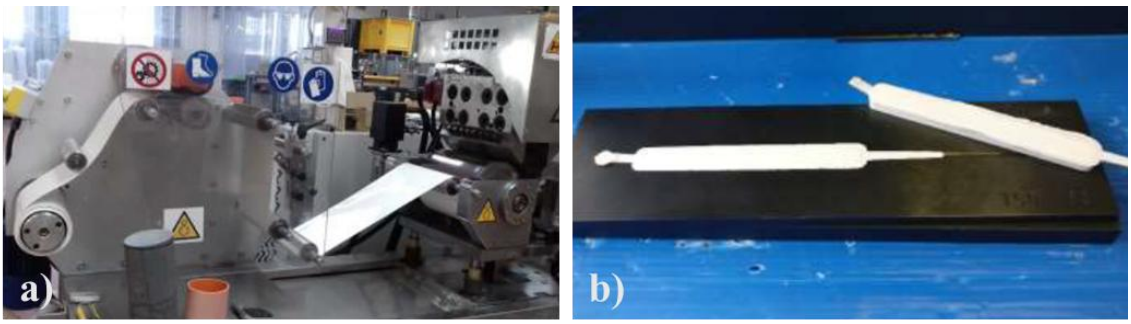

Figure 1.4 a) Cast extrusion process of the compound designed for the thermoforming process; b) Production of izod samples using the compound designed for the Injection Molding process.

Table 1.5 Processing parameters adopted during cast extrusion of the thermoforming compound

Coil ID	Thermal profile (°C)							V_e (rpm)	V_c (m/min)	V_t (m/min)	V_α (%)	Spessose (μm)	Width (mm)	Weight (kg)
	T1	T2	T3	T4	head									
					Ts	Tc	Td							
LA3CL2	175	180	180	180	185	185	185	180	1.2	2.4	27	500±50	180	-

Figure 1.4 illustrates the cast extrusion process for the thermoforming-grade formulation, alongside Izod specimen production trials for the injection-molding formulation. The critical processing parameters for the cast extrusion operation are systematically detailed in Table 1.5, providing quantitative reference points for process replication and analysis. The optimal sheet formation for the formulation LA3CL2 was achieved by casting the polymer melt between paired rollers. Although this mixture exhibited high fluidity during flat-die extrusion processing, it manifested several defects during sheet formation. The observed processing challenges likely originated from the inclusion of PCL in the formulation, a polymer renowned for its complex processing characteristics. Despite these difficulties, the produced sheet maintained a satisfactory surface finish quality. The primary defect consisted of a non-uniform thickness distribution, with the central region being notably thinner than the peripheral areas. Additionally, minor surface wrinkling appeared, presumably due to internal stress accumulation during the thermoforming process.

Figure 1.5 Thermoformed trays obtained using the PLA-based formulation

The LA3CL2 blend demonstrated superior resistance to heating time and temperature during processing, a characteristic directly attributable to its high PLA content. This formulation requires an elevated thermal energy input to achieve the viscoelastic state necessary for thermoforming, owing to PLA's glass transition temperature (Tg) of PLA significantly exceeding ambient conditions. The substantial PLA fraction complicates the optimization of the thermoforming parameters, necessitating precise thermal management throughout the process. The produced trays are shown in Figure 1.5.

The injection molding process was initially conducted using a provisional processing temperature derived from the tabulated melting and plasticization values of the individual

polymer components, with particular reference to the constituent exhibiting the highest melting point. Subsequent optimization of the processing parameters for manufacturing standardized Izod and dog-bone specimens yielded the final parameter set documented in Figure 1.6.

Figure 1.6 Izod samples produced via Injection molding using the SI LA3CL2 formulation

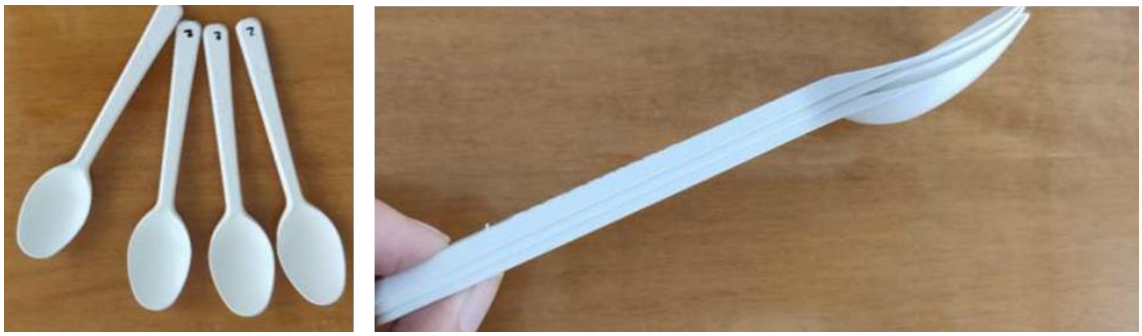

Figure 1.7 Injection molded spoons in SI LA3CL2

The materials that successfully passed the preliminary testing were subsequently subjected to industrial-scale injection molding trials, which are considered the most rigorous validation method. These trials employed a spoon mold specifically selected for its operational complexity owing to its concave geometry. The cycle time averaged approximately 15 s, with the manufactured products exhibiting exceptional aesthetic

quality, including precise geometric replication, flawless glossy surface finish, and complete absence of flash.

As illustrated in Figure 1.7, the produced spoons demonstrate both individual quality and stackability, which is a critical feature for automated packaging and subsequent rubber belt transportation systems. The stacking capability warrants particular emphasis because it directly facilitates the packaging process workflow. Notably, the part ejection system employs a sophisticated three-axis pantograph mechanism equipped with suction cups, which systematically extracts and orderly stacks the utensils directly into the packaging system according to predetermined production scheduling requirements rather than relying on conventional gravity-based bulk collection methods.

1.3 Packaging containing copolyesters of Succinic Acid

Succinic acid-based polyesters and copolyesters represent a class of materials with significant industrial potential owing to their technological properties closely resembling polyethylene. Although their cost remains elevated (ranging from €3400 to €4550 per metric ton), it is not prohibitively expensive compared to other biopolymers. Two distinct variants exist in the market:

- Fossil-derived PBS/PBSA (€3400-3800/ton) - more economically accessible but with higher environmental impact
- Bio-based PBS/PBSA (€4100-4550/ton) - commanding a premium price due to their reduced carbon footprint

The global market for polybutylene succinate (PBS) in 2019 was characterized by limited availability, with an annual production capacity of only 20,000 metric tons. At that time, Mitsubishi Chemicals maintained a near-monopoly on bio-based PBS production, although initial competitors from China were emerging. By 2020, the PBS market underwent substantial changes, marked by decreasing prices due to expanded production capacity and the emergence of new manufacturers, particularly in China. Several Chinese producers have established themselves as reliable suppliers of quality PBS at competitive prices. Among these, Xinjiang Blueridge Tunhe Chemical Industry Co. Ltd. emerged as

a significant market player, offering both fossil-based PBS at progressively lower prices and bio-based PBS at costs substantially below those of Mitsubishi Chemicals.

This shifting market landscape has renewed industrial interest in PBS, driven by its greater availability and increasingly favorable pricing. From a technical standpoint, PBS exhibits a Vicat softening temperature of approximately 93 °C, even without nucleation additives or specialized formulations, demonstrating its good thermal resistance. However, the material exhibits pronounced flexibility rather than rigidity, with an elongation at break of 210% (ISO 527-2) and a relatively low flexural modulus of 650 MPa (ISO 178). These mechanical properties make PBS suitable for applications requiring flexibility and thermal stability, but limit its use in scenarios demanding structural stiffness.

The entry of Chinese manufacturers has significantly altered the PBS market dynamics, potentially facilitating its wider adoption in flexible packaging and disposable applications. Nevertheless, the mechanical limitations of the material may necessitate blending with reinforcing agents or stiffening modifiers for semi-structural applications. The current market expansion, combined with ongoing price reductions, suggests growing opportunities for PBS in sustainable material solutions, provided that its mechanical characteristics align with application requirements. The competition between established producers and new market entrants is likely to continue to influence both pricing and quality standards in the coming years.

The research team developed a series of compounds based on PLA and PBS in collaboration with Cuki Cofresco S.r.l., a market-leading corporation specializing in the manufacturing and distribution of food packaging solutions, including food storage containers and cooking vessels. As the dominant player in this sector, the company has established itself through its comprehensive product portfolio, targeting both domestic and commercial food preservation applications. Three distinct formulations were developed (Table 1.6), each characterized by specific phase architectures and compositional ratios between polylactic acid (PLA) and polybutylene succinate (PBS). The first formulation featured a PLA-dominated matrix with PBS as a minor phase dispersed in a droplet morphology, achieved through low PBS content. The second formulation established a co-continuous phase morphology through intermediate PBS

loading, where both polymers formed interconnected networks. The third formulation inverts the phase hierarchy, utilizing PBS as a continuous matrix with discrete PLA domains obtained through low PLA incorporation.

Table 1.6 Formulations based on PLA and PBS. H: >40%; M: 5-40%; L: <5%.

	AB 400 - L	**AB 400 - LS**	**AB 400 - S**
Material	**wt.%**	**wt.%**	**wt.%**
PLA Luminy L175	H	M	M
BioPBS FZ91	M	M	H
Talc	M	M	M
EBS	L	L	L
PDLA Luminy D70	L	L	L
Melt Strength Enancher	L	L	L
Chain Extender	L	L	L

The incorporation of a droplet-dispersed PBS phase (below 20% content) within a PLA matrix enhanced the flexibility of the resulting compound. This effect stems from PBS's intrinsic material properties of PBS, particularly its low elastic modulus and high elongation at break, which collectively impart plasticizing characteristics to the blended system. The PBS phase effectively modified the stress-strain behavior of the otherwise rigid PLA matrix, improving its toughness while maintaining its structural integrity. Conversely, the inverse configuration, in which discrete PLA domains are dispersed within a continuous PBS matrix, produces an opposite modification effect. In this case, the high elastic modulus of the PLA inclusions reinforced the more flexible PBS continuous phase. This structural arrangement enhances the stiffness of the composite without compromising the inherent flexibility of the PBS matrix, which typically requires no additional flexibility enhancement in its unmodified state.

The research team incorporated a mineral phase into the formulations, which served multiple functional roles within the bioplastic compound. Primarily, the mineral component reduces the overall plastic content in the final food container. This inert fraction consequently diminishes the quantity of plastic waste requiring end-of-life management, thereby alleviating post-consumer disposal challenges associated with plastic waste. Talc was selected as the mineral additive owing to its well-documented

nucleation efficiency for PLA crystallization, commercial availability, and safety profile as a certified quartz- and asbestos-free material. From an economic perspective, the substantially lower cost of talc compared with other formulation components contributes to the overall material cost reduction. The lamellar morphology of uniformly dispersed talc particles creates a tortuous pathway within the polymer matrix, effectively impeding gas molecule permeation (particularly oxygen diffusion) and light radiation. This barrier functionality operates synergistically with the crystalline polymer phase to significantly reduce the overall material permeability. The combination of these effects addresses two critical design parameters for food packaging materials: oxidative degradation prevention and light protection, both of which are essential for maintaining food quality and extending shelf life.

The Research Group strategically combined talc with two distinct organic nucleating agents, each designed to operate through different mechanisms and temporal kinetics. Ethylene-bis-stearamide (EBS) was employed as a slow-acting nucleating agent, primarily to promote crystallization during the thermoforming reprocessing stage. This amphiphilic compound serves dual functions as both a nucleating agent and a processing aid, modifying the viscoelastic behavior of the polymer while gradually enhancing crystalline formation during secondary processing operations. PDLA (Luminy D70, Corbion) was incorporated as a stereocomplexing nucleant, which was specifically engineered to form thermally stable crystalline domains with the base PLLA matrix. The resulting stereocomplex crystals exhibited exceptional thermal stability, maintaining their structural integrity up to approximately 235 °C, which is a significant improvement over the thermal stability of conventional PLA crystals. This nucleation mechanism occurs through the formation of racemic crystallites, where D- and L-configured polymer chains establish highly ordered co-crystalline structures.

The Research Group systematically investigated the effects of process additives on the workability of compostable bioplastic formulations, with initial studies focusing on melt-strength modification. Conventional acrylic-based additives were evaluated for their ability to stabilize the polymer melt during extrusion processing. These additives promote chain entanglement within the PLA matrix, inducing the formation of an interconnected polymeric network. This molecular reorganization results in a substantial increase in the

melt viscosity of the compound, which critically influences the processability and final material properties.

The Research Group investigated the implementation of compatibilizing additives to enhance the processability and melt stability during flat-die extrusion and thermoforming of food container bioplastics. These chain-extending additives serve the critical function of molecular weight restoration, counteracting degradation-induced chain scission that occurs during melt-processing operations.

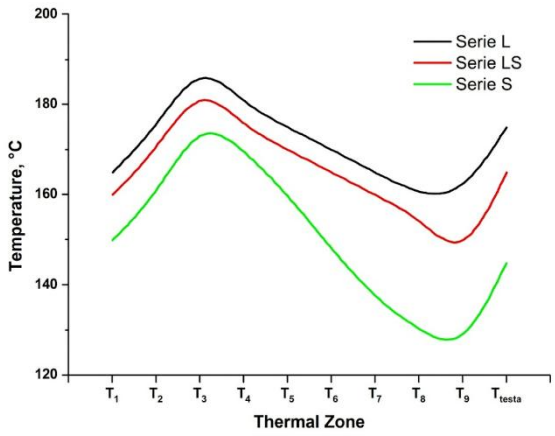

Figure 1.8 Temperature profiles adopted during the compounding process of PLA/PBS formulations

The defined compounds were produced via extrusion using a co-rotating twin-screw extruder equipped with a water-ring pelletizer system. Process control was achieved by precisely regulating three key parameters: the temperature profile along the barrel, screw rotation speed, and material feed rates from the twin gravimetric feeders. The temperature profile along the co-rotating twin-screw extruder was carefully designed to follow a parabolic trajectory (up to T9), as detailed in Figure 1.8. This thermal management strategy serves multiple processing objectives: the independent temperature control unit governing the die zone maintained temperatures 15-20 °C above the previous one to prevent melt flow obstructions through the die assembly. Significantly, the thermal profile reached its maximum value in zone 4 (powder feeding section), where the temperature was maintained 10-15 °C above the polymer melting point to optimize the

encapsulation process of powdered additives and mineral fillers within the molten polymer phase.

Table 1.7 Processing parameters set and recorded during the compounding process of the PLA/PBS blends

	Screw Speed (rpm)	**Side Feeder Spee (rpm)**	**Granule feeder (%)**	**Powder Feeder (kg/h)**	**Cutting Speed (%)**	**Melt Temp. (°C)**	**Melt Pressure (bar)**	**Torque (%)**
Serie L	420	256	22	5.9	44	170	26	35
Serie LS	420	256	23	6.1	47	165	25	35
Serie S	420	256	23	5.7	53	145	22	35

The peak temperature selection was systematically determined based on the relative composition of the primary and secondary polymer phases. For the L-series and LS-series formulations, where PLA L175 (melting temperature = 175 °C) served as the continuous matrix, the thermal profile was optimized based on PLA concentration. Conversely, the S-series formulations, featuring PBS FZ91 (melting temperature = 115 °C) as the dominant phase, required peak temperature modulation, which ensured the complete melting of both the PBS matrix and the dispersed PLA phase. The thermal profile subsequently decreased progressively along the final barrel sections to enhance the melt strength, thereby increasing the head pressure prior to the die exit. The processing parameters, including mass throughput and screw speed, were uniquely defined for each extrusion trial and are presented in Table 1.7. Screw velocity critically influences both the material throughput and melt temperature through the frictional heating generated at the screw-polymer interface. This interdependent relationship necessitates precise parameter optimization to balance production efficiency with melt quality requirements. The melt temperature is a critical process parameter resulting from both the imposed thermal profile and frictional heat generation during extrusion. Maintaining precise control over this variable is essential to prevent two key processing issues: excessive pressure drop near the die region and the thermal degradation of the material. Elevated melt pressure (P_{melt}) at the die head is crucial for ensuring homogeneous material flow through the die orifice, which is a fundamental requirement for consistent strand formation during pelletization. For all formulations investigated, the operational throughput was maintained within a narrow range of 38-40 kg/h. This throughput

optimization balances production efficiency with the need to maintain stable processing conditions across various material compositions. The produced pellets are shown in Figure 1.9. In all cases, a regular shape was obtained owing to the chosen processing parameters and selected additives. The gray color is attributed to talc.

Figure 1.9 Appearance of the produced PLA/PBS pellets: a) Series L; b) Series LS; c) Series S.

The investigated material was specifically engineered for flat-die extrusion and thermoforming processes for food packaging applications. Following dehumidification pretreatment, the pelletized compound undergoes cast extrusion to produce uniform sheets. The thermal management strategy employs a carefully designed temperature profile along three critical components: the extrusion barrel, transition elbow, and die assembly. This profile follows a progressively increasing gradient that surpasses the material's melting temperature, reaching peak values at the die head to systematically reduce the polymer viscosity and enhance the processability.

Table 1.8 Temperature profile adopted during cast extrusion of PLA/PBS compounds

	T1 (°C)	**T2 (°C)**	**T3 (°C)**	**T4 (°C)**	**Tsx (°C)**	**Tc (°C)**	**Tdx (°C)**
Serie L	170	180	188	188	188	188	188
Serie LS	180	188	190	190	192	190	190
Serie S	177	185	185	187	187	185	187

The die temperature distribution requires particular optimization because of its direct influence on the melt flow uniformity. Optimal processing conditions were achieved by

implementing higher temperature setpoints at the die extremities. This thermal compensation counteracts the "cat's tongue" effect, a phenomenon resulting from disproportionate cooling rates at the sheet edges caused by their higher surface-to-volume ratio relative to the central portion. The strategic temperature elevation at the edges maintained consistent viscoelastic properties across the entire melt curtain, ensuring dimensional stability in the extruded sheet. The temperature profile and processing parameters are presented in Tables 1.8 and 1.9, respectively. The cast extrusion process is shown in Figure 1.10.

Table 1.9 Processing parameters adopted during cast extrusion of PLA/PBS compounds

	Screw speed (rpm)	**Calander speed (m/min)**	**Draw speed (m/min)**
Serie L	150	1	1.3
Serie LS	150	1	1.3
Serie S	150	1	1.3

Figure 1.10 Cast extrusion of the formulations based on PLA/PBS

The experimental thermoforming trials conducted on the extruded sheets demonstrated exceptional replication fidelity of geometric features (Table 1.9), indicating superior

material performance in mold-detail reproduction. This characteristic behavior stems from the optimized viscoelastic properties achieved through carefully designed compounding and extrusion parameters. The comprehensive thermomechanical characterization results confirmed the suitability of these compounds for thermoformed product manufacturing. Notably, formulations with PBS as the primary polymeric phase exhibited superior heat deflection temperature (HDT) performance, indicating enhanced thermomechanical stability under load-bearing conditions at elevated temperatures.

Figure 1.11 Details of the thermoformed trays based on PLA and PBS.

1.4 Colored solutions

The development of colored polymer compounds is a technically demanding process that requires careful optimization across multiple production stages. The initial selection of a suitable color masterbatch must be followed by a comprehensive evaluation through flat-die extrusion trials with the target base compound, subsequent thermoforming into finished products, and rigorous testing of the colored articles. The chromatic properties initially achieved during compounding may be significantly influenced by several processing factors, including uneven pigment distribution within the polymer matrix, molecular orientation effects during extrusion and thermoforming operations, and potential thermal degradation of the polymer matrix or colorant system.

The introduction of coloring agents may also modify the fundamental processing characteristics of the material by altering its rheological behavior. Pigment particles can act as nucleation sites, potentially affecting the crystallization kinetics and ultimately

modifying the mechanical properties of the final product. Furthermore, the interaction between pigment concentration, particle size distribution, and polymer flow characteristics must be carefully balanced to maintain both color consistency and processing stability throughout the manufacturing process.

To obtain compounds with the desired characteristics, engineering strategies were proposed in this study aimed at: (i) customizing the thermomechanical properties of the material; (ii) minimizing polymer degradation, particularly with regard to color; (iii) adjusting the rheological properties of the melt during processing; (iv) reducing production costs through the introduction of mineral fillers; and (v) producing a bio-based, biodegradable material suitable for direct food contact.

Therefore, it was necessary to select the most suitable materials for the application under consideration from those available on the market. Polylactic acid (PLA) is a biomaterial suitable for producing compostable food-contact articles (EN 13432 standard). This polymer is currently the most widely used and prevalent in numerous market segments, particularly in the food packaging sector.

Although PLA exhibits fair thermomechanical properties, its application in the single-use food sector requires material engineering, as previously noted. In particular, this phase aims to increase the toughness of the commercial polymer, which would otherwise be too brittle. Strategies based on secondary polymer phases have been adopted for this purpose. Through compounding processes, it is possible to obtain a material that exhibits the combined properties of the polymers in the formulation, depending on their relative concentrations, miscibility, and compatibility. The use of a secondary polymer phase with greater ductility leads to the formation of rubbery segments within the rigid PLA chains, which can make the structure of the final polymer more flexible. The choice of this secondary phase must also be made in relation to its miscibility with PLA to avoid discontinuities. The proposed formulations feature PLA as the primary polymer phase and PBS (polybutylene succinate) as the secondary phase.

The use of fillers is already widespread in the thermoplastics sector and can represent an immediate and straightforward solution for reducing the cost of the final material. The use of mineral or organic fillers improves the properties of the blend, such as the gas barrier performance and mechanical strength. Furthermore, the presence of fillers can

increase the degree of crystallinity, improve strength and thermal stability, and enhance aesthetic characteristics. The use of mineral fillers does not compromise the compostability of the products, as the reference standard for packaging, EN 13432:2002, applies only to the organic fraction. Therefore, formulation scenarios have included the use of inorganic fillers.

The PLA engineering process carried out by the research team also involved the use of additive phases. The presence of active agents in the formulations is essential to obtain materials with the necessary mechanical properties for the intended application, as well as good processability. The formulations identified the need to include a release agent, chain extender, and additives to improve the toughness of the polymer melt.

The research team subsequently focused on possible innovative solutions for coloring bioplastics, exclusively using pigments not derived from chemical synthesis. Among the various solutions available on the market, a range of pigments was selected that could be integrated into the polymer matrix without altering its physical and mechanical properties. These products are commercially available as compounds that can be blended with base compounds of neutral coloration. The assessment of the quantity to be incorporated in each formulation focused on aspects such as (i) the desired final color intensity, (ii) color uniformity, and (iii) surface finish. Four different colors were tested: yellow, pink, blue, and green (Figure 1.12).

Figure 1.12 Colored masterbatches

The tested formulations are listed in Table 1.10. The concentration of the colored masterbatch was set at 4 wt %, corresponding to the maximum concentration allowed by the regulations governing compostability. In each formulation, two different grades of PLA were included, differing in their D-isomer content, to optimize the mechanical properties. PLA Luminy L175 is a high-performance grade with a high crystallization capability during processing, making it particularly suitable for the extrusion process. PLA Luminy D070 is also suitable for extrusion; however, owing to its higher D-isomer content, it exhibits a lower tendency to crystallize and is therefore characterized by greater ductility (higher elongation at break). These characteristics make them suitable for the extrusion of films with greater flexibility. PBS with a low MFR of 5 g/10 min and a high flexural modulus was selected as the secondary polymer phase.

Table 1.10 Colored formulations. H: >40%; M: 5-40%; L: <5%.

Yellow Formulation		**Pink Formulation**	
Material	*wt%*	*Material*	*wt%*
PLA Luminy L175	H	**PLA Luminy L175**	H
PLA Luminy D070	L	**PLA Luminy D070**	L
PBS Thune LMFR	M	**PBS Thune LMFR**	M
Yellow Masterbatch	4%	**Pink Masterbatch**	4%
Chain Extender	L	**Chain Extender**	L
Organic wax	L	**Organic wax**	L
Melt Strength Enhancer	L	**Melt Strength Enhancer**	L
Talc	M	**Talc**	M
Light Blue Formulation		**Green Formulation**	
Material	*wt%*	*Material*	*wt%*
PLA Luminy L175	H	**PLA Luminy L175**	H
PLA Luminy D070	L	**PLA Luminy D070**	L
PBS Thune LMFR	M	**PBS Thune LMFR**	M
Light Blue Masterbatch	4%	**Green Masterbatch**	4%
Chain Extender	L	**Chain Extender**	L
Organic wax	L	**Organic wax**	L
Melt Strength Enhancer	L	**Melt Strength Enhancer**	L
Talc	M	**Talc**	M

Based on the initial extrusion tests, a second set of formulations was defined, in which the colored masterbatch was set at a concentration of 7%, to obtain a product with greater color intensity and uniformity regardless of variations in the thickness of the film or the

final product. As previously mentioned, 4% wt constitutes the maximum concentration allowed to comply with compostability regulations; however, it is possible to submit the produced formulations for certification in the future. The optimized compositions of the colored formulations are listed in Table 1.11.

Table 1.11 High-intensity color formulations. H: >40%; M: 5-40%; L: <5%.

Yellow Formulation		**Pink Formulation**	
Material	*wt%*	*Material*	*wt%*
PLA Luminy L175	H	**PLA Luminy L175**	H
PLA Luminy D070	L	**PLA Luminy D070**	L
PBS Thune LMFR	M	**PBS Thune LMFR**	M
Yellow Masterbatch	7%	**Pink Masterbatch**	7%
Chain Extender	L	**Chain Extender**	L
Organic wax	L	**Organic wax**	L
Melt Strength Enhancer	L	**Melt Strength Enhancer**	L
Talc	M	**Talc**	M
Light Blue Formulation		**Green Formulation**	
Material	*wt%*	*Material*	*wt%*
PLA Luminy L175	H	**PLA Luminy L175**	H
PLA Luminy D070	L	**PLA Luminy D070**	L
PBS Thune LMFR	M	**PBS Thune LMFR**	M
Light Blue Masterbatch	7%	**Green Masterbatch**	7%
Chain Extender	L	**Chain Extender**	L
Organic wax	L	**Organic wax**	L
Melt Strength Enhancer	L	**Melt Strength Enhancer**	L
Talc	M	**Talc**	M

The experimental phase focused on the optimized formulation, as reported in Table 1.11. The compounds were produced using a co-rotating twin-screw extruder, model Leistritz ZSE 27 iMaxx, and the corresponding dosing systems. Before reaching steady-state conditions that led to a stable and consistent production of pellets, an optimization phase of the extrusion parameters was necessary, starting from the initial trial values set based on the research team's previous experience. In particular, the parameters on which the optimization process primarily focused were the feed rates of the volumetric and gravimetric feeders, extruder temperature profile, and screw rotation speed. The processing parameters adopted during the compounding process are presented in Table

1.12, Table 1.13, Table 1.14 and Table 1.15. The aspect of the produced pellets are presented in Figure 1.13, Figure 1.14, Figure 1.15 and Figure 1.16.

Table 1.12 Processing parameters adopted during the extrusion of the yellow compound

Steady-state machine parameters for the production of the yellow compound										
Extruder speed (rpm):	550			Melt temperature (°C):						185
Side-feeder speed (rpm):	256			Melt pressure (bar):						22
Cutter blade speed (%):	41			Extruder torque (%):						30
Machine flow rate (kg/h):	49			Measured machine flow rate (kg/h):						48
Thermal profile (°C):	T1	T2	T3	T4	T5	T6	T7	T8	T9	HEAD
	175	185	185	182	180	175	173	170	168	190

Table 1.13 Processing parameters adopted during the extrusion of the pink compound

Steady-state machine parameters for pink compound production										
Extruder speed (rpm):	550			Melt temperature (°C):						179
Side-feeder speed (rpm):	256			Melt pressure (bar):						21
Cutting blade speed (%):	48			Extruder torque (%):						30
Machine throughput (kg/h):	49			Measured machine throughput (kg/h):						48
Thermal profile (°C):	T1	T2	T3	T4	T5	T6	T7	T8	T9	HEAD
	175	185	185	182	180	175	173	170	168	180

Table 1.14 Processing parameters adopted during the extrusion of the light blue compound

Steady-state machine parameters for the production of the blue compound										
Extruder speed (rpm):	550			**Melt temperature (°C):**						179
Side-feeder speed (rpm):	256			**Melt pressure (bar):**						22
Cutting blades speed (%):	41			**Extruder torque (%):**						30
Machine throughput (kg/h):	47			**Measured machine throughput (kg/h):**						46
Thermal profile (°C):	**T1**	**T2**	**T3**	**T4**	**T5**	**T6**	**T7**	**T8**	**T9**	**DIE**
	175	185	185	182	180	175	173	170	168	180

Table 1.15 Processing parameters adopted during the extrusion of the green compound

Steady-state machine parameters for green compound production										
Extruder speed (rpm):	550			**Melt temperature (°C):**						179
Side-feeder speed (rpm):	256			**Melt pressure (bar):**						21
Cutting blade speed (%):	41			**Extruder torque (%):**						30
Machine throughput (kg/h):	49			**Measured machine throughput (kg/h):**						48
Thermal profile (°C):	**T1**	**T2**	**T3**	**T4**	**T5**	**T6**	**T7**	**T8**	**T9**	**HEAD**
	175	185	185	182	180	175	173	170	168	190

Figure 1.13 Appearance of the pellets of the yellow compound

Figure 1.14 Appearance of the pellets of the pink compound

Figure 1.15 Appearance of the pellets of the light blue compound

Figure 1.16 Appearance of the pellets of the green compound

Table 1.16 Processing parameters adopted to produce the yellow sheets with different thickness values

Compound with Yellow Master	Thermal Profile (°C)							Extruder Speed (rpm)	Calender Speed (m/min)	Puller Speed (m/min)	Winder Speed (%)
	T1	T2	T3	T4	Head						
					Ts	Tc	Td				
1st sheet	190	190	190	190	190	190	195	135	0.9	1.6	28
2nd sheet	190	190	190	190	190	190	195	135	1	1.5	28
3rd sheet	190	190	190	190	190	190	195	135	1	1.5	28

The processability of the pilot formulations was evaluated on a laboratory/semi-pilot scale plant, as was done for the pellet production process. The system used was a prototype customized to meet the processing requirements of the bio-based materials. Each formulation responded differently to the extrusion process, and individual optimization of the operating parameters was necessary. The parameters requiring optimization included the temperature profile, screw rotation speed, and parameters of the film take-off system, namely, the rotation speed of the calender rolls, haul-off, and winder. The pellets of all the studied formulations were dried for 6 h at 60 °C prior to flat-die extrusion to prevent hydrolytic degradation phenomena and defects attributable to the evaporation of moisture adsorbed on the pellet surface. For each colored formulation, three different plastic films were produced, each characterized by a different thickness. To achieve these results, each plastic film was produced by setting different processing parameters. In particular, the following parameters are of fundamental importance for varying the thickness in the flat-die extrusion process: (i) extrusion speed, (ii) calender roll speed, (iii) haul-off speed, and (iv) winder speed. The process parameters used for

the production of the films from the different compounds are reported in Table 1.16, Table 1.17, Table 1.18 and Table 1.19. For the two masterbatch concentrations tested (4 and 7 wt %), the same process parameters were applied for each color.

Table 1.17 Processing parameters adopted to produce the pink sheets with different thickness values

Compound with Pink Master	Thermal Profile (°C)							Extruder Speed (rpm)	Calender Speed (m/min)	Puller Speed (m/min)	Winder Speed (%)
	T1	T2	T3	T4	Head						
					Ts	Tc	Td				
1st sheet	190	190	190	190	190	190	195	140	0.5	1.9	30
2nd sheet	190	190	190	190	190	190	195	140	1.5	1.8	30
3rd sheet	190	190	190	190	190	190	195	140	0.8	1.5	30

Table 1.18 Processing parameters adopted to produce the light blue sheets with different thickness values

Compound with Blue Master	Thermal Profile (°C)							Extruder Speed (rpm)	Calender Speed (m/min)	Puller Speed (m/min)	Winder Speed (%)
	T1	T2	T3	T4	Head						
					Ts	Tc	Td				
1st sheet	190	190	190	190	190	190	195	135	1.1	1.6	30
2nd sheet	190	190	190	190	190	190	195	135	1.1	1.7	30
3rd sheet	190	190	190	190	190	190	195	135	1	1.4	30

Table 1.19 Processing parameters adopted to produce the green sheets with different thickness values

Compound with Green Master	Thermal Profile (°C)							Extruder Speed (rpm)	Calender Speed (m/min)	Puller Speed (m/min)	Winder Speed (%)
	T1	T2	T3	T4	Head						
					Ts	Tc	Td				
1st sheet	190	190	190	190	190	190	195	120	0.8	2.0	28
2nd sheet	190	190	190	190	190	190	195	155	1	2.4	27
3rd sheet	190	190	190	190	190	190	195	165	1.1	1.6	27

Figure 1.17 shows images of the extrusion process of compostable bioplastic films colored with four different masterbatches. As previously noted, variations in the extrusion process parameters allowed the production of films with different film thicknesses. Figure 1.18 shows the aspect of sheets after the extrusion process.

Figure 1.17 Cast extrusion process of the colored sheets

Figure 1.18 Aspect of the colored sheets after the extrusion process

Thermoforming was performed on all formulations. A ribbed tray mold measuring 130 × 180 mm² was selected, featuring a rim geometry suitable for the heat sealing of a top lid (i.e., a flexible film for sealing the tray). The phases of the thermoforming process are shown in Figure 1.19. The machine allows the control of the heating power of the quartz lamp positioned on the top of the sheet (Figure 1.20).

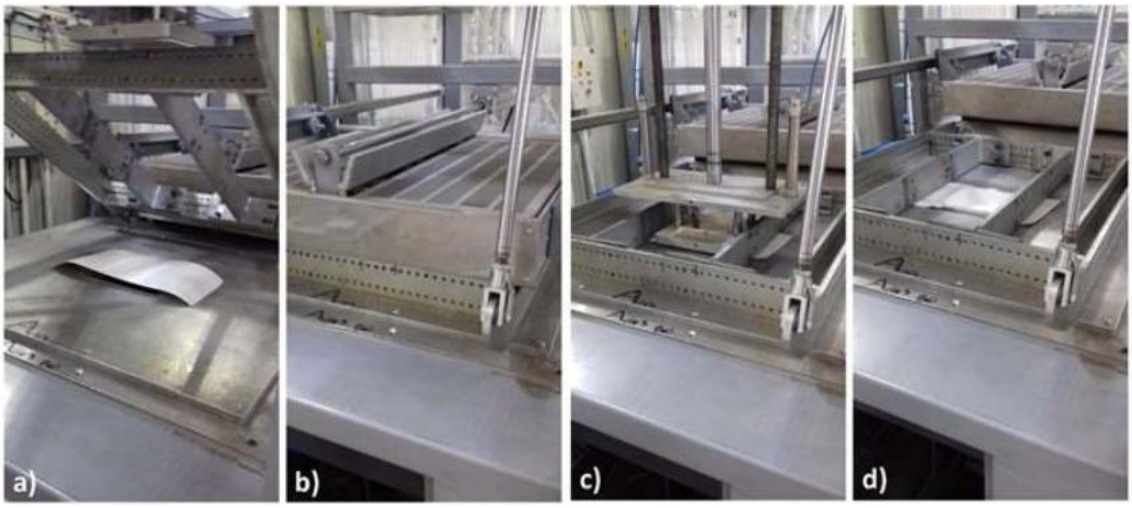

Figure 1.19 Phases of the thermoforming process

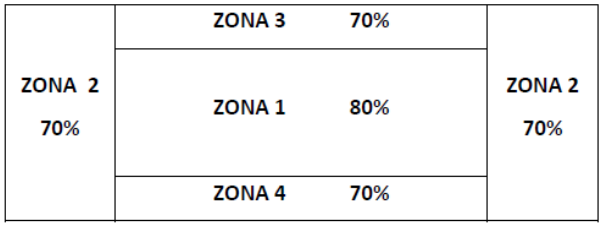

Figure 1.20 Heating power adopted during the thermoforming process of the colored sheets

Figure 1.21 and Figure 1.22 display the images of the obtained trays. The leaves were thermoformed correctly, exhibiting the proper geometry, particularly along the edges and corners. Furthermore, no significant color variations were observed despite the differing thickness-to-stretch ratios, which can cause variations in the manufactured article.

Figure 1.21 Top view of the colored thermoformed trays

Figure 1.22 Bottom view of the colored thermoformed trays

The characterization of the colored film primarily involved the evaluation of its color. The pink, yellow, green, and blue films were extruded using a flat die, as previously described. Colorimetric analysis focused on formulations containing 4% and 7% colored biomasterbatch by weight. It is essential to identify any color differences along the film

of the chosen sample to ensure chromatic homogeneity and assess the quality of the formulation used. This test was performed by measuring the color at the reference and sample points. The color differences were calculated using the resulting colorimetric values. The uniformity of the blue and green films was good; however, the pink and yellow films showed some dyschromia at certain points. This phenomenon was primarily observed at masterbatch concentrations of 4% by weight. This is attributed to the non-uniformity of the film thickness, which is more apparent with lighter colors such as pink and yellow. The objective is to optimize the film extrusion process to reduce this defect. In the specific case of the yellow film, increasing the colorant percentage appeared to mitigate this problem. Therefore, the colorant percentage will be increased accordingly, in accordance with compostability regulations. Alternatively, adjustments can be made to the formulation itself by increasing the percentage of mineral fillers, again in compliance with regulations, to make the film more amenable to lighter color tones.

1.5 Home compostable solutions

The necessity for reform in plastic waste management has led the European Commission to implement Directive (EU) 2019/904 on Single-Use Plastics (SUP), which bans the use of synthetic plastics in disposable products as of July 2021. Replacing fossil-based polymers with products made from compostable, bio-derived materials can decrease environmental impact and alleviate the challenges and costs associated with the management, recycling, and disposal of municipal waste. The subsequent stage in the investigation of novel materials involves the development of compounds suitable for home composting. Industrial and domestic composting scenarios exhibit significant differences. Industrial composting involves multiple bio-oxidation and maturation stages, characterized by temperatures that can exceed 50°C during the thermophilic phase. Conversely, home composting occurs within a simple composting unit, where the temperature and humidity levels correspond to ambient conditions or are only slightly elevated.

To develop a plastic material that complies with home composting requirements, it is imperative that all components within the formulation are compatible with this end-of-

life scenario, as previously discussed. Currently, there are no formal regulations for home composting analogous to the standards established for industrial composting, necessitating a precise definition of the term. Home compostable materials are characterized by their ability to achieve 90% degradation under conditions of relatively low and inconsistent temperatures and humidities within a period of less than six months. To ascertain a material's compliance with these criteria, certification bodies such as TÜV Austria are available for consultation. These organizations specialize in evaluating the suitability of formulations through standardized tests conducted by accredited laboratories under controlled conditions. Additionally, certain local regulations, particularly in France and Australia, are currently undergoing refinement, with the aim that their standards will eventually be internationally recognized.

The research project entailed the development of an initial series of formulations incorporating TPS as one of the polymer phases, owing to its biodegradability, extensive market availability, and cost-effectiveness, which are crucial factors in the single-use tableware industry. PLA was employed in conjunction with TPS as a reinforcing agent and stiffener. PLA exhibits significantly greater stiffness at room temperature than TPS, and when utilized in the form of dispersed particles, it can enhance the stiffness of the matrix in which it is embedded. Notably, PLA is immiscible with TPS and forms a fine and homogeneous dispersion within the matrix at specific concentrations and mixing conditions. The discontinuity of the reinforcing phase, coupled with its good homogeneity despite a small particle size, are parameters of the blend that enhance the efficiency of PLA's reinforcing effect. A third component was subsequently incorporated into the TPS/PLA formulation as a plasticizing phase, which enhanced the flexibility of the plastic material. This component will be chosen between PBAT and PBSA. The former, which is also compostable, is more cost-effective, whereas PBSA, derived from a renewable source, exhibits superior degradability in its pure state. Consequently, the initial phase of the design process was devoted to investigating ternary blends. Ternary blends, or more precisely, ternary compounds, present significant complexity in design, as the interactions between constituent pairs must also be considered. The defined formulations are presented in Table 1.20 and Table 1.21. The selected extruder type was a Leistritz ZSE 27 IMaxx model, configured as a co-rotating twin-screw system and equipped with appropriate gravimetric dosing units. This is a pilot-scale system; however, it possesses

features analogous to those of larger industrial plants, such as a high motor power relative to the screw size (40 kW). This configuration represents an optimal balance among several critical requirements. First, efficient mixing is essential because of the presence of mineral fillers and the necessity for a finely dispersed blend of immiscible polymers. Second, this must be accomplished without exerting excessive shear forces on the biopolymers.

Table 1.20 Definition of home-compostable formulations (B-TPS1)

Form	***Component***	***Wt, %***
Granule	TPS AMITROPLAST	25.0%
Granule	PLA Luminy L175	20.0%
Granule	PBAT China	45.0%
Powder	Talco Luzenac	8.0%
Powder	EBS (beads) EVIWAX 140	2.0%

Table 1.21 Definition of home-compostable formulations (B-PHBH 1)

Form	Component	Wt %
granule	**PHBH** Kaneka X131A	60,00%
granule	**MCC PBS** FD 92 PBSA	18,00%
powder	**Luzenac Talc**	15,00%
powder	**EBS** Ewivax C140	1,00%
granule	**White Masterbatch**	4,00%
powder	**Plastistrength** 550	0,90%
powder	**Paraloid** BPMS 265	0,90%
granule	**Joncryl** ADR 4400	0,20%

Figure 1.23 Aspect of the produced home compostable granules. Left: B-TPS-1; right: B-PHBH-1.

Bio-derived polymers are highly susceptible to various degradation phenomena, particularly hydrolysis at elevated temperatures, with PLA being notably prone to this phenomenon. Excessively high stress can induce localized temperature increases, which may not be detected by the thermal regulation system, leading to the progressive degradation of the material. The aspects of the produced granules are shown in Figure 1.23. The adopted processing parameters are listed in Table 1.22.

Table 1.22 Processing parameters adopted during the extrusion process of home compostable formulations

Extruder speed (rpm):	340			*Melt temperature (°C):*						125
Side-feeder speed (rpm):	256			*Melt pressure (bar):*						23
Cutter speed (%):	24			*Extruder torque (%):*						30
Machine throughput (kg/h):	8,04			*Measured machine throughput (kg/h):*						n.a.
Thermal profile (°C):	*T1*	*T2*	*T3*	*T4*	*T5*	*T6*	*T7*	*T8*	*T9*	*HEAD*
	120	135	150	140	130	126	124	122	118	135

The melt flow rate (MFR) of the synthesized compounds indicates their suitability for the injection molding process. B-TPS1 exhibited an MFR of 35.5 g/10 min at 230°C under a load of 2.16 kg. The elevated testing temperature was necessitated by the high viscosity of the resultant compound, which did not flow at lower temperatures. B-PHBH1 demonstrated an MFR of 7.4 at 160°C under a weight of 5 kg. Material B-TPS1 exhibited low thermal resistance, characterized by a Vicat temperature of approximately 44°C, attributable to its low crystallinity. Thermal analysis of B-PHBH1 revealed an initial endothermic event at approximately 84°C, corresponding to the melting of PBSA. The melting of PHBH occurred at a higher temperature of approximately 145°C. Additionally, PHBH has high crystallinity, resulting in a Vicat Softening Temperature of approximately 115°C.

The optimization of the cast extrusion process for material B-TPS1 necessitated considerable effort in refining the machine settings and pellet preparation procedure prior to flat-die extrusion. Although the formulation exhibited only minor and negligible adhesion issues with the die and pelletization system during reactive extrusion, it

encountered significant challenges during flat-die extrusion. The tackiness of the material, coupled with prominent defects caused by residual moisture in the extrudate, rendered it impossible to establish a parameter set that would produce a consistent sheet (Figure 1.24). Consequently, the assessment of processability and sheet production was deferred pending an additional drying step conducted at 60°C and extended overnight. However, as extended drying cannot be applied directly to thermoplastic starch prior to compounding, as this would result in the loss of the plasticity of the starch, some water residue inevitably remains within the extruded sheet. This residual moisture can complicate the flat-die extrusion process, potentially resulting in the production of low-quality sheets.

Figure 1.24 B-TPS1 cast extruded sheet. Left: defects related to humidity; right: sheet after the parameters optimization

The fabrication of sheets with a thickness of less than 500 μm, which is essential for assessing the home compostability of the material, has highlighted a limitation in the mechanical properties of this formulation. Specifically, sheets thinner than 120 μm exhibited insufficient strength at processing temperatures (i.e., T > Tg) to endure the tensile stresses encountered during production (Figure 1.25). This inadequacy is attributed to the presence of imperfectly dispersed starch, which introduces discontinuities in the matrix, leading to crack formation and propagation, which hinders the formation of a continuous sheet. The reduced thickness was, indeed, considered necessary to facilitate reasonably rapid biodegradation tests. However, from an

application perspective, such minimal thicknesses are not pertinent to the single-use tableware industry, where production typically commences with sheets of at least 400–450 microns in thickness to manufacture the corresponding products.

Figure 1.25 Cast extrusion of B-TPS1 sheets with thickness below 120 µm

The cast extrusion of the B-PHBH1 formulation is depicted in Figure 1.26. The resulting sheet satisfactorily achieved a target thickness of 550 ± 15 µm and marginally met the width target of 195 mm, which is inherently less critical as it is contingent upon the specific dimensions of the flat die. The surface of the sheet exhibited a glossy and uniform appearance, indicating effective material distribution within the calender nip. A well-developed white color was observed, signifying the correct integration of the corresponding masterbatch, which is the pigment used to impart a clearly defined white hue to the sheet. This white color is the standard typically employed in the single-use tableware segment, and it was utilized in the present experiment to align with customer expectations.

During the extrusion process, an atypical accumulation of material was observed along the edges of the die lip, which formed a material frame around the flat die opening by the conclusion of the production run (Figure 1.27). The mechanism underlying this phenomenon is attributed to the swelling of the exiting material, indicative of viscoelastic

behavior, with a magnitude significantly greater than initially anticipated. This observation is consistent with the substantial discrepancy between the output sheet thickness and the adjustments made to the flat-die opening and calender gap.

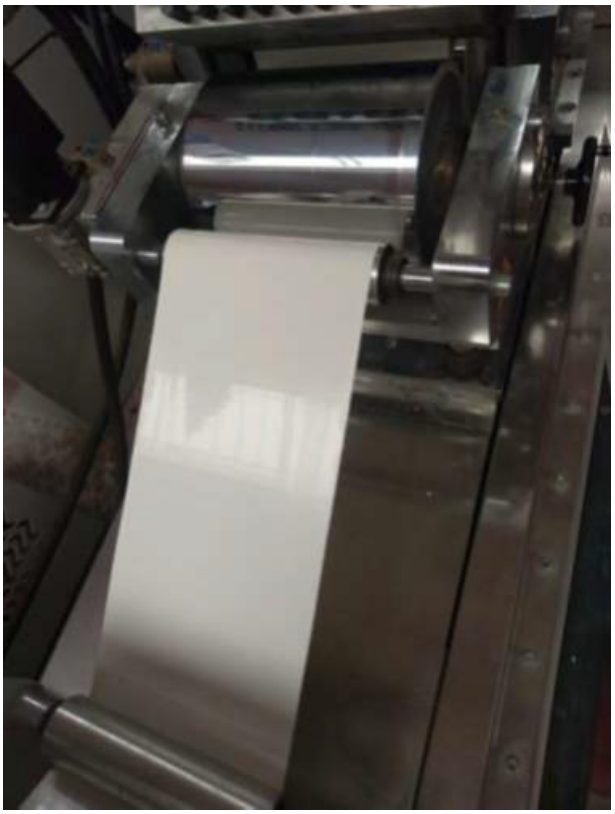

Figure 1.26 Cast extrusion process of B-PHBH1

Figure 1.27 Material accumulation at the die during the extrusion of B-PHBH1

In summary, the produced sheet did not exhibit optimal geometric accuracy; however, it remained suitable for subsequent thermoforming processes. This phenomenon is typically attributed to the "condensation" of plastic material around the calender lip. The material exiting the calender undergoes rapid undercooling, which can result in the swift recrystallization of the plastic. This recrystallized material tends to accumulate at the lip, where the temperature is insufficient to remelt it because this location is outside the die. Consequently, the material build-up progressively increases as the production run continues. During industrialization, this aspect warrants careful examination, as it may necessitate production stoppages for cleaning the lips. The sheets were used to fabricate thermoformed trays using laboratory-scale equipment. B-TPS1 exhibited a notably low viscosity. This characteristic necessitates prolonged cycle times to facilitate part ejection from the mold, without deformation. Additionally, the viscosity of the material in its plasticized state was sufficiently low to replicate the imprints of the vacuum holes from the mold surface. This was first achieved by reducing the lamp power by 5 points compared to the initial value (for samples i and ii) and subsequently by decreasing the irradiation time (for sample iii). However, a significant improvement was observed when an irradiation power between 70% and 80% was applied while keeping the irradiation times unchanged. Specifically, the optimized conditions were achieved by applying 80% of the maximum power for the central lamp and 70% for the perimeter lamps, with a heating time of 30 s. Images of the process are presented in Figure 1.28. Overall, the material demonstrated good workability, and no adhesion to the mold substrate was observed. The polyhydroxyalkanoate-based material demonstrated commendable performance in thermoforming, as evidenced by its capacity to adhere effectively to mold walls and accurately replicate their geometric details, thereby achieving the intended shape with high precision. For instance, images of two P 136 plates produced through the thermoforming of the B-PHBH1 blend are presented in Figure 1.29, illustrating the high quality of the manufactured articles and the favorable aesthetic appearance attained during the experimental trial. Empirical evaluations of thermal and mechanical resistance confirmed the viability of utilizing these compounds in the manufacture of disposable food trays. The presence of TPS and PHBH ensures the home compostability of the formulations.

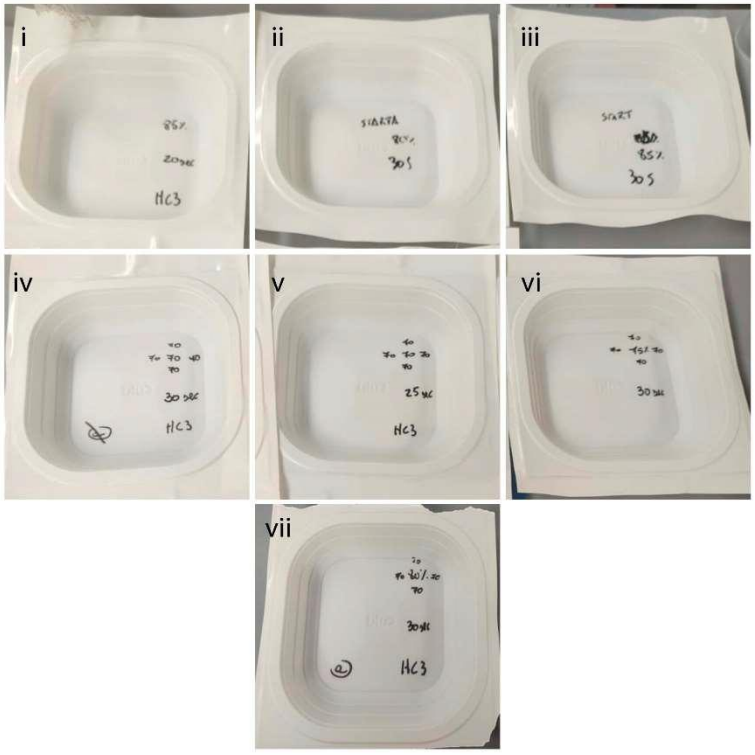

Figure 1.28 B-TPS1 home compostable trays

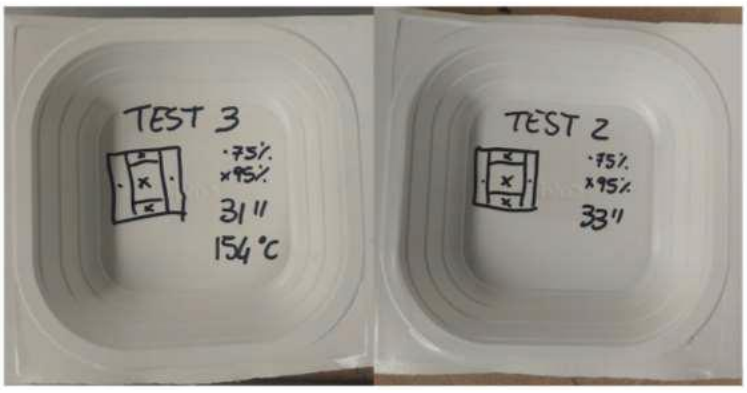

Figure 1.29 B-PHBH1 home compostable trays

1.6 Recycling of bioplastics

Mechanical recycling of plastics is predominantly applied to waste materials consisting of fossil-based polymers, such as polyolefins, which exhibit high stability and diminished propensity for degradation. There are four principal types of recycling processes [4].

1. Primary recycling involves the extrusion of pre-consumer polymers or pure polymer streams (for example, Bottle-to-bottle closed-loop recycling).
2. Secondary recycling, which requires the sorting of polymer waste streams and reduction of polymer waste size, followed by extrusion (for example, Recycling into lower-value plastics).
3. Tertiary recycling is employed for polymers that are not amenable to conventional mechanical recycling techniques and often serves as a complement to traditional methods (for example Depolymerization of polyesters).
4. Quaternary recycling pertains to the process applied to plastics that are unsuitable for other recycling methods, facilitating energy recovery through pyrolysis.

Mechanical recycling of bioplastics poses significant challenges owing to pronounced thermo-hydrolytic degradation and consequent deterioration of rheological properties associated with repeated processing. Bioplastics are susceptible to thermo-oxidative and shear-induced chain scission, crosslinking, and chain branching. Consequently, the reprocessing of bioplastics requires the incorporation of a chain extender.

Numerous studies have investigated the effects of epoxy chain extenders on pristine PLA. Cosate de Andrade et al. examined the influence of Joncryl ADR 4400 on the properties of PLA by simulating the recycling process through two successive extrusion cycles using a single-screw extruder. The incorporation of the chain extender resulted in an increase in the molecular weight, a decrease in the melt flow index (MFI) and crystalline degree, and an overall recovery of the compound's properties [5]. Agüero et al. investigated the impact of six extrusion cycles on the mechanical and thermal properties of PLA, noting a reduction in the elongation at break and an increase in crystallinity [6]. Åkesson et al. investigated the impact of repeated processing on polylactic acid (PLA) composites reinforced with cellulose fiber. The study found that these composites exhibited a reduction in both the elongation at break and elastic modulus as the number of reprocessing cycles increased [7]. Zenkiewicz et al. observed a 20% reduction in impact strength, a reduction in the melting temperature and tensile strength, and an increase in the MFR [8]. Lendvai et al. evaluated the properties of PLA when subjected to multiple injection-molding cycles. The subsequent processing resulted in a significant increase in the MFR value, which rose from 4.9 g/10 min to 150 g/10 min after ten reprocessing cycles. The mechanical properties deteriorated after the fifth processing step [9].

As previously noted, the compounding of PLA and PBS is a prevalent approach for developing bio-based materials with enhanced mechanical properties. The recycling of bioplastics is critical in the context of thermoforming or injection molding processes, which generate substantial waste material. The next step in this research path was to study the recyclability of PLA/PBS compounds [10].

Table 1.23 PLA/PBS recycling study: definition of the formulations [10]

	Sample ID		PLA	PBS	Talc	Joncryl	First cycle material	Second cycle material	Other additives
First extrusion cycle	L(1)	wt%	67.32	15.53	12.43	0.17			4.56
	LS(1)	wt%	51.78	31.07	12.43	0.17			4.56
	S(1)	wt%	15.53	67.32	12.43	0.17			4.56
Second extrusion cycle	L(2)	wt%	37.02	8.54	6.84	0.09	45		2.52
	LS(2)	wt%	28.48	17.09	6.84	0.09	45		2.52
	S(2)	wt%	8.54	37.02	6.84	0.09	45		2.52
Third extrusion cycle	L(3)	wt%	37.02	8.54	6.84	0.09		45	2.52
	LS(3)	wt%	28.48	17.09	6.84	0.09		45	2.52
	S(3)	wt%	8.54	37.02	6.84	0.09		45	2.52
Third extrusion cycle + R	L + R(3)	wt%	36.99	8.54	6.83	0.14		45	2.52
	LS + R(3)	wt%	28.46	17.07	6.83	0.14		45	2.52
	S + R(3)	wt%	8.54	36.99	6.83	0.14		45	2.52

The PLA/PBS studied formulations are presented in Table 1.23. To simulate the aging of the polymeric material, the compounds were subjected to multiple extrusions for up to three cycles. The raw polymeric material was subjected to extrusion during the first extrusion cycle. Subsequently, for the second extrusion cycle, 45% of the material from the first cycle was blended with fresh raw polymeric materials. This resulting blend, comprising 45% previously extruded material and 55% new raw material, underwent extrusion once more. The objective of incorporating 45% of the material from the first cycle was to simulate the industrial practice of recovering post-process waste coming from thermoforming, which typically generates around 35% of waste material during the product manufacturing process. Furthermore, a third extrusion cycle was conducted, involving a mix of 45% material from the second cycle and 55% raw material, followed by another extrusion cycle. Notably, this study explored two distinct scenarios in the third extrusion cycle, with one scenario involving a higher quantity of chain extenders, as

shown in Figure 1.30, which summarizes the experimental campaign conducted in this study. Talc was used as a processing aid to improve the crystallization speed and processability of the resulting compound. The processing parameters adopted during the twin-screw extrusion of the compounds are presented in Table 1.24. To assess the processability of the produced samples, the pellets were dehumidified and used to produce cast-extruded sheets. The adopted processing parameters are listed in Table 1.25.

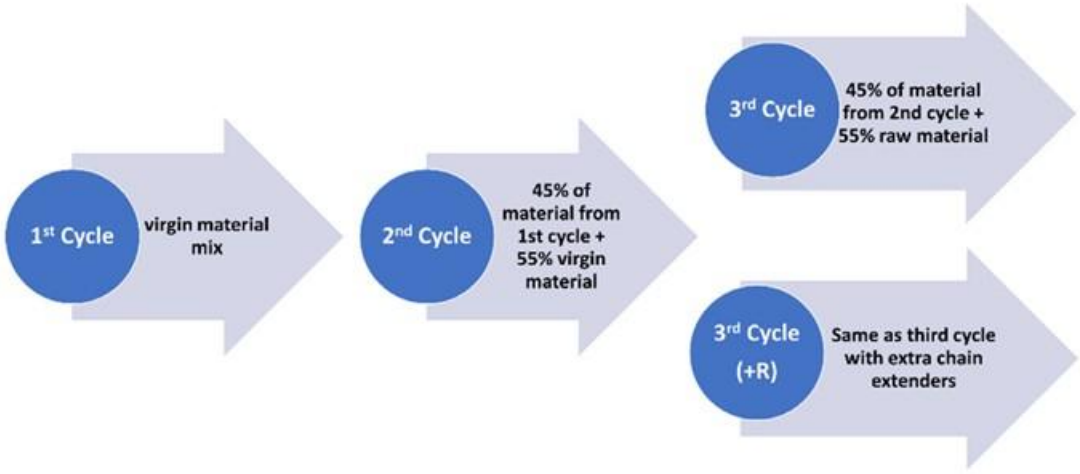

Figure 1.30 PLA/PBS recycling study: schemes of the extrusion process [10]

Table 1.24 Processing parameters adopted during twin screw extrusion [10]

Sample	T_1 (°C)	T_2 (°C)	T_3 (°C)	T_4 (°C)	T_5 (°C)	T_6 (°C)	T_7 (°C)	T_8 (°C)	T_9 (°C)	T_{head} (°C)
L	165	175	190	180	175	170	165	160	160	175
LS	160	170	185	175	170	165	160	155	145	165
S	150	160	177	170	160	148	137	130	125	145

Rheological analysis of the synthesized compounds revealed that an increase in the number of consecutive extrusion cycles promoted polymer degradation, ultimately leading to a reduction in viscosity. Notably, for the L and LS formulations, the melt flow rate (MFR) values exhibited a declining trend with each extrusion step. This observation can be attributed to the influence of the chain extenders on the melt viscosity of the polymers. Chain extenders possess the capability to reconnect the chains of degraded

polymers by forming a bridge between their functional groups and the degraded chain ends, thereby increasing the polymer's molecular weight and enhancing its properties. The FTIR analysis performed on the produced compounds showed that the introduction of the epoxy chain extender reduced the chain scission and thermo-oxidative degradation.

Table 1.25 Processing parameters adopted during cast extrusion [10]

Sample	T_1 (°C)	T_2 (°C)	T_3 (°C)	T_4 (°C)	T_5 (°C)
L	170	180	188	188	188
LS	180	188	190	190	190
S	177	185	185	187	185

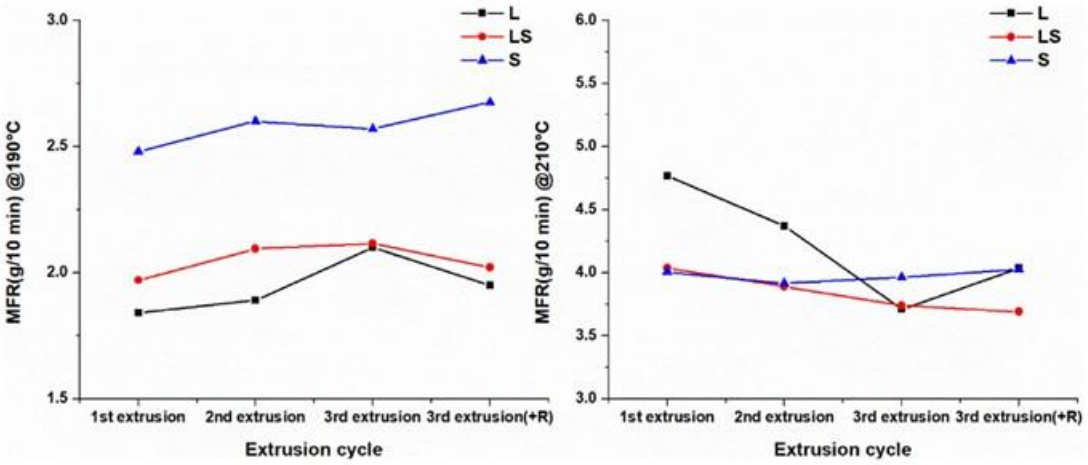

Figure 1.31 Results of the rheological characterization performed on the PLA/PBS aged compounds [10]

1.7 Multilayer thermoformed trays with high thermal stability

The subsequent research conducted by the team focused on developing solutions characterized by high thermal stability. Regarding the thermoforming process, the most promising solution involves the fabrication of multilayer sheets. These sheets consist of an inner core layer containing a high concentration of talc, flanked by two outer layers with a lower talc concentration designed for direct food contact. The presence of talc at high concentrations facilitates increased crystallinity within the layer, thereby enhancing

its thermal stability. Three distinct formulations were developed to produce three separate materials. Two alternative configurations of a tri-layer sheet were designed to identify the optimal solution that offers a structural inner core layer characterized by high impermeability and low material cost, alongside two identical outer surfaces exhibiting high flexibility. The three materials were compounded via twin screw extrusion, while the tri-layer sheets were fabricated through multilayer cast extrusion. Subsequently, the semifinished products underwent thermoforming to produce a prototype food tray composed of bio-based, biodegradable, and compostable polymeric materials. [11]

Table 1.26 First set of formulations studied for multilayer thermoformed trays [11]

Sample ID	**INN (Inner layer)**	**OUT_T1p (Outer layer Type 1)**	**OUT_T2p (Outer layer Type 2)**
Components	***wt.%***	***wt.%***	***wt.%***
PLA Luminy L175	48%	20%	0%
PBS A200 MF	12%	80%	80%
PLA Luminy D120	2%	0%	0%
Talc CHX05L	36,9%	0%	0%
EBS EVIWAX	1%	0%	0%
Joncryl ADR 4400	0,1%	0%	0%
PBAT KB100	0%	0%	20%

The initial material formulations are detailed in Table 1.26. The first formulation (INN) is intended to function as the core layer of the sheet, while OUT_T1p and OUT_T2p are designed to serve as the outer surface layers. During the cast extrusion process, the outer layer materials in both formulations exhibited processability issues, as the film surfaces were excessively adhesive on the calenders, resulting in delamination of the multilayer sheet.

Table 1.27 Optimized formulations studied for multilayer thermoformed trays [11]

Sample ID	**INN (Inner layer)**	**OUT_T1 (Outer layer Type 1)**	**OUT_T2 (Outer layer Type 2)**
Components	***wt.%***	***wt.%***	***wt.%***
PLA Luminy L175	48%	18%	0%
PBS A200 MF	12%	72%	72%
PLA Luminy D120	2%	0%	0%
Talc CHX05L	36,9%	10%	10%
EBS EVIWAX	1%	0%	0%
Joncryl ADR 4400	0,1%	0%	0%
PBAT KB100	0%	0%	18%

Consequently, OUT_T1p and OUT_T2p were reformulated by incorporating 10% talc into both formulations. It is often the case that a preliminary compound can reveal, during processing, the necessity for mineral fillers and rheological additives to enhance its processability. A mineral additive such as talc is cost-effective and can function as an anti-blocking agent, reducing moisture absorption and increasing scratch resistance. OUT_T1p and OUT_T2p were subsequently re-extruded with the optimized formulations presented inTable 1.27to produce the OUT_T1 and OUT_T2 surface materials. Table 1.28, Table 1.29, and Table 1.30 present the processing parameters employed during the twin screw extrusion of the defined compounds.

Table 1.28 Temperature profile and processing parameters for INN inner layer material extrusion [11]

Temperature profile [°C]									
T1	**T2**	**T3**	**T4**	**T5**	**T6**	**T7**	**T8**	**T9**	**Die**
170	172	175	177	180	180	180	175	175	173
Processing parameters									
Screws speed [rpm]	**Feeder speed [rpm]**	**Granules flow [%]**	**Powders flow [kg/h]**	**Melting temperature [°C]**	**Pressure [bar]**	**Torque [%]**	**Cutting speed [%]**		
250	256	15	8,77	182	62	30	80		

Table 1.29 Temperature profile and processing parameters for OUT_T1p [11]

Temperature profile [°C]									
T1	**T2**	**T3**	**T4**	**T5**	**T6**	**T7**	**T8**	**T9**	**Die**
150	152	153	155	160	160	160	160	155	153
Processing parameters									
Screws speed [rpm]	**Granules flow [%]**	**Pressure [bar]**	**Torque [%]**	**Cutting speed [%]**					
270	35	14,1	81	3,5					

Table 1.30 Temperature profile and processing parameters for OUT_T2p [11]

Temperature profile [°C]									
T1	**T2**	**T3**	**T4**	**T5**	**T6**	**T7**	**T8**	**T9**	**Die**
150	152	153	155	160	160	160	160	155	153
Processing parameters									
Screws speed [rpm]	**Granules flow [%]**	**Pressure [bar]**	**Torque [%]**	**Cutting speed [%]**					
270	50	9,4	78	3,5					

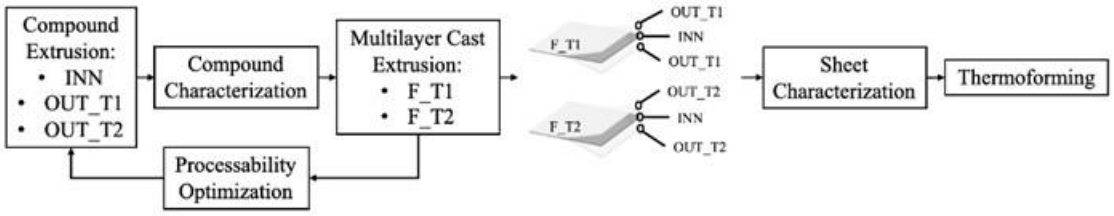

Figure 1.32 Process scheme [11]

Table 1.31 Temperature profile and processing parameters for cast extrusion of F_T1 and F_T2 [11]

			Temperature profile [°C]						
	Rotational speed [m/min]	**Screw speed [rpm]**	**Zone 1**	**Zone 2**	**Zone 3**	**Central back zone**	**Central front zone**	**Left lateral zone**	**Right lateral zone**
Drive	1,1								
Calender 1	0,6								
Calender 2	0,8								
Extruder A (outer layer)		71	140	145	145				
Extruder C (inner layer)		73	200	200	200				
Extruder B (outer layer)		71	140	145	145				
Die						150	165	155	155

The study entailed the fabrication of two multilayer sheets with distinct configurations (Figure 1.32). Type 1 film, designated as F_T1, comprises an inner layer of INN material flanked by two identical outer layers of OUT_T1p on both external sides. Conversely, Type 2 sheet, referred to as F_T2, features the same inner layer with two outer surfaces composed of OUT_T2p. The parameters for the cast extrusion process are consistent for both F_T1 and F_T2 (Table 1.31). The rotational speed of the screw for the inner layer was marginally higher than that selected for the extrusion of the outer layers of the sheet. This adjustment was made to reduce the thickness of the surfaces relative to the core layer. The temperature profile for the outer layers was set to slightly lower values compared to the corresponding twin screw extrusion profile, aiming to achieve a reduced flow of the melt with the already processed material. For the inner layer, it is crucial to attain the activation temperature between 190°C and 200°C for the chain extender Joncryl ADR 4400, followed by a reduction in temperature to decrease the melt flow through the die. The die temperature profile was determined by considering the distinct heat transfer

characteristics of the die's external surfaces. In each sheet configuration, the cast extrusion process revealed that the outer layers exhibited excessive stickiness on the calenders, preventing the completion of the process. Consequently, the design of the surface layers was modified to enhance processability in cast extrusion. To mitigate the adhesion phenomenon on the calenders, 10% talc was incorporated into the original design as a solid lubricant. The produced sheets where then thermoformed into trays using a lab-scale equipment (Figure 1.33).

Figure 1.33 Food trays thermoformed from F_T1 sheet (left) and F_T2 sheet (right) [11]

The produced granules, sheets and trays were characterized in order to evaluate the thermal, mechanical and rheological properties and the suitability to be used to produce multilayer food trays. The results of the mechanical characterization of the sheets are presented in Table 1.32. All the structures present a high elastic modulus, which is related to the presence of PLA within the formulation and to the presence of talc, which posses a higher stiffness compared to polymeric materials.

Table 1.32 Results of the mechanical characterization of the cast extruded sheets [11]

Sample ID	Max Stress [N/mm²]	Max Strain [%]	Young Module [N/mm²]	Yield Stress [N/mm²]
F_T1 MD	46,2 ± 2,7	13,3 ± 2,8	837,5 ± 235,4	42,2 ± 3,5
F_T2 MD	45,9 ± 2,5	35,4 ± 1,7	726,2 ± 116,9	15,2 ± 2,1
F_T1 TD	34,3 ± 1,5	4,3 ± 0,2	977,8 ± 120,5	15,7 ± 4,5
F_T2 TD	37,2 ± 1,7	20,9 ± 12,2	953,8 ± 374,7	27,1 ± 7,5

The differential scanning calorimetry (DSC) results are presented in Table 1.33. The DSC analysis of the inner layer revealed a glass transition at -32.8°C for the PBS phase and at 61.8°C for the PLA phase. An endothermic peak at 115.5°C is associated with the melting point of PBS, while another endothermic peak at 177.3°C corresponds to PLA. Additionally, two endothermic peaks were observed in the second heating curve for the INN material, detected at 148.2°C and 216.0°C, respectively. These peaks are attributable to the presence of more stable crystalline regions of PBS and PLA, which melt at elevated temperatures. These structures may be generated by the presence of talc, acting as a nucleating agent during the twin-screw extrusion process. For the PBS–PBAT blend, distinguishing the respective peaks is challenging due to their similar thermal characteristics.

Table 1.33 DSC analysis for INN, OUT_T1 and OUT_T2 [11]

Material	Component	wt%	T_g [°C]	T_m [°C]
INN	PLA	48%	61,8	177,3
	PBS	12%	-32,8	115,5
OUT_T1	PLA	20%	61,7	174,0
	PBS	80%	-33,8	116,5
OUT_T2	PBS	80%	-31,5	114,8
	PBAT	20%	-31,5	114,8

The mechanical, thermal, and rheological analyses confirmed that the designed materials exhibit properties comparable to those of traditional polymers and can be processed using established industrial technologies. Proper tuning and optimization of the manufacturing processes and material formulations were necessary to address processability issues of the new materials. The developed solutions, based on PLA, PBS, PBAT, and talc blends, enable a significant reduction in the overall environmental footprint of the products at the end of their life cycle, as all the materials used for the main polymeric phases of the compounds are biodegradable and compatible with composting processes, allowing for disposal alongside organic waste. With advancements in waste management infrastructure, this product has the potential to reduce the burden on landfills and contribute to the mitigation of environmental plastic pollution. A final thermal empirical test demonstrated that the prototypes of the final products were not prone to hot water

damage. Future developments of this research will focus on conducting a comprehensive life cycle assessment (LCA) of the final product to validate its overall environmental impact in more detail. Additionally, further studies may investigate the feasibility and cost-effectiveness of industrial-scale production.

1.8 Aim of the research

The food service industry has experienced a significant transformation in recent years, characterized by a substantial increase in the consumption of disposable plastic tableware, primarily driven by the rise in take-away and delivery orders.[12]. Food packaging waste constitutes approximately 30% of residential waste in the United States and significantly contributes to the expansion of landfills [13]. Polystyrene (PS) is one of the most widely utilized materials for disposable packaging and fast-food containers [14]. The adoption of compostable plastics has emerged as a viable strategy to mitigate landfill accumulation [15]. Bioplastics, an increasingly prominent category of polymers, present a compelling alternative to traditional petroleum-derived plastics [16].

Polylactic acid (PLA) is regarded as one of the most promising bioplastics currently available on the market. However, its commercial viability is constrained by its inadequate thermal stability, mechanical properties, and processability [17]. In contrast, Poly (3-hydroxybutyrate-co-3-hydroxyhexanoate) (PHBH) is a biobased, biodegradable, and biocompatible polyester that has not yet garnered significant attention. This is primarily due to its limited availability, challenging processability, and the stringent confidentiality maintained by manufacturers [18].

Epoxy chain extenders are frequently employed to enhance the interfacial compatibilization of bio-polyesters. The production process is pivotal in determining the efficacy of the chain extender. Soleymani Eil Bakhtiari et al. investigated the impact of an epoxy chain extender on PLA-PBAT blends produced through film extrusion, compression molding, and injection molding [19]. The most effective compatibilization was observed when the chain extender was pre-mixed with either PLA or PBAT using single-screw extrusion. However, reactive extrusion is more commonly conducted with twin-screw extruders [20]. The presence of mixing elements in twin-screw extruders

enhances the uniformity of melt composition through the synergistic effects of distributive and dispersive mixing [21]. Furthermore, the shear rate attainable in a twin-screw extruder surpasses that of a single-screw extruder [22]. Zhou et al. previously explored the potential for producing compatibilized PLA/PHBH blends using an epoxy chain extender. The addition of the chain extender enhanced the elongation at break and impact strength of the PHBH/PLA blends, facilitated a uniform distribution of the polymeric phases, and decreased the particle size of the dispersed phase [23].

The cost of bioplastics is generally higher than that of fossil-based polymers. For instance, the price of polylactic acid (PLA), one of the more affordable biopolymers, ranges from 2.3 to 2.9 $/kg, whereas the cost of poly(3-hydroxybutyrate-co-3-hydroxyhexanoate) (PHBH) can reach up to 6 €/kg. In contrast, most single-use trays are manufactured from polypropylene or polystyrene, with market prices ranging from 1 to 1.6 €/kg, which are significantly lower than those of bioplastics. This cost disparity remains a primary obstacle to the widespread industrial adoption of these polymers [24]. Over time, the optimization of production processes and the advancement of production technologies can result in a reduction in the cost of these materials, thereby potentially satisfying market demands [25]. A well-established strategy for reducing product costs involves the incorporation of mineral fillers into formulations. In addition to cost reduction, fillers are employed in the packaging industry to enhance processability [26] and to improve certain mechanical properties, such as stiffness and strength [27]. Furthermore, PHBH is characterized by a slow crystallization rate, necessitating the use of nucleating agents to enhance its processability. Talc is recognized for its exceptional nucleating properties in conventional polymers and can effectively increase the crystallization rate of various polyhydroxyalkanoates [28]. For potential industrialization and scale-up, minimizing thermal crystallization time is crucial for enhancing production efficiency [29]. The extrusion of polyhydroxyalkanoates necessitates meticulous control of processing parameters, as their degradation temperature is proximate to their melting point, rendering them vulnerable to chain scission [30]. PHBH exhibits a broader processing window compared to other polyhydroxyalkanoates (PHAs), due to the presence of 3HH units, which also reduce crystallinity and enhance flexibility [31]. However, the shear stress generated during twin-screw extrusion can further reduce the molecular weight of polyhydroxyalkanoates [32]. The introduction of mineral fillers at high concentrations

increases overall shear stress during extrusion. Post et al. reported a significant decrease in the molecular weight of PHBH when compounded with talc or calcium carbonate [24]. In this context, the use of a reactive epoxy chain extender may contribute to mitigating the degradation of bio-polyesters during extrusion [33], while also facilitating the compatibilization of different polymer phases. However, it is important to note that the use of a chain extender adversely affects the cycle time by reducing the crystallization rate [34].

Polybutylene adipate terephthalate (PBAT) is a bioplastic known for its high flexibility and strength; however, its relatively high cost and low elastic modulus limit its broad application as a cost-competitive commodity plastic [35]. Another limitation to the widespread use of PBAT is that it is mainly synthesized from fossil-based feedstocks [36], potentially limiting its environmental benefits. In recent years, advancements have been made in the production of polybutylene adipate terephthalate (PBAT) from bio-based feedstocks, reducing the environmental impact by up to 85% compared with fossil-based PBAT. As the leading global producer and exporter of PBAT, China is actively developing facilities to enhance the production of bio-based plastics and PBAT. The goal is to achieve an annual production capacity of 200,000 tons of bio-based butanediol, a primary precursor of PBAT, by 2026 [37], thus opening the market to cost-effective bio-based PBAT. Polybutylene succinate (PBS) is a thermoplastic aliphatic polyester synthesized from bioderived materials such as succinic acid and 1,4-butanediol [38]. Its mechanical properties are comparable to those of polyethylene; however, its processability poses several challenges related to its thermal stability, processing window, and the need for specific additives to enhance its stiffness, impact strength, and flexibility [38]. Both PBS and PBAT are promising alternatives to nonbiodegradable packaging materials, and their blends exhibit distinctive properties that can broaden their application potential. In PBS/PBAT blends, PBAT is often used as secondary phase to improve the mechanical properties of PBS due to the good compatibility between the two polymers [39–44]. PBAT/PBS blends, where PBAT is the main polymeric phase, have been explored in relation to antimicrobial properties using small amounts of Zinc Oxide [45], in combination with linear low-density polyethylene (LLDPE) for bread packaging [46], as food packaging with tunable mechanical and barrier properties [47], or with essential oils to enhance barrier properties [48]. As previously mentioned, the incorporation of

mineral fillers is a common strategy for reducing the cost of the final plastic product [49]. Compounding polymers and fillers can be complex, as fillers increase the shear stress within the extrusion cylinder, potentially leading to the degradation of the blend [50]. Talc is also used to improve the processability of compounds, as it increases the crystallization rates and decreases the production cycle time [51]. In the literature, blends of polylactic acid (PLA) and polybutylene succinate (PBS) containing 36% talc have been produced through extrusion to obtain thermoformed multilayer trays. These trays exhibit properties comparable to those of conventional polymers while offering a reduced environmental impact.[11]. Hassan et al. investigated the effect of 20%wt of talc on the properties of ternary blends of PLA, PBS, and PBAT to enhance the thermal performance and dimensional stability of 3D printed structures [52].

This study examines the synergistic effects of reactive epoxy chain extenders and mineral fillers on various bioplastic blends, with the objective of evaluating their potential for the cost-effective production of single-use trays through thermoforming. The blends were processed using twin-screw extrusion, followed by the production of cast films and subsequent thermoforming. The functional properties of the resulting products were then assessed. Two distinct sets of formulations were evaluated and produced: one based on PBAT/PBS, noted for its high flexibility and significantly reduced cost, and another based on PLA/PHBH, which is characterized by its reduced environmental impact and potential for marine biodegradability.

In the context of industrialization, the primary requirements for a PLA-PHBH blends include a cost not exceeding €0.03 per tray, comparable to that of polypropylene, a cycle time of less than 5 seconds, and a retention of more than 90% of PHBH molecular weight following processing at 150°C. Talc serves as an effective nucleating agent [28] and enhances thermal diffusivity [53], thereby reducing cooling durations and shortening the thermoforming cycle. The chain extender obstructs terminal acid groups and stabilizes PHBH [54], preserving molecular weight provided that the moisture content remains below 250–300 ppm and the residence time is kept under 3 minutes. Polypropylene (PP) costs €1.5/kg, and a typical tray weighs 20 g. To achieve the same cost per tray, the mass of the bioplastic blend must be less than 13 g, assuming a blend cost of ~€2.3/kg. A 30–35% weight reduction is technically achievable if the processability of the sheet is confirmed at low thicknesses, since 20% talc doubles the flexural modulus of the blend

compared to neat PLA [55]. For a PBAT-PBS blends, the requirements of cost are more easily met. The cost of PBS ranges between $2900/MT and $3100/MT whereas the cost of PBAT ranges between $1500/MT and $1800/MT. The introduction of 40% of talc in the formulation allows to obtain a bio-based blend with a cost of 1.60 €/kg. To obtain the same cost per tray, a 5 – 10% weight reduction per item is required, which is technically achievable when the compounds present good processability.

2 Materials

2.1 Bioplastics

Plastic is a polymer-based formulation composed of one or more polymers (homopolymers, copolymers, or blends) along with additives and fillers. Many polymers exist in nature, such as starch, cellulose, lignocellulose, and various proteins, which are often referred to as biopolymers or naturally occurring polymers. Bioplastics are formulations derived from biopolymers. The properties of a plastic material, whether fossil-based or bio-based, are determined by the specific combination of its constituent polymers and additives. [56]

The term "bioplastics" encompasses a diverse range of materials with varying properties and applications. European Bioplastics defines a "bioplastic" as a plastic material that is either bio-based, biodegradable, or features both properties. Biodegradability is not dependent on the feedstock but is linked to the chemical structure. Some fossil-based plastics can degrade under certain environmental conditions, and there are fully bio-based plastics that are not biodegradable. Figure 2.1 provides a classification of the most common plastic materials according to their biodegradability and bio-based origin. [57]

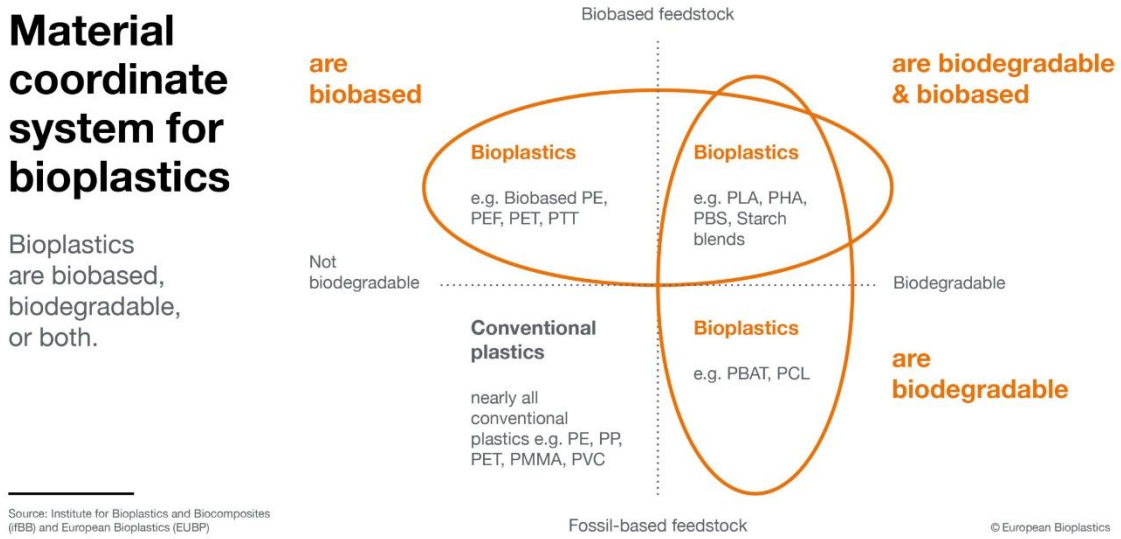

Figure 2.1 Classification of bioplastics [57]

The term bio-based indicates that a material is at least partially derived from biomass. A widely accepted method for determining the bio-based carbon content in materials and products is the 14C-method. This technique is formally recognized by several standards, including the EU standard EN 16640, the international standard ISO 16620-2, and the corresponding US standard ASTM 6866. Certification programs and associated product labels based on European and U.S. standards are available. These are provided by various certification organizations, such as the Belgian certifier TÜV Austria and the German certifier DIN CERTCO, which offer labels such as "OK biobased" and "DIN geprüft biobased" (Figure 2.2). [58]

Figure 2.2 "OK biobased" and "DIN geprüft biobased" labels

Biodegradability indicates that some microorganisms available in certain environments can convert materials into water, carbon dioxide, and biomass. The term biodegradability differs from compostability, which indicates the properties of being biodegradable under industrial or home composting conditions. European Bioplastics advises that, whenever feasible, emphasis should be placed on the specific claim of industrial compostability.

Figure 2.3 "OK industrial compost label" and "Seedling" labels

This claim should be substantiated by referring to relevant standards, such as EN 13432, EN 14995, ISO 18606, ISO 17088, or ASTM D6400. Additionally, the organization recommends supporting this with a formal certification and an appropriate label, such as the Seedling or OK industrial compost label, which is issued by certifiers such as TÜV Austria Belgium or DIN CERTCO (Figure 2.3). [58] However, bioplastics are not suitable for direct processing. All plastics present poor processability, as they are generally sticky, subjected to thermal and mechanical degradation, or present poor thermal and mechanical properties. Therefore, plastic compounds are generally produced to combine the good properties of different bioplastics via melt blending and, at the same time, enhance some properties via the use of specific processing aids and additives. Mineral fillers can also be included to improve the mechanical properties and reduce the cost of the overall formulation.

2.1.1 Poly (Lactic Acid) – PLA

Poly(lactic acid) (PLA) is a linear aliphatic thermoplastic polyester, and its chemical structure is presented in Figure 2.4. It is derived from renewable sources, such as corn starch and sugarcane, and is biodegradable under composting conditions. Microbial enzymes break down the polymer chains into lactic acid, which is then metabolized to carbon dioxide and water. The degradation rate strongly depends on temperature, moisture, and microbial activity [59]. PLA can be synthesized via ring-opening polymerization of cyclic lactide diester monomers or via direct condensation of Lactic Acid (LA) monomers [60]. Lactic Acid has an asymmetric atom in its molecule; therefore, LA can exist in two forms: L-LA and D-LA, as shown in Figure 2.5 [61].

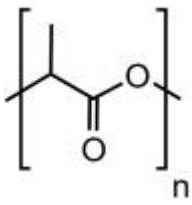

Figure 2.4 Poly(lactic acid) structure [60]

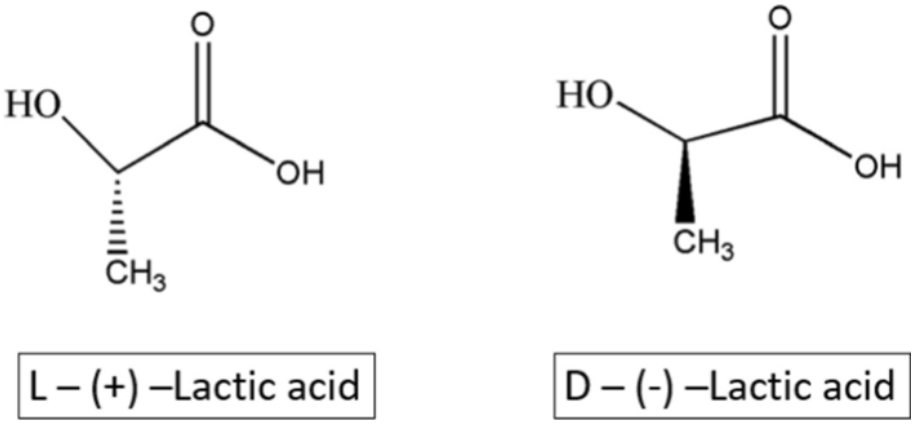

Figure 2.5 L-LA and D-LA molecular structure [61]

Poly(L-lactic acid) (PLLA), which is composed of L-LA units, is a transparent and rigid polymer that exhibits a tensile strength of 45–70 MPa. Its thermal properties include a melting point of 170–180 °C and glass transition temperature (T_g) of 53 °C. The thermal performance of PLLA can be improved by physically blending it with poly-D-lactide (PDLA). This method has been shown to increase the melting and heat deflection temperatures of PLLA by 40–50 °C and 60–190 °C, respectively. Conversely, PDLLA does not have a melting point because it is an amorphous polymer, but it possesses a T_g of approximately 55 °C, which contributes to its lower tensile strength. The recrystallization rate during cooling from the melting stage is a critical property of semicrystalline thermoplastics.

Table 2.1 General properties of PLA [62]

Property	**Value**	**Unit**
Density	1.210 – 1.250	kg/m^3
Price	2.4 - 3	USD/kg
Young's modulus	3.45 – 3.83	GPa
Yield Strength (elastic limit)	48 - 60	MPa
Tensile Strength	48 - 60	MPa
Compressive Strength	48 – 60	MPa
Elongation	5 - 7	%
Fracture toughness	0.7 – 1.1	MPa $m^{1/2}$
Melting point	160 – 177	°C
Glass transition temperature	56 – 58	°C

While pure poly(L-lactic acid) (PLLA) exhibits spontaneous crystallization, the rate of crystallization decreases as the D-lactic acid (D-LA) content increases. This leads to the formation of a quasi-amorphous phase in less refined PLLA, which has inferior mechanical properties. Consequently, the manufacture of commercial poly(lactic acid) (PLA) relies on polymer-grade L-lactic acid, which typically contains over 98–99% L-LA and a D-LA content of less than 1–2%. [61] The general properties of PLA are listed in Table 2.1. The PLA production industry has come a long way since its inception, and nowadays, there are mainly two big PLA producers that dominate the market. Different grades are produced, each with distinct properties and processability. The first company is NatureWorks LLC. NatureWorks is a global company specializing in biopolymer production and innovation. The Ingeo line of materials is composed of advanced substances manufactured from sustainable and available feedstocks. These materials are notable for their superior performance and cost-effectiveness compared to traditional oil-based intermediates, plastics, and fibers. The use of these products provides brand owners with novel alternatives to traditional methods. NatureWorks is one of the earliest and most prominent producers of polylactic acid (PLA) [63]. NatureWorks commercializes different series of polylactic acids, depending on the final destination and the requirements of the processing technology (Figure 2.6). In particular, 2 Series is designed for Extrusion and Thermoforming, presenting a high molecular weight and 3 Series is designed for Injection Molding, consisting of polymers with low viscosity. [64]

The second largest PLA producer is Total Corbion. Total Corbion is a recognized global leader in the production of polylactic acid (PLA), with market leadership extending to both manufacturing and marketing and sales of the polymer. The Luminy® PLA collection is considered an advanced material, featuring a range of high-heat and normal grades. This material is employed in a diverse array of applications, including fresh food packaging, household products, fabrics, food service ware, and 3D printing. [63] The Luminy product range is shown in Figure 2.7. High-heat PLA grades are used for demanding applications, whereas standard PLA is used for general-purpose applications. Low heat is often used as a seal layer, whereas PDLA grades are used either as nucleating agents or to create full stereocomplex compounds [65].

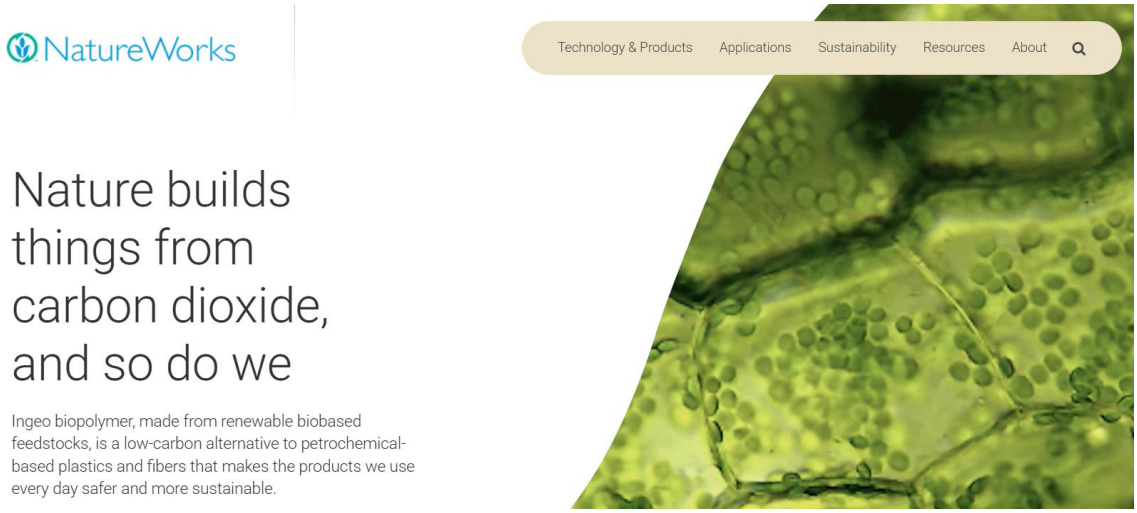

Figure 2.6 Natureworks Ingeo products [64]

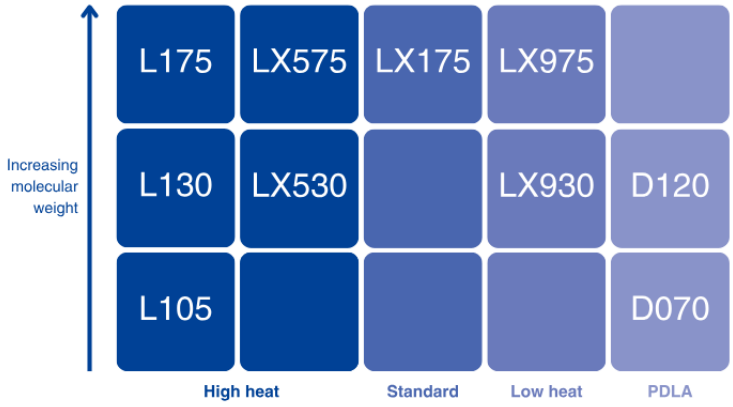

Figure 2.7 Total Corbion Luminy products [65]

2.1.2 Poly (Butylene Succinate) – PBS

Poly (Butylene Succinate) (PBS) is a thermoplastic biopolyester synthesized via the polycondensation of succinic acid (SA) and 1,4-butanediol (BDO), which can be derived from either fossil-based or renewable feedstocks. The chemical structure is visible in Figure 2.8.

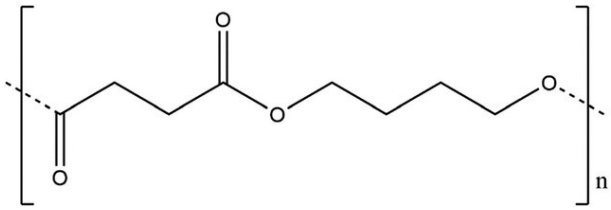

Figure 2.8 Chemical structure of PBS [66]

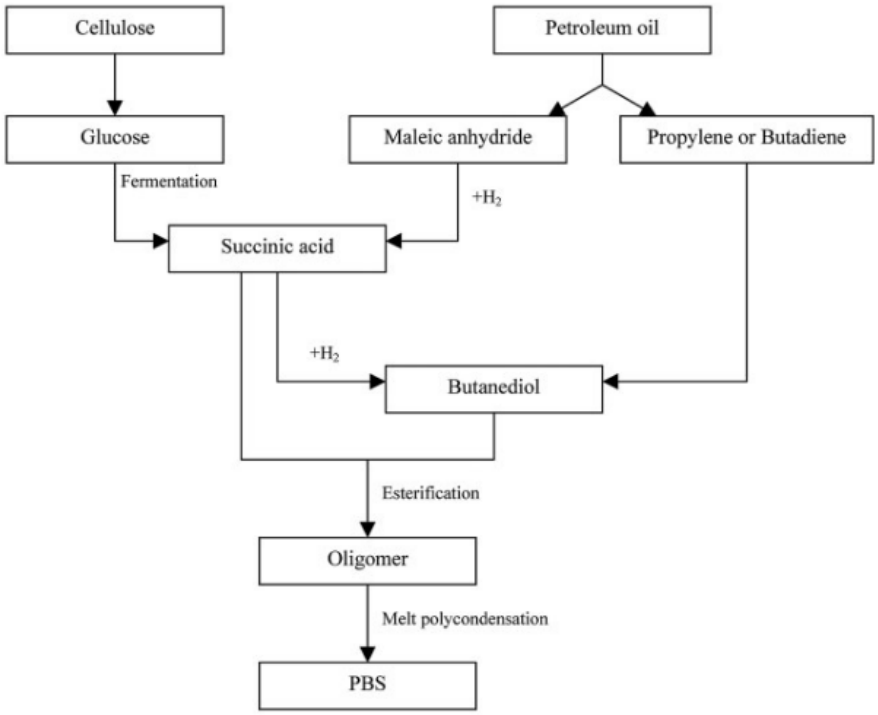

Figure 2.9 Production process of PBS [67]

A schematic of the PBS production process is presented in Figure 2.9. Currently, succinic acid is produced commercially through a chemical process that involves hydrogenating maleic anhydride to create succinic anhydride, which is then hydrated to yield succinic acid. This maleic anhydride is obtained from the oxidation of either butane or benzene. An alternative method for producing succinic acid is through the fermentation of renewable feedstocks, such as glucose, starch, or xylose, by microorganisms. Traditional commercial methods for synthesizing butanediol (BDO) rely on petrochemical sources. An alternative biobased process for BDO production allows to synthesize it form corn has recently been announced. Polybutylene succinate (PBS) synthesis is a two-step

process. First, an oligomer is created through either the esterification of succinic acid and BDO or the transesterification of dimethyl succinate and BDO. Subsequently, the oligomers undergo polycondensation to remove BDO, resulting in high-molecular-weight PBS [67].

Table 2.2 General properties of PBS [68]

Property	Value	Unit
Density	1.230 – 1.260	kg/m^3
Young's modulus	300 – 700	MPa
Tensile Strength	20 – 34	MPa
Glass Transition Temperature	-45 - -30	°C
Glass transition temperature	109 - 115	°C

PBS exhibits excellent mechanical properties, which are similar to or even better than those of polyethylene (PE) and polypropylene (PP). The thermal properties of PBS depend on its molecular weight (Mw). In general, the glass transition temperature of PBS ranges between -40 °C and -10 °C, and the melting point ranges between 90 °C and 120 °C [69]. An overview of the general properties of PBS is provided in Table 2.2. A few large producers currently dominate the PBS production market. The first company is PTT MCC Biochem Co., Ltd., which commercializes a bio-based PBS under the commercial name BioPBS. The two main grades are BioPBS FZ91/PB and BioPBS FZ71/PB, which are low and high flow, respectively. The former is suitable for compounding and extrusion technologies, whereas the latter is suggested for injection molding. BioPBS is soft and flexible, and exhibits good dimensional stability and flowability. It is food contact safe, being listed in U.S.FCN, JCII and complying with EU10/2011 and China GB. In the European Union, it is certified as K compost INDUSTRIAL by TÜV Austria. Its renewable content is certified by DIN CERTCO, JBPA, and USDA. Xinjiang Blue Ridge Tunhe Sci. &Tech. Co., Ltd. is a Chinese company and a global leader in PBS production. The company produces a wide range of polyesters, mainly from fossil-based sources. The commercial name of the PBS is TH803S, which is commercialized in both an HMFR version, characterized by a high melt flow rate and therefore suitable for injection molding, and an LMFR version, suitable for extrusion and with a higher viscosity.

Figure 2.10 BioPBS commercialized by PTT MCC Biochem Co., Ltd. [70]

Typical Property	Unit	4-8	Test Method
Density	g/ cm³	1.27	ISO 1183
MFR (190℃,2160g)	g/10min	5-8	ISO 1133
Carboxyl End Groups	Mol/mt	15-20	GB/T14190
Moisture	%	≤0.05	GB/T14190
Melt Point	℃	114	ISO 11357
Hundred-grain Weight	g/100 grain	1.6	/
Shore Hardness	D/15	70	ISO868
Tensile Strength	MPa	41	ISO527
Elongation	%	280	ISO527
HDT B/Tff0.45	℃	90	ISO75-1:2013&ISO75-2:2
Flexural Strength	MPa	35	ISO178:2010/Amd.1:2013
Flexural Modulus	MPa	610	ISO178:2010/Amd.1:2013
Izod Impact Strengt	KJ/㎡	6	ISO180:2000/Amd.2:2013

Figure 2.11 Properties of PBS TH803S [71]

Kingfa Sci & Tech Co., Ltd. is a Chinese company that has been active in the bio-polyester market since 2004. PBS is commercialized under the name ECOPOND® Compostable Polyesters A200 in three grades, each characterized by a different viscosity. The typical mechanical and thermal properties are shown in Figure 2.12. The MFR at 190 °C and 2.16 kg can vary from 4 g/10' to over 30 g/10', depending on grade. All grades have a biobased content of 48%, and their commercialization has recently begun in the European Union.

Properties		Test Method	Test Condition	S.I. Units	Typical Values
Mechanical Property	Tensile Strength	ISO 527-2	50 mm/min	MPa	37
	Elongation	ISO 527-2	50 mm/min	%	62
	Flexural Strength	ISO 178	2 mm/min	MPa	29
	Flexural Modulus	ISO 178	2 mm/min	MPa	600
	Impact Strength, IZOD	ISO 180	4 mm，23 ℃	KJ/m^2	6.6
Thermal Property	Melting Point	DSC	10 ℃/min	℃	112-116
	HDT	ASTM D648	0.45 MPa	℃	93
Others	Melt Mass-Flow Rate	ISO 1133	190 ℃, 2.16 kg	g/10min	18.0
	Moisture Content	ISO 15512	Method C	ppm	240
	Specific Gravity	ISO 1183	23 ℃	g/cm^3	1.26

Figure 2.12 Typical properties of PBS KingFa A200 series

2.1.3 Poly (Butylene Adipate – co – Terephthalate) – PBAT

Poly (Butylene Adipate-co-Terephthalate) (PBAT) is one of the most extensively utilized bioplastics. In 2021, it accounted for 19.2% of the total bioplastic production, with an annual output exceeding 460 thousand tons [72]. PBAT is synthesized through the polycondensation of adipic acid, 1,4-butanediol, and terephthalic acid. The synthesis process encompasses esterification, condensation, and melt polymerization, as illustrated in Figure 2.13. The synthesis of PBAT is contingent upon the reaction conditions. The molecular weight of PBAT can be modulated by adjusting the esterification temperature, the ratio of reactants, and the reaction duration [73]. PBAT exhibits exceptional processability due to its low viscosity, rendering it suitable for film production through cast extrusion or blown extrusion techniques. However, its high stickiness necessitates

the use of anti-block processing aids. Table 2.3 presents the typical properties of commercial grades of PBAT. PBAT is distinguished by its high ductility and low elastic modulus, exhibiting characteristics similar to those of low-density polyethylene (LDPE) [74].

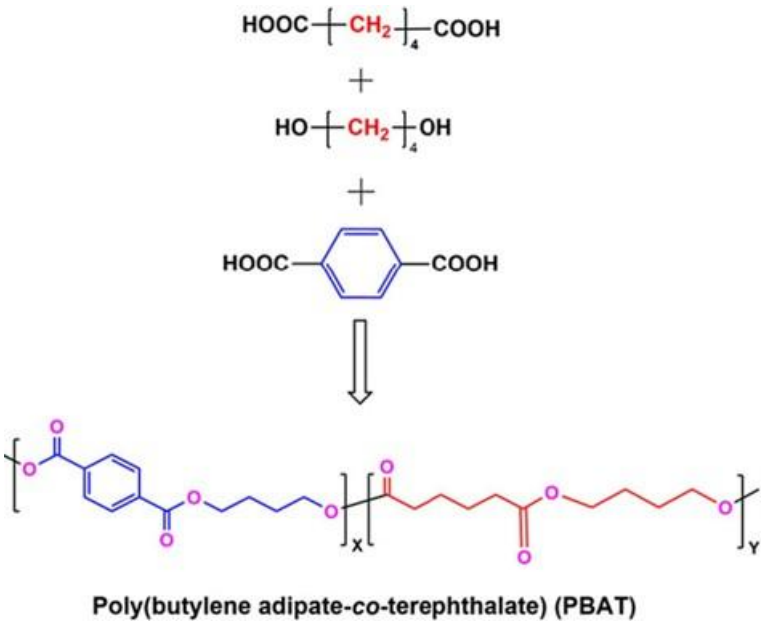

Figure 2.13 Synthesis of PBAT [73]

Table 2.3 Properties of PBAT (Adapted from [72])

PBAT tradename	Melting temperature (°C)	Glass transition temperature (°C)	Elongation at break (%)	Elastic Modulus (MPa)	Tensile Strength (MPa)	Ref.
Ecoflex FBX 7011			600	117.3	14.2	[75]
ECOPOND	115-125		670		21	[76]
	110-115	-30	>500	52	9	[77]
SolPol-1000	130.4		330	52	15.5	[78]
Produced by Xinfu Pharmaceutical Co., Ltd.	114	-34.1	927	38.9	11	[79]
Produced by Xinjiang Blue Ridge Tunhe Polyester Co			1252	122.3	49.9	[80]

Table 2.4 Major commercially available PBAT grades [76]

Company	Country	Brand name	Capacity (t/y)
BASF	Germany	ECOFLEX®	60,000
KINGFA	China	ECOPOND®	50,000
NOVAMONT	Italy	Origo-Bi®	40,000
TUNHE	China	–	30,000
XINFU	China	–	20,000
JINHUI	China	ECOWORD®	20,000

The principal PBAT grades available in the market are detailed in Table 2.4. PBAT is typically synthesized from fossil-based resources. As the foremost global producer and exporter of PBAT, China is currently advancing facilities to augment the production of bio-based plastics and PBAT. The objective is to attain an annual production capacity of 200,000 tons of bio-based butanediol, a primary precursor of PBAT, by 2026 [37], thereby expanding the market for cost-effective bio-based PBAT. Moreover, the current price of PBAT is approximately 1.7 €/kg, rendering it a cost-effective bioplastic alternative from an economic perspective as well.

2.1.4 Polyhydroxyalkanoates – PHAs

Polyhydroxyalkanoates (PHAs) are biogenic polyesters synthesized by a diverse range of bacterial species. Since their discovery in the 1980s, PHAs have garnered significant attention as potential alternatives to fossil-based plastics. These polyesters are naturally produced by at least 75 different bacterial genera, encompassing both gram-positive and gram-negative bacteria, as a means of energy storage. Bacteria capable of PHA production can be categorized into two primary groups based on the environmental conditions necessary for PHA synthesis. Certain bacteria synthesize PHAs in response to nutrient stress, particularly when there is a limitation of essential nutrients such as nitrogen, phosphorus, magnesium, or sulfur, coupled with an excess of carbon sources. Once the carbon source is depleted, these polymers are subsequently degraded and utilized as a source of energy and carbon. On the other hand, the second type of bacteria tend to accumulate PHA during their growth, without requiring any nutrient limitation. The constituent molecular blocks are hydroxyalkanoate (HA) units (Figure 2.14)

connected together by ester bonds. The HA units are all in the D(-) configuration because of the stereospecificity of the biosynthetic enzymes. The molecular mass of the produced polymers is in the range of 50.000 – 1.000.000 Da and is comparable to the one of classic fossil-based plastics. [81–84]

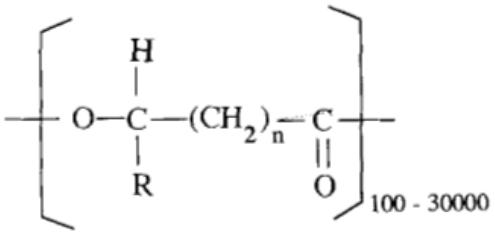

Polymer		
n = 1	R = hydrogen	Poly(3-hydroxypropionate)
	R = methyl	Poly(3-hydroxybutyrate)
	R = ethyl	Poly(3-hydroxyvalerate)
	R = propyl	Poly(3-hydroxyhexanoate)
	R = pentyl	Poly(3-hydroxyoctanoate)
	R = nonyl	Poly(3-hydroxydodecanoate)
n = 2	R = hydrogen	Poly(4-hydroxybutyrate)
n = 3	R = hydrogen	Poly(5-hydroxyvalerate)

Figure 2.14 General structure of Polyhydroxyalkanoates [82]

Up to now, more than 150 different types of polyhydroxyalkanoates, intended as unique monomer units, have been discovered. A primary classification of PHAs can be made depending on the dimensions of the constituent monomers (Figure 2.15): short-chain length PHAs (SCL) present three to five carbon atoms; medium-chain length PHAs (MCL) present more than five carbon atoms. PHAs can be classified also according to their structure (Figure 2.15), in Homopolymers PHA and Copolymers PHA. The strategy of copolymerization is widely applied in order to improve the mechanical properties and the processability of these bioplastics. The most evident example is represented by the co-polymerization of PHB and the wide range of commercial products that derived from it (PHBH, PHBV, P3HB4HB, …). The PHA molecular composition and structure can be tailored using different strategies. Chemical modifications, such as the introduction of C-

C double bonds, can be obtained by genetically modifying the bacterial strain that produces the PHA. By feeding different substrates to producing bacterial strains, it is also possible to tailor the properties of the final polymer. For example, by using mixed substrates it is possible to obtain PHA copolymers. Block copolymers can be synthesized by means of periodical substrate addition. Genetical modifications can be also induced in the producing bacterial strains in order to improve the production capacity. [83, 85–87]

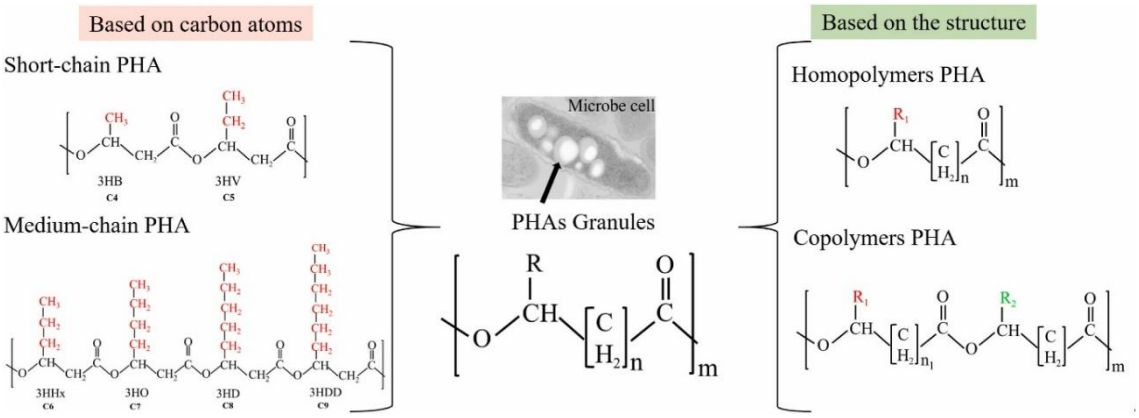

Figure 2.15 Classification of PHAs based on number of carbon atoms of the monomeric units and based on their structure [87]

Another appealing property of this family of bioplastics is its high biodegradation rate and its ability to biodegrade also in marine environment. Since PHAs are naturally produced by bacteria, there exist in nature specific enzymes able to biodegrade them. The principal enzyme for the degradation of PHB is PHB depolymerase. In the degradation process, the PHA chains are broken down into their molecular building blocks, the hydroxyacids (HA), that can be used as a carbon source for growth. The biodegradation of PHAs leads to non-toxic and natural products: in anaerobic conditions, carbon dioxide and methane are produced; under aerobic conditions, the resulting products are carbon dioxide and water. Most of biodegradable bioplastics, such as Polylactic acid (PLA), Polybutylene succinate (PBS) and Polybutylene adipate co – terephthalate (PBAT), are chemically synthesised polymers. Therefore, even if these bioplastics are both bio-based and biodegradable, they are susceptible to enzymic and microbial attack but do not present any specific enzyme able to completely biodegrade them. [84, 88, 89].

Poly-3-hydroxybutyrate (PHB) is by far the most studied component of the PHA family, being also the first one to be identified and characterized. On an industrial level, it is produced by fermentation of a various number of bacteria, such as *Ralstonia eutropha*, *Alicaligenes spp*., *Azotobacter spp*., *Bacillus spp*. *Nocardia spp*., *Pseudomonas spp*. and *Rhizobium spp*.. PHB presents very high crystallinity levels (up to 95%) because it is produced in only one optical form and in linear chains (Figure 2.16). However, the crystallinity percentage may depend upon the origin of the polymer. Its mechanical properties (Table 2.5) are similar to the ones of polyethylene terephthalate (PET). It presents a glass transition temperature of around 10°C and a melting temperature of around 165 – 180°C. [90–92]. During melt crystallization, PHB forms α crystals, an orthorhombic crystal system consisting of left-hand 2_1 helix structures. The unit cell parameters are a = 0.576 nm, b = 1.320 nm and c (fibre axis) = 0.596 nm [93].

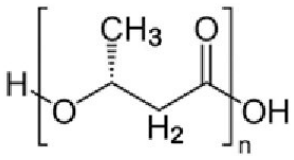

Figure 2.16 Chemical Structure of PHB [94]

Table 2.5 Properties of PHB

	PHB [95]
Tensile strength (MPa)	40
Young modulus (MPa)	3500
Strain at break (%)	5
Glass transition temperature (°C)	4
Melting temperature (°C)	180

Poly(3-hydroxybutyrate-co-3-hydroxyhexanoate) (PHBH) is constituted of medium and long chains of 3-hydroxyhexanate (3HHx) units and short chains of 3-hydroxybutyrate (3HB) units (Figure 2.17). The production of this polymer was aimed by the need of increasing the flexibility of PHB. 3-hydroxybutyrate (3HB) units are extremely brittle and tend to form different types of crystals. On the other hand 3-hydroxyhexanate (3HHx)

units have an elastomeric behaviour and act as plasticizers of P(3HB) units, also decreasing the glass transition temperature of the resulting polymer [18, 96]. Therefore, depending on the percentage of HHx chains, the mechanical properties of the polymer may vary from brittle to ductile. In Table 2.6 a summary of the properties of melt – processed PHBH is presented. It is evident how the polymer grade and, therefore, the percentage of 3HH has an influence on the polymer behaviour. With respect to pure PHB, 3HH units have a beneficial effect also on the processability. 3HH chains broaden the melting peak, thus increasing the processing window and allowing a better control on thermal degradation [18]. 3HH units also induce changes in the crystallization kinetics of the polymer. It is widely assessed in literature that only P(3HB) region participate to the crystalline lattice. 3HH units act as impurities in PHBH, preventing self-diffusion of 3HB units and, therefore, inhibiting nucleation and crystal growth [96]. Therefore, P3HB and PHBH present the same peaks in the wide-angle X-ray diffraction (WAXD) pattern, but PHBH peaks have a lower intensity. This result confirms that 3HH units do not alter P(3HB) crystalline structure but merely reduce the overall crystallinity of the material [93].

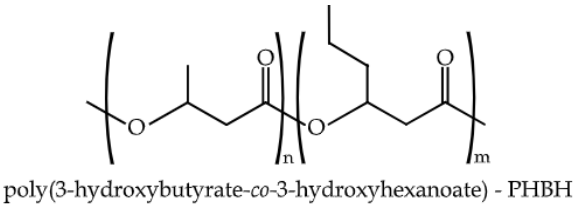

poly(3-hydroxybutyrate-*co*-3-hydroxyhexanoate) - PHBH

Figure 2.17 Chemical structure of PHBH [97]

Table 2.6 Properties of melt processed PHBH.

	PHBH (MAIP Group) [98]	**PHBH (Kaneka X151A)** [99]
Tensile strength (MPa)	23.1	
Young modulus (MPa)	1715	1000 – 1500
Strain at break (%)	3.7	400 - 600
Glass transition temperature (°C)	5.9	4.5
Melting temperature (°C)	141.2	119.4
Degree of crystallinity (%)	30.0	51.2

The polymer properties, such as the heat resistance, the mechanical properties and the crystallization rate, are strongly affected by the percentage of 3HHx units. PHBH is compostable at room temperature. However its high sensitivity to heat treatments, its difficult processability and insufficient barrier properties make the direct replacement of fossil-based plastics hard. [18, 100–102]

2.2 Chain Extenders

The rheological properties of polymer compounds can be adjusted via reactive melt modification using appropriate chemical agents called chain extenders (CE). The most popular is a multifunctional styrene-acrylic oligomeric chain extender commercialized under the trade name Joncryl® ADR, which is used to improve the processability and properties of recycled polymers. Joncryl® ADR comprises multifunctional molecules (functional groups fn > 4) with a molecular weight lower than 3000. The chemical structure of the Joncryl ADR chain extender is presented in Figure 2.18. Epoxy functional groups can react efficiently with hydroxyl and preferably with carbonyl groups of polymers [103], leading to chain extension or branching reactions [104]. Joncryl ADR 4400 and Joncryl ADR 4468 are the most purchased grades, whose main properties are listed in Table 2.7. The correct amount of chain extender is of utmost importance because it can initiate a reticulation reaction that radically changes the properties and processability of the compound. The weight average functionality Efw is the parameter used to determine the proper amount. The definition of Efw is presented in Equation 2.1 [104].

$$Efw = Weight\ average\ functionality = \frac{M_w Joncryl}{Epoxy\ Equivalent} \qquad 2.1$$

The extrusion process can lead to the degradation of polycondensates via hydrolysis, alcoholysis, and thermal cleavage owing to the high processing temperature or shear forces. This process causes a loss of molecular weight and, consequently, a reduction in viscosity and mechanical performance. The reactive parts of Joncryl can react with the functional groups of the polymers, reducing degradation. A schematic illustration of the

reaction of an epoxy chain extender with a degraded polymer is presented in Figure 2.19. [104]

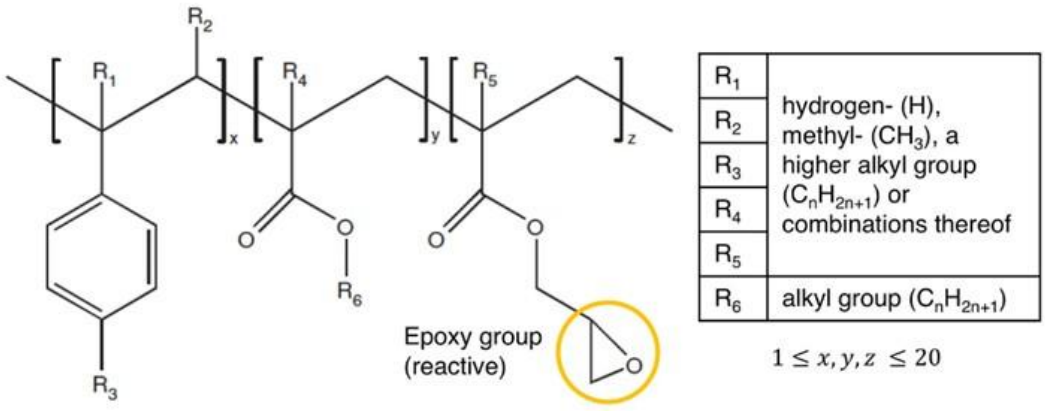

Figure 2.18 Chemical structure of a generic Joncryl ADR chain extender [104]

Table 2.7 Typical properties of Joncryl ADR chain extender [104]

Name	Molecular weight	Glass transition temperature (°C)	Epoxy equivalent weight (g/mol)	Equivalent functionality
Joncryl ADR 4468	7250	59	310	~ 24
Joncryl ADR 4400	7100	65	485	~ 14

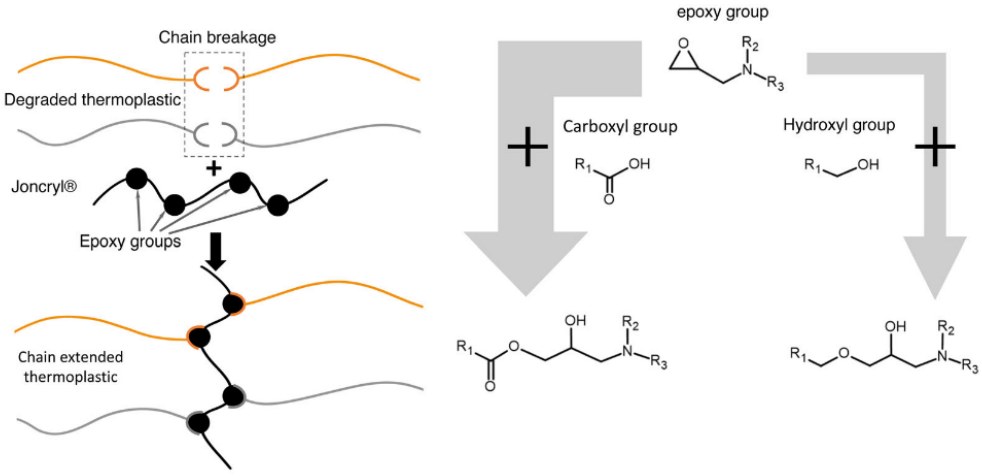

Figure 2.19 Schematic mechanism of the reaction of an epoxy chain extender with a degraded polymer [104]

2.3 Antioxidants

Stability and resistance to thermal and oxidative degradation are fundamental requirements for polymer processing. Exposure to heat, oxygen, and catalyst residues can lead to material degradation, compromising the properties of the material. The incorporation of antioxidants (AO) is a powerful solution to overcome this issue. [105]

Phenolic compounds constitute a category of substances frequently employed as antioxidants. They operate by donating phenolic hydrogen to generate a resonance-stabilized free radical that reacts with other free radicals. Antioxidant activity is influenced by the chemical structure and position of the -OH groups. The chemical structures of some commonly used antioxidants are shown in Figure 2.20 [106]. Sterically hindered phenols are called “Primary Oxidants” because they act as radical scavengers by reacting quickly with free radicals.

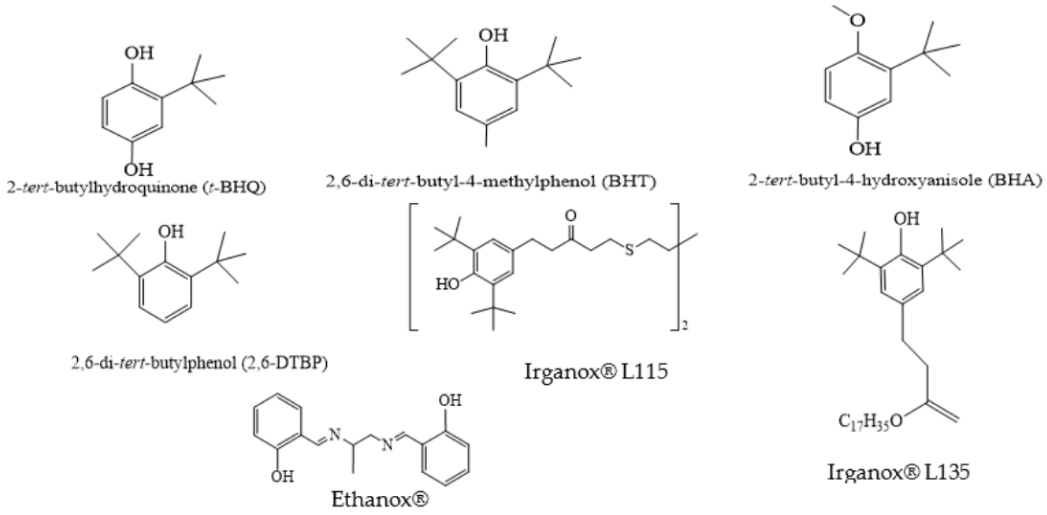

Figure 2.20 Structure of commercial primary antioxidants [106]

Esters of phosphorous and phosphonic acids are a class of materials used on a large scale as antioxidants to stabilize organic materials against degradation during the production process. Phosphites and thioesters are secondary antioxidants. They react with

hydroperoxides to obtain non-radical products, and are particularly effective in combination with primary antioxidants. [107, 108]

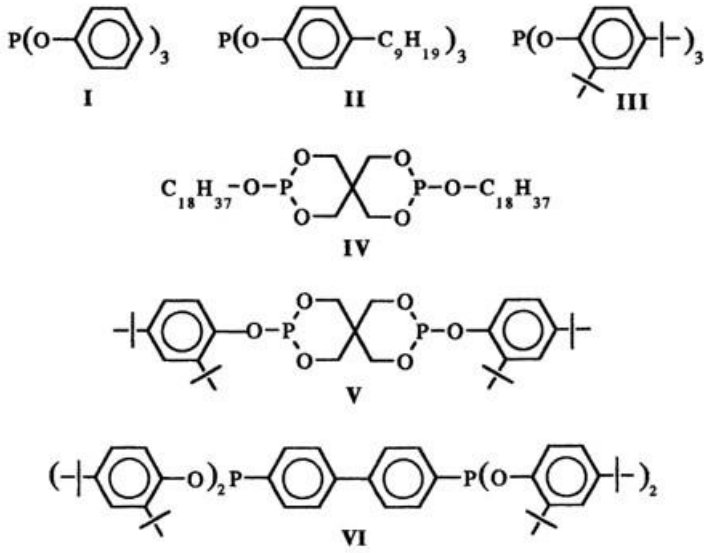

Figure 2.21 Structure of commercially available secondary antioxidants [109]

The reaction mechanism of antioxidants is as follows [110]:

1. The combined effect of heat and mechanical stress removes a hydrogen atom from the polymeric chains (RH) and forms a free alkyl radical (R•).
2. Oxygen combines with free radicals and creates new reactive species, mainly peroxides and hydroperoxides (O_2 + R• → ROO• + RH → ROOH + R•) and other minor species (H_2O, H_2, H_2O_2).
3. Hydydroperoxides are also reactive and create new reactive species, such as hydroxyl radicals or alkali radicals (ROOH → OH + RO•).

The process can end without the intervention of antioxidants over time, but it is a slow process. Reaction propagation can lead to chain scission and a reduction in the molecular weight and viscosity of the polymer. This also leads to a loss of color and mechanical properties. Therefore, the use of antioxidants is of utmost importance in polymeric compounds. [110]

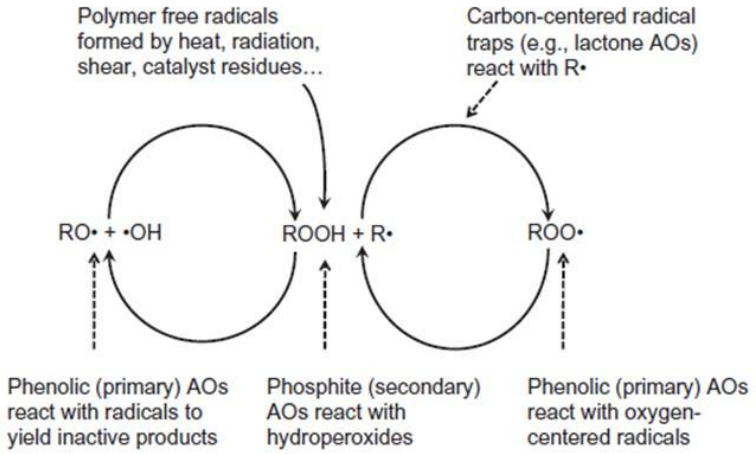

Figure 2.22 Auto-oxidation reaction of a polymeric compounds and effect of primary/secondary antioxidants [110]

ADEKA Amazing Chemicals | Polymer Additives | TECHNICAL INFORMATION

June 1, 2009

ADK STAB A-611
ADK STAB A-611RG

— Antioxidant blend system—

Identification

This product is a mixture of phenolic antioxidant and phosphite as following.

Trade name	COMPONENT	%	CAS No.
ADK STAB AO-60	Benzenepropanoic acid, 3,5-bis(1,1-dimethylethyl)-4-hydroxy-, 2,2-bis[[3-[3,5-bis(1,1-dimethylethyl)-4-hydroxyphenyl]-1-oxopropoxy]methyl]-1,3-propanediyl ester	50	6683-19-8
ADK STAB 2112	Phenol, 2,4-bis(1,1-dimethylethyl)-, phosphite (3:1)	50	31570-04-4

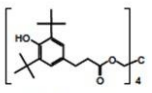

ADK STAB AO-60

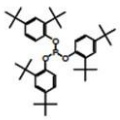

ADK STAB 2112

Features

- ADK STAB AO-60 is the most common hindered phenolic antioxidant which shows very low volatility and excellent retention within the polymer due to high molecular weight.
- ADK STAB 2112 is a very common phosphite which exhibits the most excellent hydrolytic stability among commercial phosphites and shows low volatility and excellent retention within the polymer.
- Highly protects polymers against thermal degradation during/after processing and provides long-term heat stabilization for the life time of the article due to the synergistic effect of ADK STAB AO-60 and ADK STAB 2112.
- Approved as an indirect additive in food contact substances in US, EU, and Japan. Potential application is food packaging. (For additional information such as kind of adaptable polymers, please ask our Sales Department.)

Figure 2.23 Technical data sheet of ADK STAB A611

Primary antioxidants stabilize free radicals by donating hydrogen atoms, effectively neutralizing unpaired electrons, and restoring molecular stability. Although the antioxidant loses a hydrogen ion, it remains more stable than other radical species and does not propagate degradation. Secondary antioxidants decompose relatively unstable hydroperoxides via oxidation. These often function synergistically with primary antioxidants, as their combined action provides superior protective effects on the polymer matrix. The antioxidant selected for this initial experimental campaign was ADK STAB A611, whose technical data sheet is shown in Figure 2.23. This formulation comprises a blend of AO-1 (CAS 6683-19-8), a phenolic primary antioxidant with a molecular weight of 1178 g/mol and a melting point between 110 and 125°C, and P-1 (CAS 31570-04-4), a phosphitic secondary antioxidant with a molecular weight of 646 g/mol and a melting point ranging from 181–187°C.

2.4 Mineral Filler

Fillers are widely employed as additives in plastics, constituting the most crucial components for enhancing the physical properties of the compound. In general, they are largely inert foreign constituents integrated into the polymer matrix. Inorganic fillers are commonly used to reduce the cost of plastic products by effectively increasing the volume of the blend [111]. Talc, calcium carbonate and silica are among the most widely used ones [112].

Talc is a widely utilized mineral filler, possessing a bulk density of 0.75 g/cm^3 [111], which is significantly lower than that of bioplastics, typically ranging from 1.1 to 1.2 g/cm^3. Talc is a layer silicate mineral, characterized by a structure comprising three octahedral magnesium (Mg) positions for every four tetrahedral silicon (Si) positions, with the chemical formula $Mg_3Si_4O_{10}(OH)_2$. Talc is characterized by a neutral charge, signifying the absence of interlayer metal cations, and exhibits hydrophobic properties, which complicate its dispersion in aqueous environments. Consequently, it has been effectively utilized as a filler in various polymers, including polyethylene, polystyrene, poly(vinyl chloride), and poly(3-hydroxybutyrate-co-3-hydroxyvalerate) [113].

Talc has a platelet structure and low hardness and it is extremely effective in improving processing and mechanical properties, other than reducing the overall cost of the formulation [114]. Regarding mechanical properties, talc significantly enhances the flexural modulus due to the increased crystallinity of the resulting compound and due to the greater stiffness of talc relative to the polymeric matrix [115]. Talc functions as a nucleating agent [113], reducing crystallization time and thereby potentially decreasing the cycle time for thermoformed or injection-molded components, improving the processability and furtherly reducing the overall cost. The benefits of talc in terms of processability are also related to a lower stickiness of the compound, facilitating the cutting process of the pellets during compounding and avoiding the formation of twin pellets.

The incorporation of mineral fillers within the extrusion cylinder results in an increase in shear stress, which may adversely affect the polymeric phase and potentially initiate the chain scission process. This issue is particularly critical for polyhydroxyalkanoates, which are prone to thermo-oxidative degradation and may experience a reduction in molecular weight. In contrast, polyesters exhibit less susceptibility to this phenomenon, and the addition of talc reduces chain mobility, which can ultimately decrease the viscosity of the compound [24].

2.5 Slip and Anti-block Agents

The production of commercially viable plastic products necessitates the use of processing aids that reduce surface friction, facilitating the rapid extrusion and subsequent storage of the film. The competitive pricing of the resultant material is influenced by the production speed and the film's ability to slide on processing equipment. Moreover, given that 80% of a film's cost is attributed to resin expenses, the efficient utilization of raw materials and the minimization of waste are of paramount importance [116].

Slip agents operate by diminishing the coefficient of friction between a film and processing equipment or other surfaces, including the surface of the film or extruded product itself. Analogous in function to antistatic agents and mold release agents, effective slip agents must exhibit incompatibility with the base polymer resin. This

incompatibility facilitates their migration to the surface as the extruded polymer cools [116]. The most commonly utilized migratory fatty acid primary amides include erucamide (melting point 81–83°C), oleamide (73–78°C), and stearamide (101–102°C). In the current study, ethylene bis-stearamide (EBS) was employed due to its superior thermal stability, with a melting point reaching up to 143°C. Additionally, zinc stearate serves as an aid in high-speed extrusion processes [116].

Anti-block agents serve a function analogous to that of slip agents, as they prevent polyolefin films from adhering to one another. Mineral fillers, such as talc, can be employed to introduce surface roughness or protrusions to the film, thereby mitigating blocking. Erucamide and ethylene bis-stearamide are among the most frequently utilized anti-block agents [116].

2.6 Definition of the formulations

In the present thesis, two different sets of formulations were evaluated. The formulations based on PLA-PHBH are detailed in Table 2.8. The PLA utilized was Ingeo Biopolymer 2003D (NatureWorks LLC, Plymouth MN, USA), an extrusion grade characterized by a melt flow rate (MFR) of 6 g/10 min (210°C, 2.16 kg) and a tensile elongation of 6 MPa. The PHBH grade employed was GreenPlanet X331N (Kaneka Belgium NV, Westerlo-Oevel, Belgium), an injection molding grade with an MFR of 10 g/10 min (160°C, 5 kg) and an elongation at break of 4%. A lamellar talc (Imerys S.A., Paris, France) served as the mineral filler. The epoxy chain extender was sourced from BASF (Ludwigshafen, Germany), and the primary/secondary antioxidant was procured from Adeka (Mulhouse, France). Ethylene bis(stearamide), an organic wax, and zinc stearate, a lubricant, were employed as processing aids. Each formulation comprises 20 wt% talc, 0.3% epoxy chain extender, 0.2% antioxidant, 1% EBS, and 0.1% zinc stearate. In all instances, the polymeric phase is PLA-PHBH. In PLA-PHBH 82, the polymeric phase consists of 80% PLA and 20% PHBH; in PLA-PHBH 55, it consists of 50% PLA and 50% PHBH; and in PLA-PHBH 28, it consists of 20% PLA and 80% PHBH.

Table 2.8 PLA – PHBH based formulations

	PLA-PHBH 82	**PLA-PHBH 55**	**PLA-PHBH 28**
	wt%	*wt%*	*wt%*
PLA INGEO 2003D	64.9	39.2	13.5
PHBH Green Planet X331 N	13.5	39.2	64.9
Talc	20.0	20.0	20.0
Chain Extender	0.3	0.3	0.3
Antioxidant	0.2	0.2	0.2
EBS	1.0	1.0	1.0
Zinc Stearate	0.1	0.1	0.1
tot	*100.0*	*100.0*	*100.0*

The formulations based on PBS-PBAT are detailed in Table 2.9. The PBAT utilized was PBAT TH 801T/2 RESIN, procured from Xinjiang Blue Ridge Tunhe Polyester Co. Ltd. (Wulumuqi, CN). Bio PBS FZ91PM, an extrusion-grade PBS, was obtained from PTT MCC Biochem (Bangkok, Thailand). In both formulations, the ratio between the two polymeric phases was maintained at 70/30. Lamellar talc (Imerys S.A., Paris, France) was incorporated at 30 wt% in T733 and at 40 wt% in T734. The epoxy chain extender was obtained from BASF (Ludwigshafen, Germany). Additionally, a primary-secondary antioxidant, commercialized by Adeka (Mulhouse, France), and ethylene bis(stearamide) (EBS), an organic wax were employed as processing aids.

Table 2.9 PBAT – PBS based formulations

	T733	**T734**
	wt%	*wt%*
PBAT TH 801T/2 RESIN	48.2	41.7
BIO PBS FZ91PM	20.7	17.9
Talc	30.0	40.0
Chain Extender	0.1	0.1
EBS	0.8	0.2
Antioxidant	0.2	0.2
tot	*100.0*	*100.0*

3 Plastic Processing Technology

3.1 Twin – screw extrusion

Innovative compounds require reactive extrusion for their production. Compared to the compounding process of plastic materials, reactive extrusion entails that, in addition to the plasticization and homogenization of the input materials, a chemical reaction occurs within an extruder. Therefore, the extruder acts as a continuous chemical reactor. The reagents for the process were dosed into the barrel at the initial zones of the extruder to maximize the residence time. The temperature is selected based on the polymer phase to be extruded to avoid the onset of degradation phenomena and the type of additive involved in the reaction. The operating temperature must be higher than the activation temperature of the reagents for the reaction to occur. Activators and catalysts can also be used to improve the efficiency of the process. At the end of the extruder, the melt is pelletized using a cutting system (strand, liquid ring, or underwater pelletizing), or profiles, sheets, or films are directly produced. Figure 3.1 presents a diagram highlighting the fundamental differences between the compounding and reactive extrusion processes.

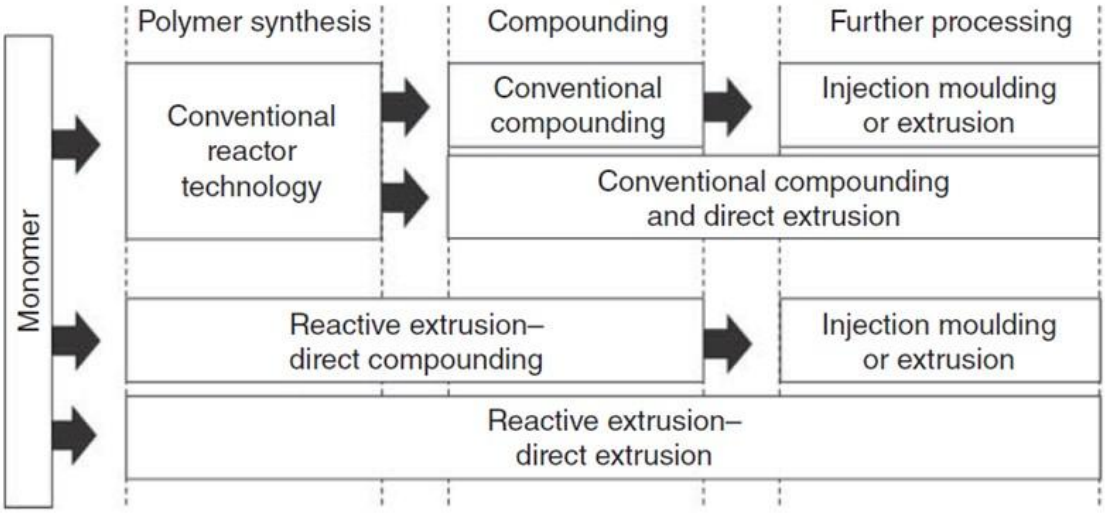

Figure 3.1 Production process routes for polymeric compounds [117]

3.1.1 Types of twin screw extruders

Twin-screw extruders are particularly well-suited for the engineering of commercially available products, as they can process materials with a wide range of viscosities and exhibit excellent mixing capabilities for the input materials. Their straightforward operation also contributes to reducing production costs, particularly when compared to complex batch-type reaction systems. The operating principle of twin-screw extruders ensures a high degree of flexibility, allowing the testing of various formulations, compounds, and reaction strategies. In addition, the use of small-scale laboratory extruders, which can operate efficiently even at very low throughputs, makes it possible to address a broad range of study cases.

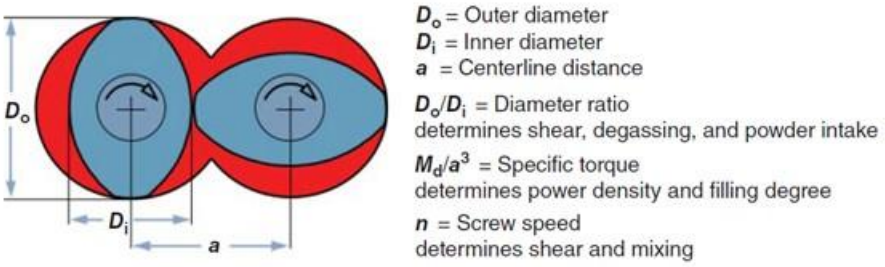

Figure 3.2 Screw parameters of a twin screw extruder [118]

The definition of the characteristic geometric parameters of the screws is critically important because the reaction occurs during the extrusion process. These parameters influence the thermomechanical stress state of the melt, efficiency of material transport through the barrel, and onset of potential degradation phenomena affecting the polymeric material. Twin-screw extruders are categorized based on the rotation type of the screws. In co-rotating extruders, the screws turn in the same direction, whereas in counter-rotating extruders, the screws revolve in opposite directions relative to one another (Figure 3.3). The inter-screw distance is another critical parameter influencing the stress conditions imparted to the polymeric melt and the subsequent degree of mixing of the polymer melt. The most common intermeshing screw configurations are shown in Figure 3.4.

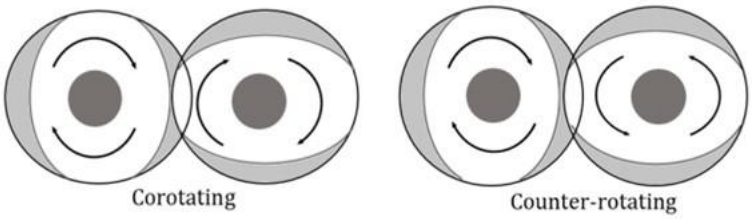

Figure 3.3 Differences between co-rotating and counter-rotating twin screw extruders [119]

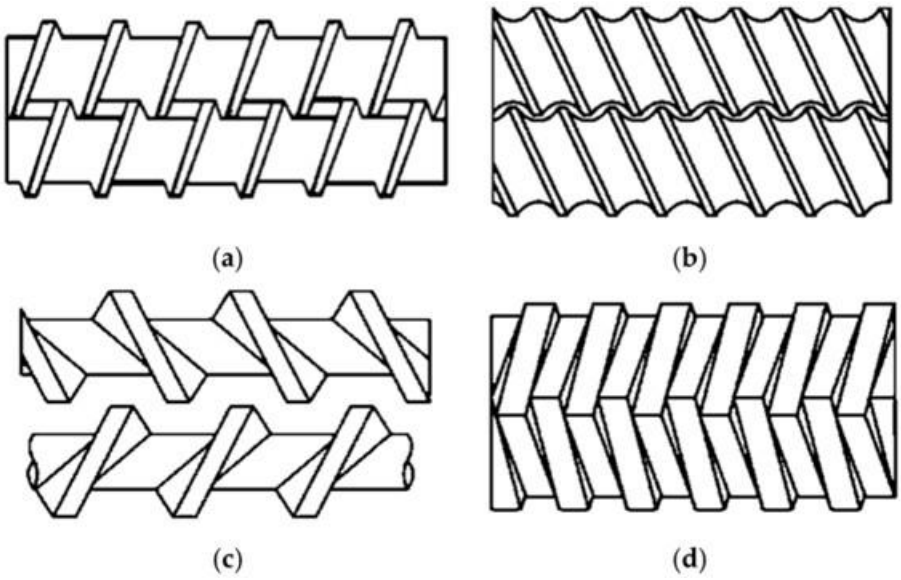

Figure 3.4 Compenetrating screw types [119]

The main geometric parameters of the twin-screw extruder are shown in Figure 3.2. The section shown in the figure refers to a co-rotating, intermeshing-type extruder, characterized by interpenetrating screw profiles capable of mutual self-cleaning of both the screw and barrel surfaces during the extrusion process. This design ensures that no material accumulates inside the barrel, which could otherwise undergo degradation phenomena owing to excessive residence time.

The first parameter that can be used to describe a co-rotating twin-screw extruder with intermeshing profiles is the ratio between the outer diameter D_0, that is the diameter of the extrusion barrel, and the inner diameter D_i, namely the diameter of the screw core. The D_0/D_i ratio is correlated with the free volume inside the extruder. The second parameter used to characterize the co-rotating twin-screw extruder is the specific torque

M_d/a^3. The specific torque is defined as the ratio between the driving torque M_d and the cube of the centerline distance between the screws a. This value determines the ability of the extruder to transfer energy to the polymer melt and the degree of barrel filling. The third parameter is the screw rotation speed n, expressed in revolutions per minute (rpm). Laboratory-scale twin-screw extruders, such as those used in the preliminary stages of the present experiment, generally reach rotation speeds not exceeding 1200 rpm. The screw rotation speed affects the magnitude of the shear stresses imparted to the material and the mixing efficiency of the extruder.

3.1.2 Screw design

A major advantage of using twin-screw extruders is their high degree of flexibility, both in terms of the wide range of materials that can be processed with a single configuration and the possibility of modifying the configuration of the extruder according to the specific reaction to be performed. Both the barrel and screw of twin-screw extruders are modular, and the individual elements can be selected independently.

Figure 3.5 Co-rotating Twin-Screw Extruder: Examples of Barrel and Screw Element Modularity [120]

Figure 3.5 shows some examples of the barrel and screw components of a co-rotating twin-screw extruder. The barrel elements were independently temperature-controlled. Temperature regulation is achieved through a system of heating resistors, generally accompanied by compressed air or a water cooling circuit. The barrel sections can be either closed, corresponding to the melting or mixing regions of the screw, or open to allow the feeding of raw materials or degassing.

Polymer exposure within the extruder can be divided into eight main areas: feed, plastication, conveying, mixing, downstream feeding, devolatilization, pumping, and die [121]. The screw design aims to create a homogenous product to feed the die and obtain a constant melt temperature and melt pressure.

The raw materials can be fed as either solids or liquids. The main feeding is usually performed in the first zone of the barrel, and the downstream addition of liquids or solids is also possible. Co-rotating extruders are typically operated under starve-fed conditions, which dictate that the extruder throughput is controlled by the material feed rate rather than the screw rotational speed. The initial screw element is generally characterized by a low pitch and short length, which is a design feature implemented to inhibit any material backflow towards the screw seals. The subsequent element is designed with a high pitch, single flight, or undercut profile, creating an open volume intended to accommodate incoming raw materials, such as pellets, powder, or flakes.

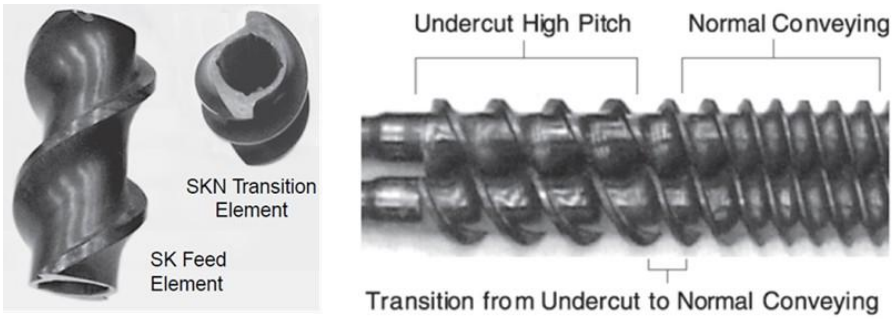

Figure 3.6 Design of the screw in the feeding section [121]

The introduction of materials downstream is usually performed for temperature-sensitive materials, reinforcements that require maintaining their aspect ratio (e.g., fibers), shear-sensitive materials, or liquids, which can be uniformly dispersed into the melt.

The polymer in the extruder is melted via four main mechanisms: conduction melting without melt removal, conduction melting with drag melt removal, melt initiation by plastic energy dissipation and frictional energy dissipation, and dissipative mix melting. The extruder motor supplies 80 – 90% of the energy required to plasticate the polymer, and heat is transferred to the plastic to the barrel walls. After the feeding section, the resin and additives are compressed by reducing the conveying element pitch, and the material moves forward. The position of the complete polymer melting depends on the screw length and screw elements (Figure 3.7).

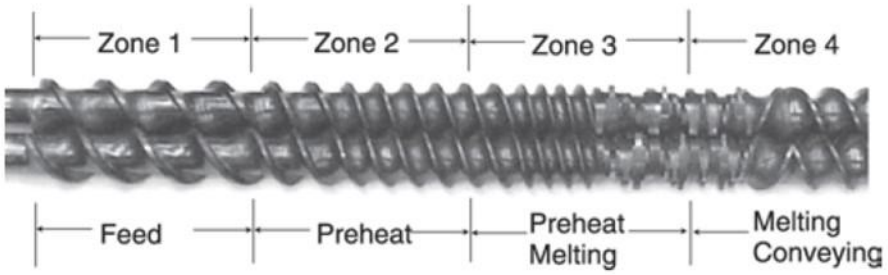

Figure 3.7 Screw design to melt the polymer [121]

Conveying elements are identified by their pitch, length and conveying direction. The nomenclature is pitch/length (e.g. 60/30 indicates that a flight makes one complete revolution around the screw element every 30 mm in length). A smaller pitch increases the percent fill and the residence time within the barrel. Forward conveying elements transport the material towards the extrusion die whereas rear conveying elements transport the melt towards the feeding zone [121].

The mixing sections of the extruder are usually made of kneading blocks (Figure 3.9), defined by their length, stagger angle, number and width of disks, number of flights and conveying direction. Their nomenclature is in the form of angle/number of disks/kneading block length (e.g. 40/5/60 indicates a 5 disks element where the first element is vertical,

the second is rotated by 45 degrees and the third one is rotated by 45 degrees from the second. The overall length of the element is 60 mm). Depending on the width of the disks and on the stagger angle, the effect of the elements on the melt flow varies ().

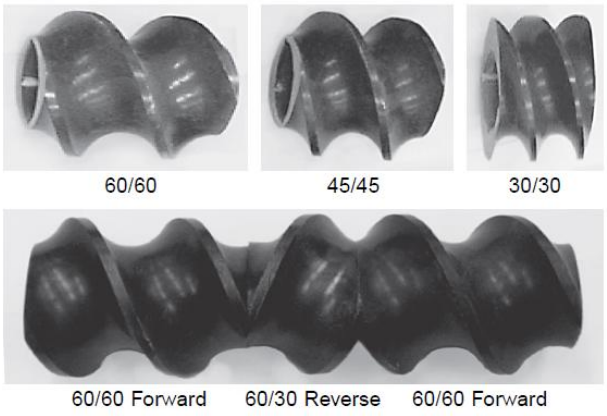

Figure 3.8 Conveying elements [121]

Figure 3.9 Example of kneading blocks (lesunscrew.com)

	Narrow Forward Conveying	Narrow Reverse Conveying	Narrow Neutral Kneading Block	Wide Forward Conveying	Wide Reverse Conveying	Wide Neutral Kneading Block
Conveying Efficiency	Good	Negative	None	Poor	Negative	None
Distributive Mixing	Good	Excellent	Excellent	Poor	Okay	Okay
Dispersive Mixing	Poor	Okay	Good	Excellent	Excellent	Excellent
Shear Heating	Low	Average	Average	High	Very High	High
Pressure Generation	Average	High	High	Very High	Exceptionally High	Very High

Figure 3.10 Effect of the kneading block geometry on the polymer melt [121]

In the process of compounding, the extruder operates under starve-fed conditions, wherein the throughput is dictated by the rate of the feeders. Feeders consist of a feeding device, a weighing platform, and a control system, and they can be categorized into two primary types: gravimetric and volumetric. In gravimetric feeders, the control system determines the actual feed rate by calculating the mass loss measured by the weighing platform over time. This method allows for the consideration of any variability during the extrusion process, such as changes in density due to a reduction in the material level within the hopper. In contrast, volumetric feeders operate by displacing a constant volume of material per unit time, with the screw speed of the feeder maintained at a constant rate [122]. Consequently, to ascertain the mass feed rate of a volumetric feeder, a pre-calibration process is necessary.

3.1.3 Feeding systems

Twin screw extruder systems are typically equipped with feeders, which play a crucial role in the process. In compounding and reactive extrusion, operations are often conducted in a starving mode, wherein the feed rate is exclusively determined by the feeders rather than the screw speed. This configuration enables precise control over the system's throughput and allows for the accurate calibration of the compound's constituents. Materials may be introduced in the initial zone of the extruders or subsequently into the barrel via side feeders. The latter approach, involving the delayed introduction of powders and mineral fillers, is frequently employed to mitigate the degradation of polymers caused by high shear stresses.

Feeders can be categorized as either volumetric or gravimetric. Volumetric feeders regulate only the screw speed, thereby allowing the setting of the system's volumetric displacement. To ascertain the material rate, it is necessary to conduct feeder calibration. In contrast, gravimetric feeders are equipped with an integrated scale and continuously monitor the feed rate through a feedback control system. This configuration permits more precise rate control, as adjustments can be made based on the apparent density of the materials, which is associated with the total weight of the material and its compacting effect. A schematic representation of the gravimetric feeders utilized in this experimental campaign is presented in Figure 3.11.

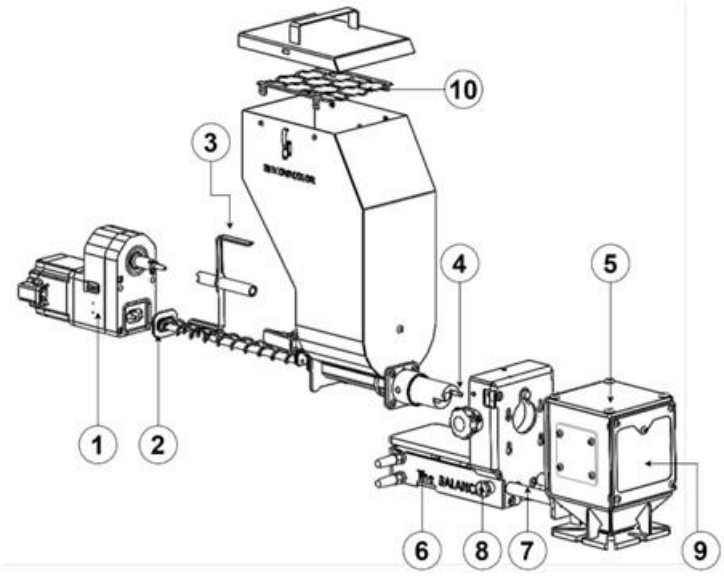

Figure 3.11 Representation of the Movacolor gravimetric feeders

3.1.4 Compounding of the defined blends

In the present experimental study, a twin-screw extruder EBC25HT – D26 – 48d (COMAC srl, Cerro Maggiore (MI), Italy) was employed. A comprehensive image of the extruder is depicted in Figure 3.14. The screws possess a diameter of 26 mm, with a length-to-diameter (L/D) ratio of 48. The high length-to-diameter (L/D) ratio facilitates uniform mixing of the compound and ensures an extended residence time, both of which are essential for the completion of chemical reactions occurring during reactive extrusion. The screw configuration is depicted in Figure 3.13. The screw alternates between conveying and mixing elements, which facilitates the elastic recovery of the melt, thereby mitigating degradation phenomena. The extruder independently regulates 12 temperature zones, thereby enabling precise control over the thermal profile of the melt. The extrusion system is equipped with five gravimetric feeders MDS Balance (Movacolor, Sneek, The Netherlands), three of which introduce material directly into the first zone of the extruder. Additionally, two side feeders allow the introduction of powders into subsequent zones of the extruder. A strand pelletizing system equipped with a dual cooling tub is employed for pellet production. This system is particularly suitable for research and laboratory-scale production, as it facilitates direct feedback on extrusion quality and the impact of

processing parameters on the melt. An overview of the used system is shown in Figure 3.14.

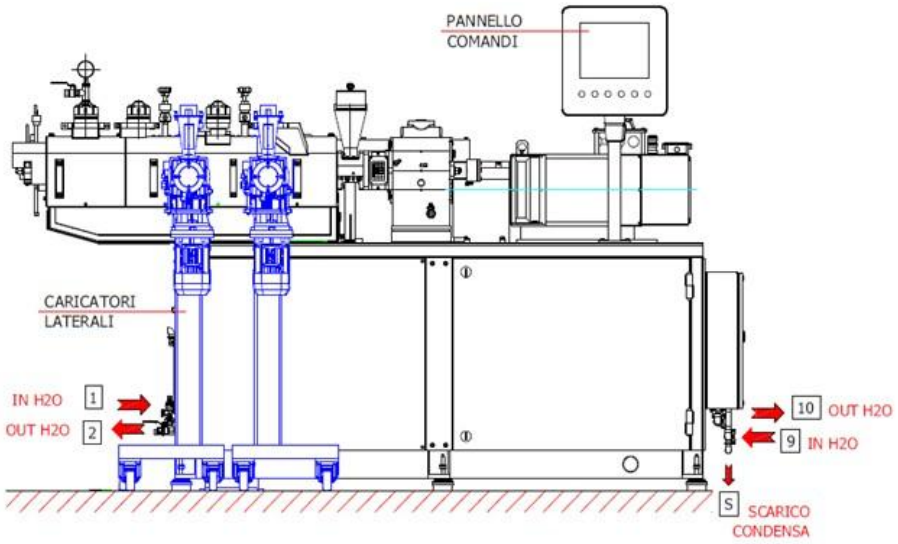

Figure 3.12 Scheme of the COMAC 26 extruder

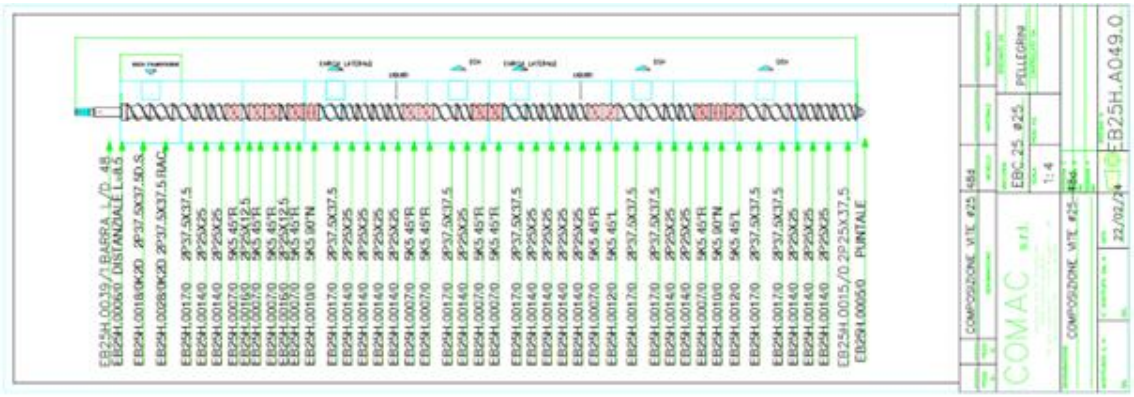

Figure 3.13 Screw profile of the COMAC 26 extruder

In the compounding process of PLA/PHBH based compounds, all materials, with the exception of talc, were initially pre-mixed manually and subsequently introduced into the first zone of the extruder via a gravimetric feeder. Talc was introduced into the fourth zone of the extruder through a side feeder, also utilizing a gravimetric feeder. The extrusion process employed a hump temperature profile, recognized for its optimal

efficiency in minimizing overall energy consumption [123]. The peak temperature was achieved immediately following the introduction of talc into the barrel, thereby enhancing fluidity and ensuring the effective incorporation of the mineral filler.

Figure 3.14 COMAC 26 extrusion system

A maximum temperature of 150°C was selected to prevent thermo-oxidative degradation of the polyhydroxyalkanoates. The melt temperature recorded at the extrusion head was approximately 140°C, which exceeded the set value but remained within the processing range of the polymers utilized. Notably, the maximum operational temperature for the PHBH grade employed is 170°C, as specified by the manufacturer in the technical data sheet. The screw speed was maintained at 280 rpm, while the side feeder speed was set at 100 rpm during the production of all compounds. The operational throughput was 18 kg/h. Table 3.1 provides a comprehensive overview of the processing parameters employed. Figure 3.15 illustrates the extrusion process of the PLA-PHBH compounds. All compounds exhibit a characteristic gray coloration, attributed to the presence of talc.

No evidence of melt degradation or rheological instability was observed at the extrusion die exit. The double tub configuration facilitated effective cooling and cutting of the strands, resulting in pellets with a consistent cylindrical shape.

Table 3.1 Processing parameters adopted for the twin screw extrusion

Thermal profile (°C)											
T1	*T2*	*T3*	*T4*	*T5*	*T6*	*T7*	*T8*	*T9*	*T10*	*T11*	*T12*
130	130	135	140	145	150	150	150	145	140	135	130
Side feeder speed				100 rpm		**Twin screw extruder speed**				280 rpm	

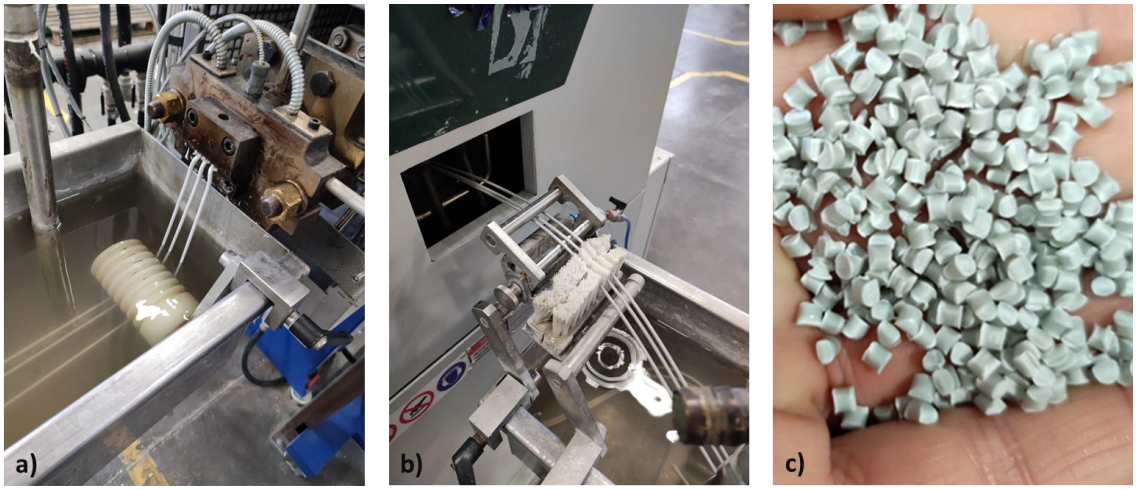

Figure 3.15 Compounding process of PLA-PHBH blends: a) strands exiting the die of the extruder, b) strands entering the pelletizer system, and c) pellets after the cut.

In the compounding process of PBAT-PBS based blends, all the constituents except talc were premixed by hand and fed in the first zone of the extruder. Talc was introduced into the fourth zone of the extruder through a side feeder, using a gravimetric MDS Balance feeder (Movacolor, Sneek, The Netherlands). The pellets were cut using a strand-pelletizing system. The temperature profile used is presented in Table 3.2, and the processing parameters are listed in Table 3.3. A hump temperature profile was used to produce T733 and T734. The T734 temperature profile attained a maximum temperature of 185 °C in the eighth temperature zone, whereas the T733 profile reached a maximum temperature of 180 °C in the seventh zone. For T734 extrusion, elevated temperatures

towards the exit were also necessary to ensure stable and uniform flow. In both instances, the die temperature was maintained at 135 °C to ensure adequate melt strength and facilitate the strands being drawn through the cooling tubs (Figure 3.16). The produced pellets exhibited a uniform cylindrical shape and were subsequently dehumidified for 3 h at 70 °C prior to further processing.

Table 3.2 Temperature profiles adopted during twin screw extrusion

	Thermal profile (°C)											
	T1	*T2*	*T3*	*T4*	*T5*	*T6*	*T7*	*T8*	*T9*	*T10*	*T11*	*T12*
T733	**130**	**140**	**155**	**160**	**165**	**175**	**180**	**175**	**160**	**155**	**150**	**135**
T734	**130**	**140**	**150**	**155**	**160**	**165**	**175**	**185**	**175**	**170**	**150**	**135**

Table 3.3 Processing parameters adopted and recorded during twin screw extrusion

	T733	**T734**
Extrusion speed	260 rpm	260 rpm
Torque	29.10%	42.20%
Side feeder speed	100 rpm	100 rpm
Melt temperature	151 °C	155 °C
Melt pressure	17.8 bar	22.0 bar

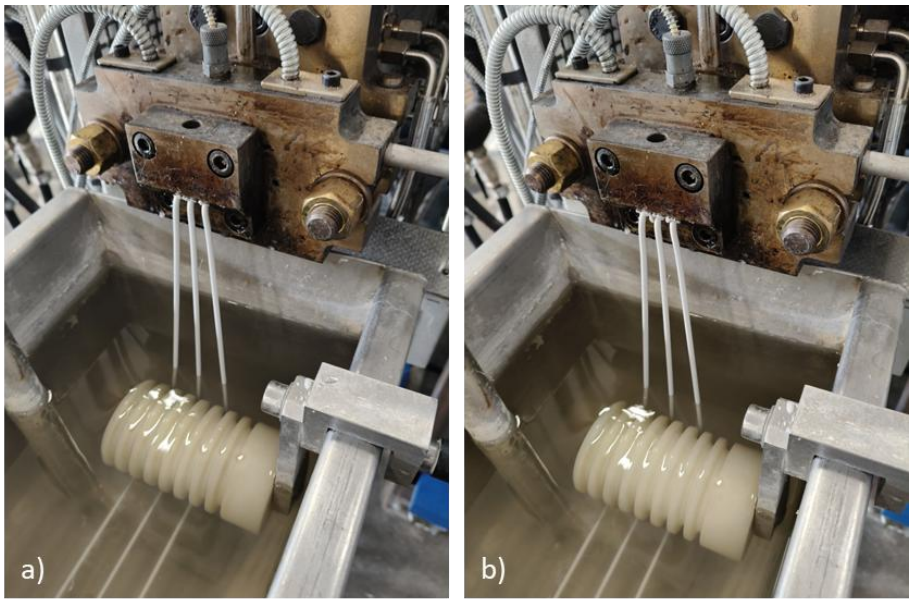

Figure 3.16 Strands at the exit of the extrusion die: a) T733, and b) T734.

3.2 Cast extrusion

Cast extrusion is one of the most prevalent technologies employed in the production of polymeric material sheets. Depending on the specific equipment utilized, it is feasible to manufacture sheets with thicknesses ranging from 10 μm to 5 mm. This process is executed using a single screw extruder, which reduces the overall cost of the equipment compared to a twin screw extruder and ensures greater simplicity of operation. Conversely, single screw extruders exhibit a reduced mixing capacity, necessitating the use of twin screw extrusion for compound production prior to sheet formation. In the process of cast film extrusion, the polymeric material is extruded through a narrow slit die and subsequently drawn from the extruder by calender rolls. The thickness of the resultant film can be regulated by adjusting the speed of the screw, the calender rolls, and the drawing rolls. A schematic representation of this process is provided in Figure 3.17.

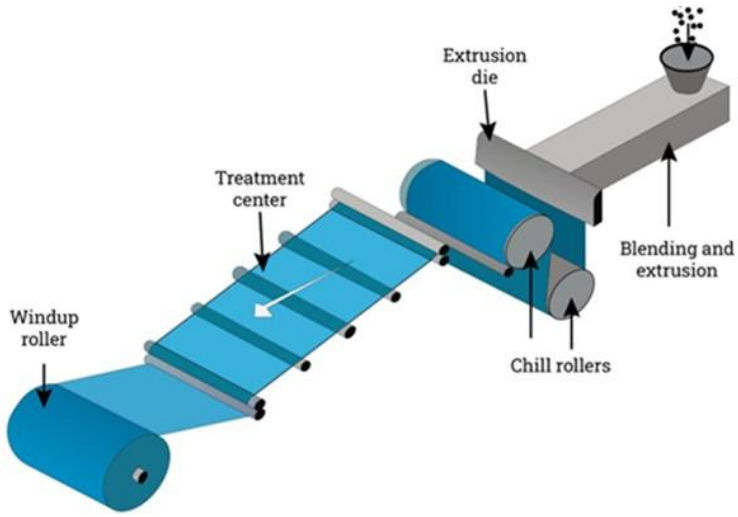

Figure 3.17 Scheme of the cast extrusion process [124]

3.2.1 Single screw extruders

The main components of a single screw extruder are visible in Figure 3.18. The screw-barrel system is the fundamental component of the extrusion process, significantly influencing its overall performance. Material flow is generated by the interaction of the

screw flights with the polymer in contact with the inner wall of the barrel. The efficiency of the extrusion process is contingent upon specific frictional conditions: if the polymer adheres to the screw, the process is hindered and fails to advance; in contrast, flow is optimized when the polymer adheres to the barrel. The screw are conventional in most cases, having a pitch equal to the diameter [125].

Figure 3.19 illustrates the functional zones of a single screw extruder. Commencing with the feeding stage, the initial zone is the solid conveying zone, where materials are introduced into the barrel in a solid state, either as powder or pellets. In the subsequent melting or compression zone, the polymer undergoes progressive melting. Within this region, the channel depth decreases progressively, attributable to either an increase in screw diameter or a reduction in barrel diameter. The final zone preceding the die is the metering zone, characterized by a constant and shallower channel depth compared to the feed zone.

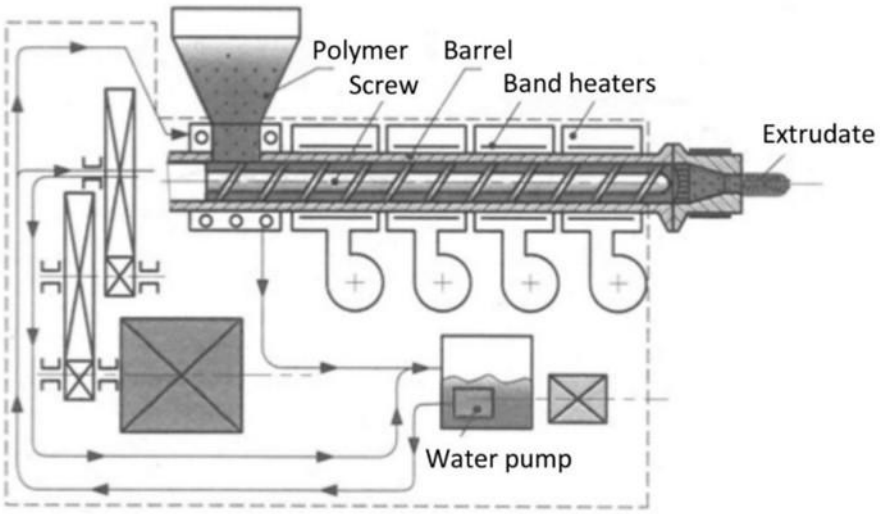

Figure 3.18 Elements of a single screw extruder [125]

The geometric parameters of the channel are detailed in Figure 3.20. Here, *b* represents the screw pitch, which generally equals the screw diameter in conventional screws. D_F denotes the nominal barrel diameter, and *h* signifies the channel depth. δ represents the

clearance between the flights and the barrel, while *e* indicates the flight width, which may be constant or a function of the radial position [125].

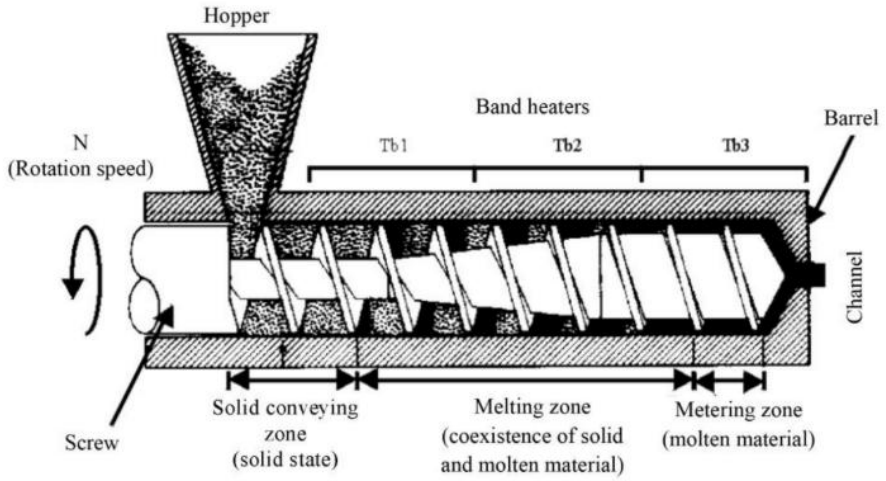

Figure 3.19 Functional zones of a single screw extruder [125]

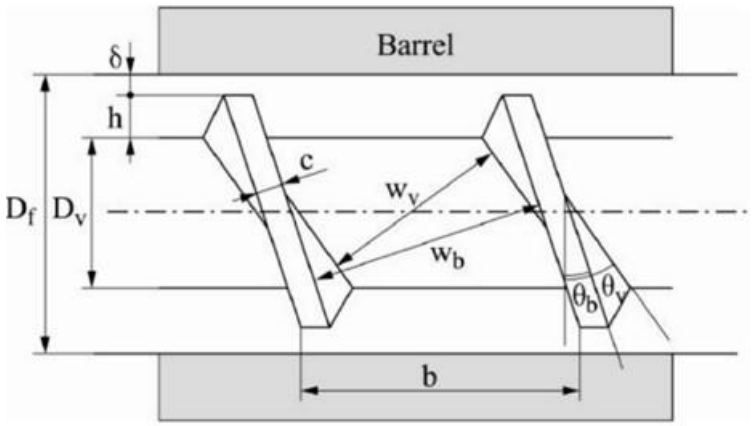

Figure 3.20 Geometric parameters of the screw of a single screw extruder [125]

3.2.2 Cast extrusion dies

Polymers exhibit viscoelastic behavior, which must be considered in the design of extrusion dies. Upon exiting the die, the polymeric melt experiences swelling due to alterations in the velocity profile, as illustrated in Figure 3.21.

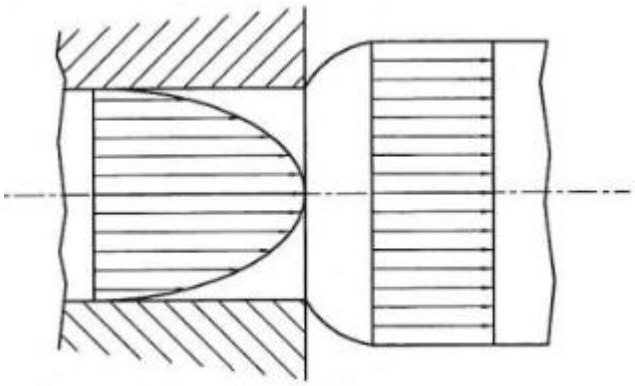

Figure 3.21 Variation of the velocity profile within the polymer melt at the exit of a die [126]

Among the simplest forms of cast extrusion dies is the manifold die, as illustrated in Figure 3.22. In this configuration, the polymer melt flows from a central channel and is subsequently distributed across the lip via a channel of constant cross-section. This design is particularly advantageous for multilayer extrusion processes. The coathanger die, depicted in Figure 3.23, distributes the polymer melt across the extrusion lip through a Y-shaped channel, also maintaining a constant cross-section. The fishtail die, shown in Figure 3.24, resembles the coathanger die in shape; however, in this instance, the polymer melt is distributed through a channel with a varying cross-section. These distinct shapes are engineered to compensate for the pressure drop associated with the polymer melt exiting the die.

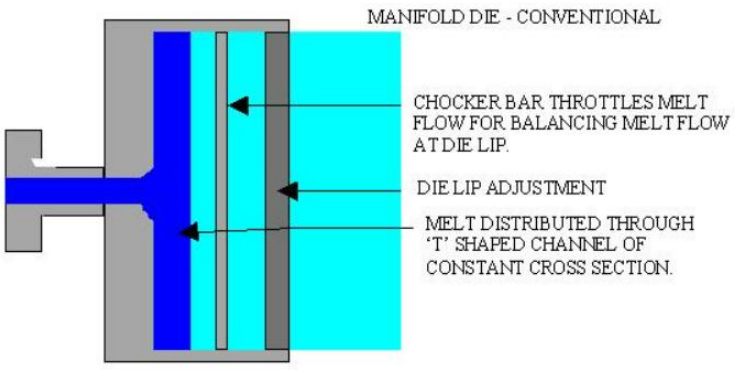

Figure 3.22 Manifold die [127]

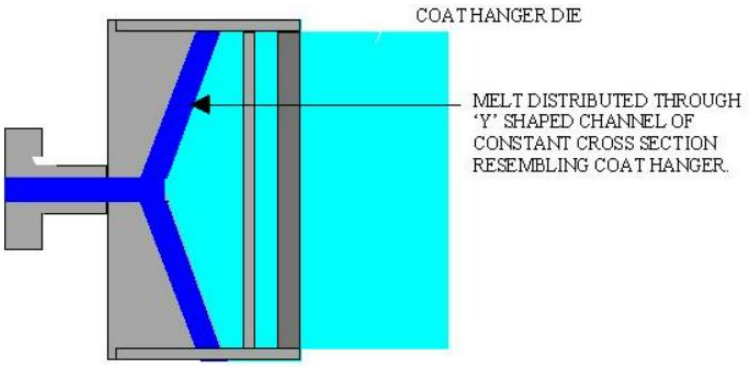

Figure 3.23 Coathanger die [127]

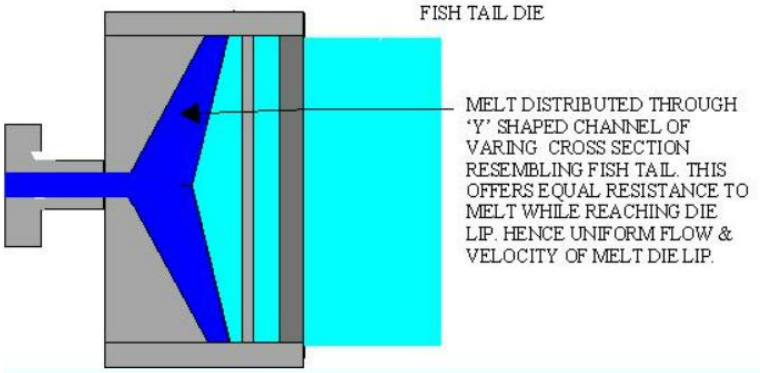

Figure 3.24 Fishtail die [127]

The coathanger die is the most used type. At the axis of symmetry, the length is typically less than ten times the die width. The flow path from the melt tube to the center of the die lips is relatively short, causing the molten polymer to preferentially flow through the central region, resulting in a thicker film or sheet at the center. The primary challenge for die designers is to restrict flow in the central die area and redirect it toward the side edges [128]. During processing, the melt distribution through the die can be adjusted by selecting appropriate extrusion temperatures.

3.2.3 Production of the sheets via cast extrusion

The cast extrusion process was performed using an Eurexma Minicast 20 extrusion system (Eurotech Extrusion Machinery srl, Tradate (VA), Italy). An overview of the used

extruder is presented in Figure 3.25. The extruder was equipped with a 20 mm screw with a length-to-diameter ratio of 25. The strand die is 200 mm wide, and the two calendaring rolls have a diameter of 150 mm and are liquid cooled. The system allows for the independent control of four different temperature zones of the cylinder and three temperature zones of the extrusion die. The temperature profile and processing parameters adopted during extrusion are presented in Table 3.4.

Figure 3.25 Eurexma Minicast 20 extrusion system

Table 3.4 Processing parameters adopted for the cast extrusion process

Temperature profile						
Cil.1(°C)	*Cil.2(°C)*	*Cil.3(°C)*	*Cil.4(°C)*	*Head right (°C)*	*Head Center (°C)*	*Head Left (°C)*
130	140	150	155	153	155	153
Processing parameters						
Calander 1			0.9 m/min	*Calander 2*		0.9 m/min
Screw speed			140 rpm	*Draw speed*		1.2 m/min

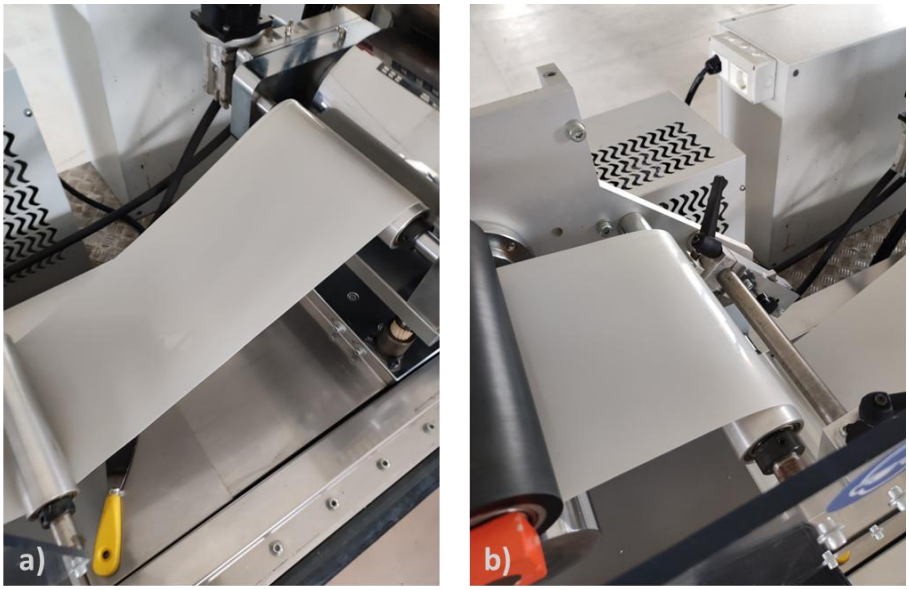

Figure 3.26 Cast extrusion process: a) Sheet after the calanders; b) Sheet before drawing.

Table 3.5 Processing parameters adopted during cast extrusion of T733

T733			
Calender 1	0.9 m/min	**Draw**	1.2 m/min
Calender 2	0.9 m/min	**Screw speed**	120 rpm
Thermal profile (°C)			
Cil.1	*Cil.2*	*Cil.3*	*Cil.4*
155	165	175	180
Head	*Right*	*Center*	*Left*
	195	195	195

Table 3.6 Processing parameters adopted during cast extrusion of T734

T734			
Calender 1	0.6 m/min	**Draw**	1.1 m/min
Calender 2	0.6 m/min	**Screw speed**	130 rpm
Thermal profile (°C)			
Cil.1	*Cil.2*	*Cil.3*	*Cil.4*
155	165	175	180
Head	*Right*	*Center*	*Left*
	195	195	195

The processing parameters employed during cast extrusion of PBAT-PBS blends are listed in Table 3.5 and Table 3.6. An identical temperature profile was used for the production of both T733 and T734 sheets. These parameters were selected to produce sheets with thicknesses ranging from 700 to 800 μm (Figure 3.27). To ensure the production of high-quality sheets, it was necessary to reduce the humidity level of the compounds to below 500 ppm. Elevated humidity levels resulted in surface defects on the film and adversely affected the thermoforming process.

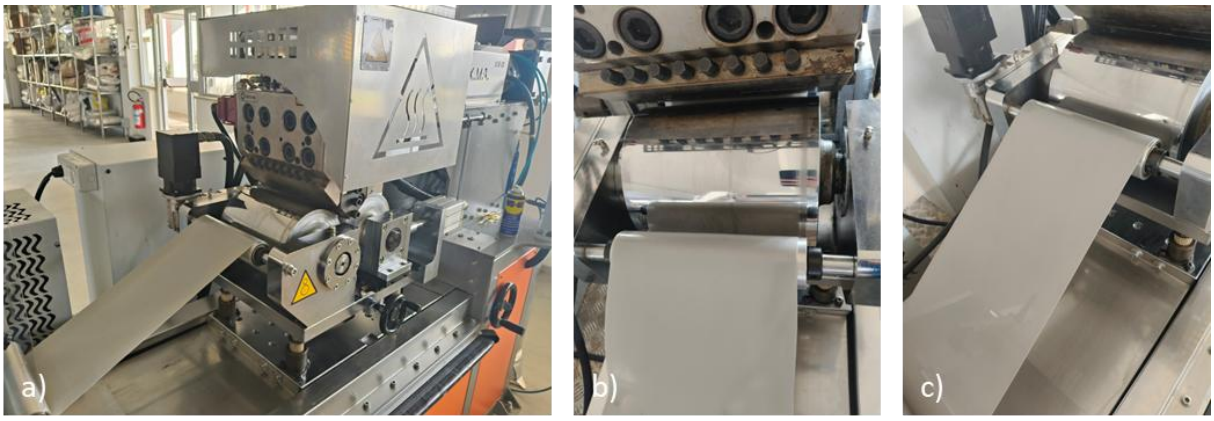

Figure 3.27 Cast extrusion process: a) overview of the extruder, b) sheet of T733 after the calender, and c) sheet of T734 after the calender.

3.3 Thermoforming

Thermoforming is a process used to produce complex geometries through the plasticization and shaping of a plastic sheet. According to American technical literature, the thermoforming process is categorized into three types: thin-gauge, which operates on sheets thinner than 1.5 mm; medium-gauge, which involves sheets with a thickness between 1.5 and 3.0 mm; and heavy-gauge, where the sheet thickness exceeds 3.0 mm. The plastic sheet, typically manufactured through cast extrusion, is heated to a temperature that permits deformation. Subsequently, the sheet conforms to the mold's shape through the application of either pressure or vacuum, contingent upon the specific configuration. Following a cooling period, the thermoformed piece can be extracted from the mold and trimmed. Thermoforming is currently employed in the production of a

diverse array of items. Amorphous plastic is predominantly utilized for this application, with polystyrene (PS) being among the most extensively used resins [126].

The requirement for tooling of thermoforming is among the most cost-effective compared to other prevalent plastic processing techniques. In contrast, processes such as injection molding, extrusion, and blow molding demand the use of steel or aluminum tooling, even for minimal production quantities. Fundamental thermoforming tooling comprises a mold for shaping the product and a method for trimming. In some instances, molds may also require internal water-cooling. For in-line thermoforming of light-gauge products, a means for rapid part removal from the processing equipment is also required [129].

3.3.1 Thermoforming process

The thermoforming process involves an initial phase in which the polymeric sheet is heated to a temperature that permits it to be deformed into a sagged configuration, after which it is drawn towards a mold. Following the cooling process, the product can be removed or ejected in preparation for the subsequent cycle. A schematic representation of thermoforming cycle time is provided in Figure 3.28.

Figure 3.28 Schematic representation of thermoforming cycle time [130]

The most basic techniques employed in thermoforming are the male mold drape and the female mold drape (Figure 3.29), contingent upon the type of mold utilized during the forming process. In both instances, the application of pressure or vacuum is necessary post-heating to ensure proper adhesion to the mold [129].

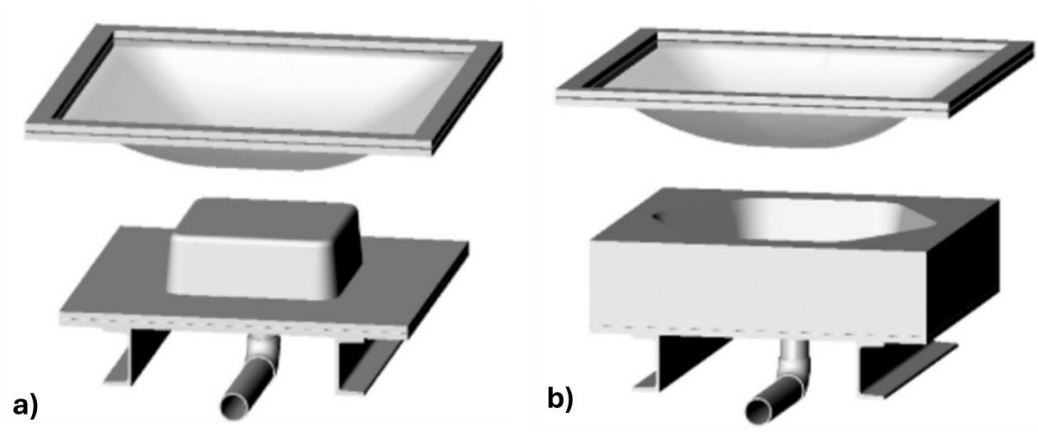

Figure 3.29 Typical thermoforming processes: a) Male mold drape and b) Female mold drape. [129]

The selection of the heating temperature is contingent upon the material being processed and the desired cycle time. There are primarily four characteristic thermoforming temperatures that must be considered. The first is the consolidating temperature, which is the temperature that permits the safe removal of the item from the mold without compromising its shape. The lower thermoforming limit temperature refers to the minimum temperature at which the material can be deformed. The normal thermoforming temperature is the temperature that must be achieved within the core sheet to ensure product quality. Finally, the upper thermoforming limit temperature is the maximum temperature before the resin undergoes degradation. Resins characterized by higher crystallinity necessitate greater energy input for heating, consequently extending the cooling duration required prior to extraction. In contrast, semi-crystalline polymers exhibit superior thermal diffusivity, facilitating more rapid and uniform heating of the sheet. The heating of these sheets can be achieved through conduction, convection, or irradiation, with the latter being the most efficient and manageable method, thus making it the predominant choice in industrial applications [126]. Figure 3.30 shows an example

of a thermal cycle that a sheet undergoes during the thermoforming cycle. In all instances, the temperature of the sheet must fall within the processability window of the resin in order to avoid degradation phenomena.

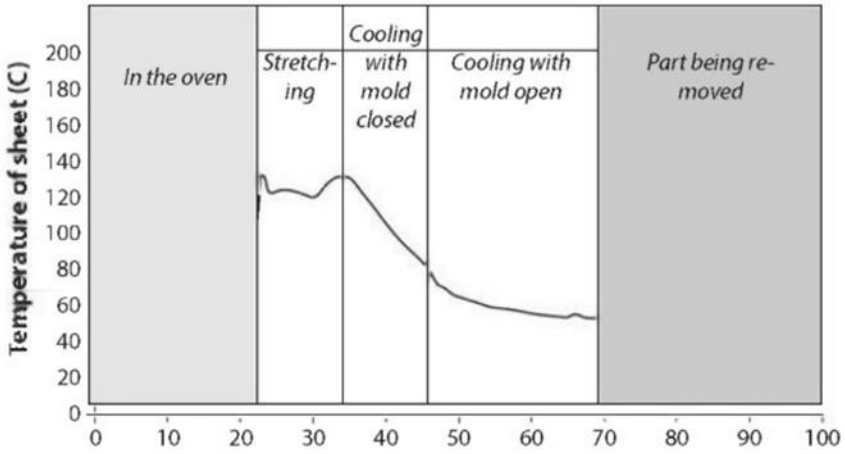

Figure 3.30 Example of thermal history of a part during a thermoforming cycle [130]

Two primary strategies ensure proper adhesion between the sheet and the mold: vacuum and pressure. In vacuum forming, the pressure must be maintained below 0.02 MPa to achieve high geometric fidelity and prevent tension in the item. A vacuum–vessel system is typically employed to ensure process stability and minimize cycle times. A schematic of vacuum forming with both male and female molds is depicted in Figure 3.31 [126].

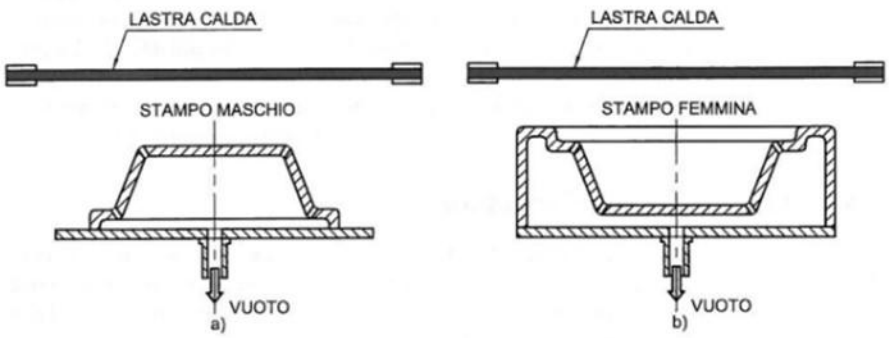

Figure 3.31 Vacuum forming: a) Male mold and b) Female mold [126].

Pressure thermoforming is employed when high fidelity in detail, strict tolerances, uniform material distribution, and minimal sheet deformation are required. Compressed air is utilized to deform the sheet. The high deformation speed necessitates the use of a pump-tank system. The working pressure differentials, Δp, range from 0.35 to 0.85 MPa, contingent upon the material's formability. A schematic of the process is presented in Figure 3.32 [126].

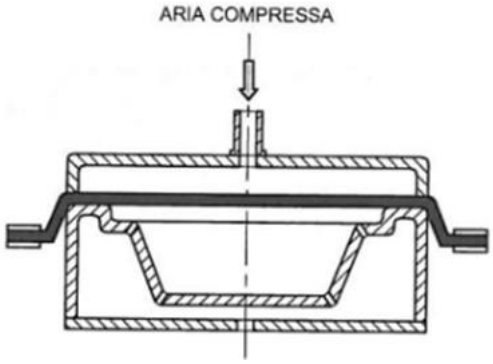

Figure 3.32 Pressure forming [126].

One of the most critical parameters for quantifying the processability of a resin through thermoforming is the maximum achievable draw ratio. This ratio serves as a measure of the elongation capability of a thermoplastic sheet when it is pressed against a mold. It is assessed as the ratio of the surface area of the final part to the initial area of the sheet prior to forming, expressed in terms of linear dimensions or cross-sectional areas. Understanding this parameter enables designers to account for the thinning of the sheet [130].

3.3.2 Production of the thermoformed trays

The thermoforming process was performed using a Formech 450DT (Formech International Limited, Thrales End, United Kingdom), a pilot-scale device equipped with a single-cavity mold in the shape of a tray. The machine features a maximum working area of 430 mm × 280 mm and is heated by four quartz lamps, each of which can be

individually controlled by adjusting the heating power of the lamp. In this laboratory-scale setup, the selection of an appropriate heating time was the primary parameter influencing the sheet quality. For all formulations, a heating time of 30 s was optimal. Shorter heating times resulted in poor detail fidelity (Figure 3.33a), whereas longer heating times led to the formation of wrinkles (Figure 3.33b). Pellet dehumidification prior to cast extrusion also plays a critical role in determining tray quality. Inadequate drying led to the formation of surface defects, particularly lumps at the bottom of the trays (Figure 3.33c). The trays produced after the manual trimming process are shown in Figure 3.34. For all formulations, it was possible to produce high-quality trays with excellent detail fidelity.

Table 3.7 Processing parameters adopted during thermoforming of PLA-PHBH based sheets

<table>
<tr><th colspan="4">Heating power</th></tr>
<tr><td rowspan="3">2

550 W</td><td>3</td><td>250 W</td><td rowspan="3">2

550 W</td></tr>
<tr><td>1</td><td>350 W</td></tr>
<tr><td>4</td><td>300 W</td></tr>
<tr><td colspan="2">Heating time</td><td colspan="2">60 s</td></tr>
</table>

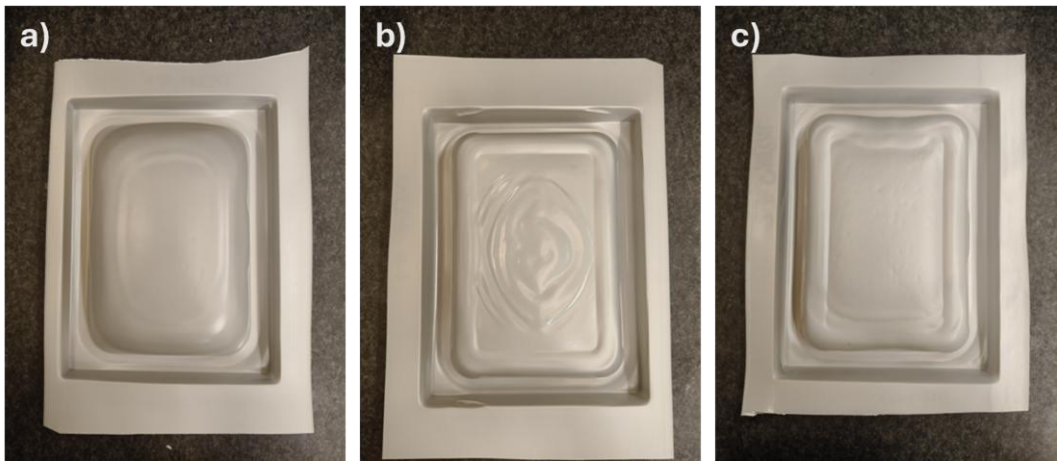

Figure 3.33 Defects observed during thermoforming: a) insufficient heating time and poor detail fidelity; b) excessive heating time causing wrinkles on the bottom of the tray; c) presence of humidity during the cast extrusion of the sheets.

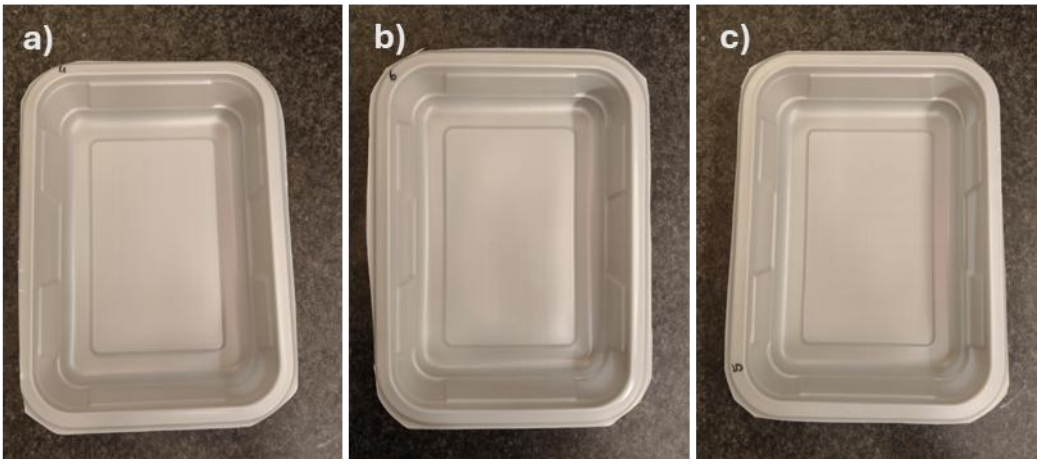

Figure 3.34 Final aspect of the trays after manual trimming: a) PLA-PHBH 82, b) PLA-PHBH 55, c) PLA-PHBH 28.

The specified heating powers of the quartz lamps used in the production of trays T733 and T734 are listed in Table 3.7. To counteract environmental influences and achieve uniform heating across the entire working area, the front and lateral zones were configured to a higher heating power. Figure 3.35 illustrates the T733 and T734 trays before their removal from the mold.

Table 3.8 Processing parameters adopted during thermoforming of PBAT-PBS based sheets

Heating power			
2	*3*	250 W	*2*
550 W	*1*	350 W	550 W
	4	300 W	
Heating time (T733)	100 s		
Heating time (T734)	70 s		

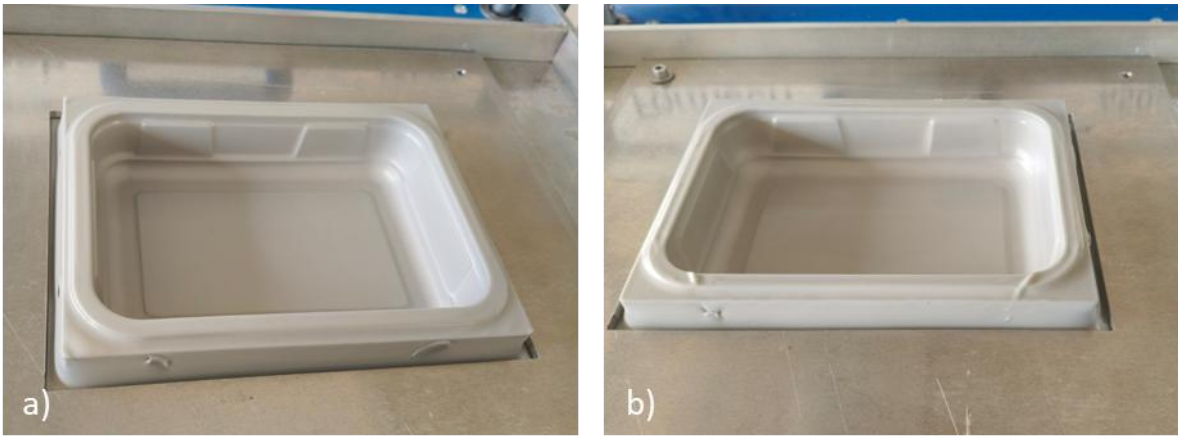

Figure 3.35 Aspect of the trays at the end of the thermoforming cycle: a) T733 and b) 734.

4 Experimental Methods

In this chapter, the experimental methods adopted to evaluate the properties of the compounds and of the semi-finished products are described.

4.1 Rheological Characterization

4.1.1 Melt Flow Rate – MFR

The Melt Flow Rate (MFR) is a fundamental rheological measurement that quantifies the extrudability of molten polymers under standardized conditions. Expressed in grams per 10 min (g/10 min), this parameter measures the mass of thermoplastic material forced through a calibrated capillary die under prescribed temperature and load conditions (Figure 4.1).

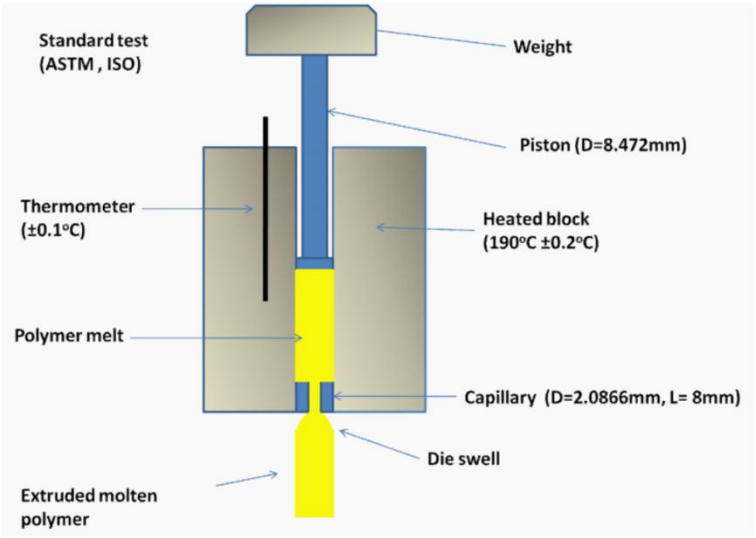

Figure 4.1 Schematic representation of a Melt Flow Rate tester[131]

The Melt Flow Rate (MFR) was evaluated in accordance with ISO 1133 standards using an ASME MFI-1221 XNR 400B (AMSE S.r.l., Torino, Italy). Mass measurements for

MFR determination were conducted using a precision balance exhibiting a measurement uncertainty of ±0.5 mg, ensuring metrological traceability for the rheological data.

Melt Flow Rate (MFR) measurements provide critical insights into material processability and serve as key industrial parameters for viscosity assessment. As documented in Table 4.1, specific MFR value ranges determine a compound's suitability for particular transformation processes. This correlation stems from the fundamental relationship between MFR and the molecular characteristics of the polymer, where higher MFR values indicate lower molecular weight and reduced chain entanglement density, whereas lower MFR values reflect greater molecular weight and increased chain interactions.

Table 4.1 MFR Range used in specific Polymer Processes [132]

Process	**MFR Range**
Injection Molding	5 – 100
Rotational Molding	5 – 10
Extrusion Coating	4 – 12
Film Extrusion	0.3 – 7
Blow Molding	0.1 – 2
Pipe and Profile Extrusion	0.2 - 2

4.1.2 Capillary Rheometer

The capillary rheometer was the first device used to measure fluid viscosity because of its simplicity, and it is one of the most widely used devices. The test fluid is placed in a reservoir, and gravity, compressed gas, or a piston is used to apply pressure. A capillary tube with radius R and length L is connected to the reservoir, and the fluid can flow through it. By measuring the pressure drop and flow rate through the capillary, it is possible to determine the viscosity of the material. The important assumptions on the basis of which viscosity measurement is possible are [133]

1. Fully developed, steady, isothermal, laminar flow.
2. No velocity in the radial and tangential directions.
3. No slip at walls.

4. The fluid is incompressible, and the viscosity does not depend on the pressure.

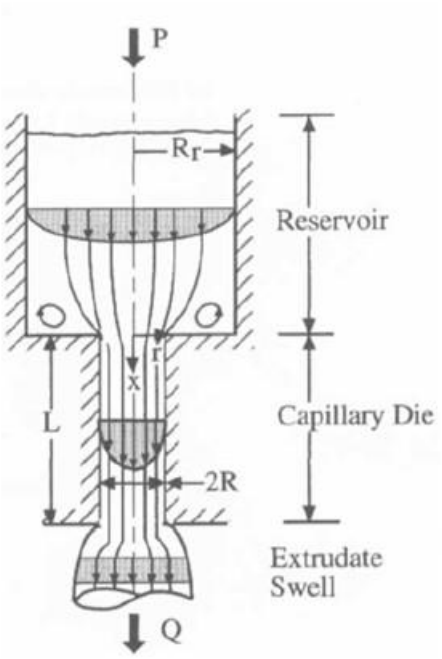

Figure 4.2 Schematic representation of a die in a capillary rheometer [133]

Capillary rheometry analysis was performed using a CEAST SmartRHEO R20 system (Instron, Pianezza, Italy) equipped with a 1 mm diameter die featuring a length-to-diameter (L/D) ratio of 20. The experimental protocol incorporated a 600-second isothermal conditioning period within the barrel to ensure thermal equilibrium prior to testing. Rheological characterization spanned shear rate conditions from 0 to 2000 s^{-1}, generating comprehensive flow curves for viscometric analysis.

Polymeric systems typically exhibit non-Newtonian flow behavior, which is characterized by pronounced shear-thinning phenomena. This rheological response manifests as progressive viscosity reduction with increasing shear rate, eventually reaching a pseudoplastic plateau region. The viscoelastic properties of the investigated compounds were quantitatively described using the Carreau-Yasuda constitutive model, which provides a robust mathematical framework for capturing the complete shear-thinning profile across multiple flow regimes. The Carreau-Yasuda model expresses the viscosity (η) as follows (4.1) [134]:

$$\eta(\gamma) = \eta_\infty + (\eta_0 - \eta_\infty)[1 + (\lambda\gamma)^a]^{\frac{n-1}{a}} \quad 4.1$$

Where:

- γ represents the shear rate (s^{-1});
- $\eta(\gamma)$ is the viscosity value, which depends on the shear rate ($Pa \cdot s$);
- η_∞ is the infinite – shear viscosity ($Pa \cdot s$);
- η_0 is the zero-shear viscosity ($Pa \cdot s$);
- λ is the time constant, called the relaxation time (s);
- n is a power-law index that determines the length of the thinning region.
- a is the Yasuda parameter, which determines the length of the transition region of the curve.

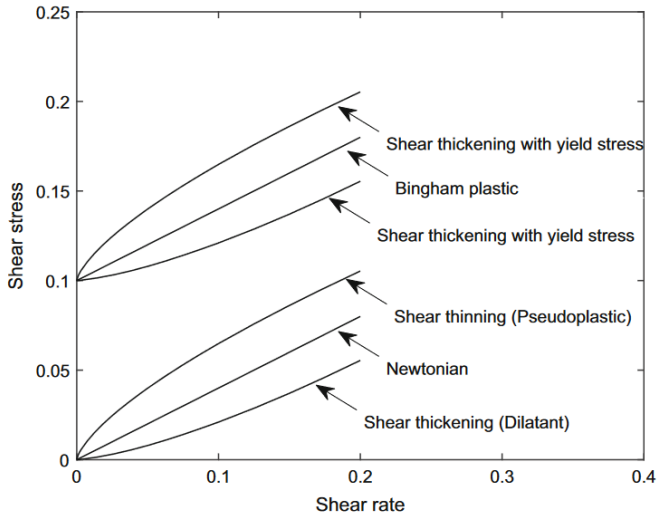

Figure 4.3 Schematic diagram for different kinds of time-independent fluids [135]

4.2 Mechanical Characterization

4.2.1 Tensile Test

The tensile test was performed using a Shimadzu AGS-X Tensile tester (Shimadzu Corporation, Kyoto, Japan) (Figure 4.4). The system was equipped with a load cell of 3

kN. Tensile tests were performed on the cast extruded films according to ISO 527 [136] in both the Machine Direction (MD) and Transverse Direction (TD). The imposed strain rate was 200 mm/min.

Figure 4.4 Shimadzu AGS-X Tensile tester

4.2.2 Compression Test

The compression test was performed on thermoformed trays using a Shimadzu AGS-X Tensile tester (Figure 4.4) equipped with a 3 kN load cell. The compression strain rate was 20 mm/min and the test was performed up to a displacement of 25 mm, which corresponds approximately to 83% of the total height of the tray.

4.3 Fourier Transform Infrared Spectroscopy – FTIR

he infrared absorption of the pellets was measured using Fourier transform infrared spectroscopy (FTIR) (Jasco FT/IR-6600 Spectrometer; JASCO Europe s.r.l., Cremella (LC), Italy) in attenuated total reflectance mode (ATR). The spectra were measured between 600 and 4000 cm 1 at 4 cm^{-1} resolution (co-added 128 scans).

4.4 X-Ray Diffractometry – XRD

The crystalline structures of compounds were analyzed by x-ray diffraction using a Rigaku Smartlab (Rigaku Corporation, Austin, TX). Spectra were recorded over a 2θ range of 5°–60° at a scanning speed of 1°/min.

4.5 Thermal Characterization

4.5.1 Differential Scanning Calorimetry – DSC

The differential scanning calorimetry (DSC) analysis was performed to assess the thermal properties of pellets. A DSC3 (Mettler Toledo, Columbus, Ohio) was used to perform the measurement. Each sample was put into an aluminium crucible. Nitrogen with a flow rate of 50 mL/ min was used as purge gas, according to ISO11357.44 Three thermic ramps were applied to the sample: a first heating ramp from -70 to 190°C with a heating rate of 10°C/min, a cooling ramp from 190 to -70°C with a cooling rate of -10°C/min and a second heating ramp from 70 to 190°C with a heating rate of 10°C/min. Enthalpies and characteristic temperatures were evaluated from all the ramps.

4.5.2 Functional Heat Resistance Tests

A functional assessment was conducted on the trays to evaluate their thermal stability and simulate their operational conditions. Specifically, 400 mL of water was heated to 100°C

and subsequently poured into the trays. After a duration of 5 minutes, the hot water was removed, and the trays were meticulously examined for any signs of deformation.

5 Results and Discussion

In this chapter, the results of the characterization performed on the compounds and semi-finished products are presented. A discussion with reference to the available literature on the matter is also provided.

5.1 Rheological properties

5.1.1 MFR Analysis

The melt flow index (MFI) of the compounds is presented in Table 5.1 and Table 5.2. For PLA-PHBH 28 and PLA-PHBH 55, the test was conducted at 160°C under a load of 5 kg, utilizing the parameters specified by the PHBH manufacturer. These parameters are designed to mitigate the degradation of PHBH caused by prolonged exposure to high temperatures within the cylinder. In contrast, for PLA-PHBH 82, the test was conducted at 190°C under a load of 2.16 kg, in accordance with the parameters established for PLA characterization. This is because, in PLA-PHBH 82, PLA constitutes the primary polymeric phase, and the melting process does not occur at lower temperatures. The MFR values obtained align with those provided by the manufacturers of the raw materials and fall within the processability range suitable for cast extrusion and thermoforming.

Table 5.1 MFR values of the PLA – PHBH blends

	Test temperature	Weight	MFR
PLA – PHBH 28	160°C	5 kg	16.2 ± 0.5
PLA – PHBH 55	160°C	5 kg	15.6 ± 0.5
PLA – PHBH 82	190°C	2.16 kg	6.0 ± 0.3

Table 5.2 MFR values of the PBAT – PBS blends

	Test temperature	Weight	MFR
T733	190°C	2.16 kg	1.27 ± 0.05
T734	190°C	2.16 kg	0.90 ± 0.12

The grade of polybutylene succinate (PBS) utilized exhibited an MFI of 5 g/10 min (190 °C, 2.16 kg), while the grade of polybutylene adipate terephthalate (PBAT) employed had an MFI ranging from 2.5 to 4.5 g/10 min (190 °C, 2.6 kg). The incorporation of talc resulted in a significant reduction in the MFI value; however, it remained within the processability parameters necessary for cast extrusion. A comparable trend was observed for pure PBS incorporated with talc or calcium carbonate. The incorporation of substantial quantities of mineral fillers in PBS resulted in an increase in the molecular weight and a consequent decrease in the melt flow rate, indicating the occurrence of secondary crosslinking reactions [24]. In the PBS/PBAT blends, an inverse trend was observed, as all the PBS/PBAT blends exhibited a higher MFR than the unprocessed reference materials [39].

5.1.2 Capillary Rheometer

The capillary rheometer viscosity curves of PLA-PHBH based compounds are presented in Figure 5.1, Figure 5.2 and Figure 5.3. All the curves exhibit the typical shear-thinning behavior of non-Newtonian fluids, as the melt viscosity decreases with increasing shear rate [137].

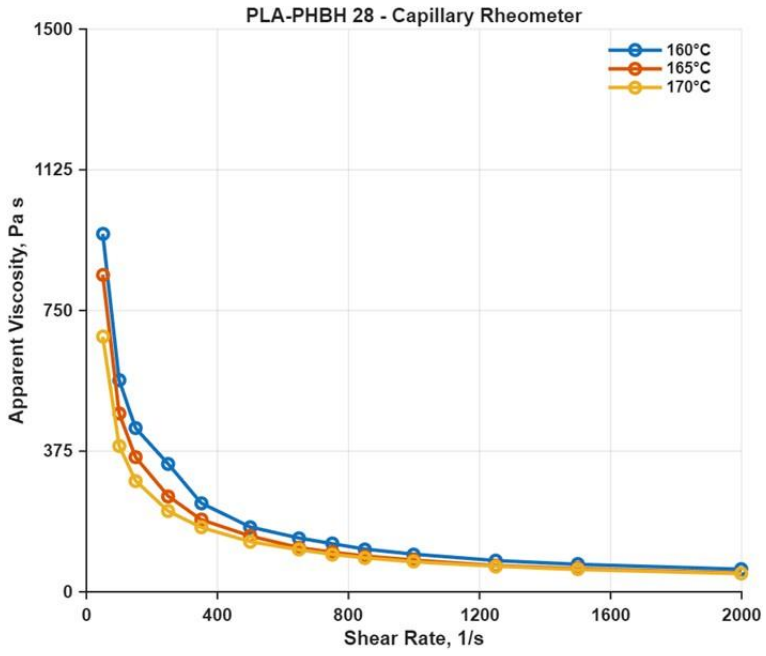

Figure 5.1 Apparent viscosity vs shear rate curves at different temperatures – PLA-PHBH 28

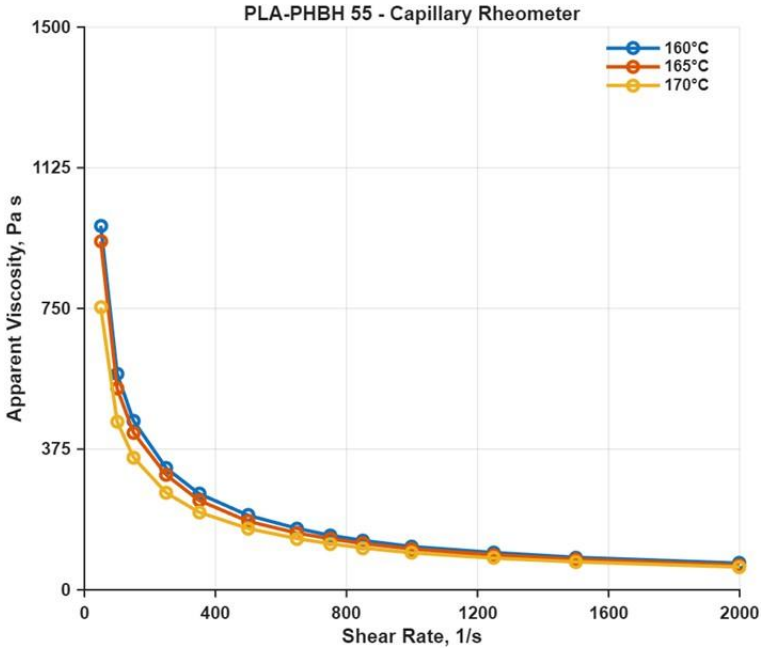

Figure 5.2 Apparent viscosity vs shear rate curves at different temperatures – PLA-PHBH 55

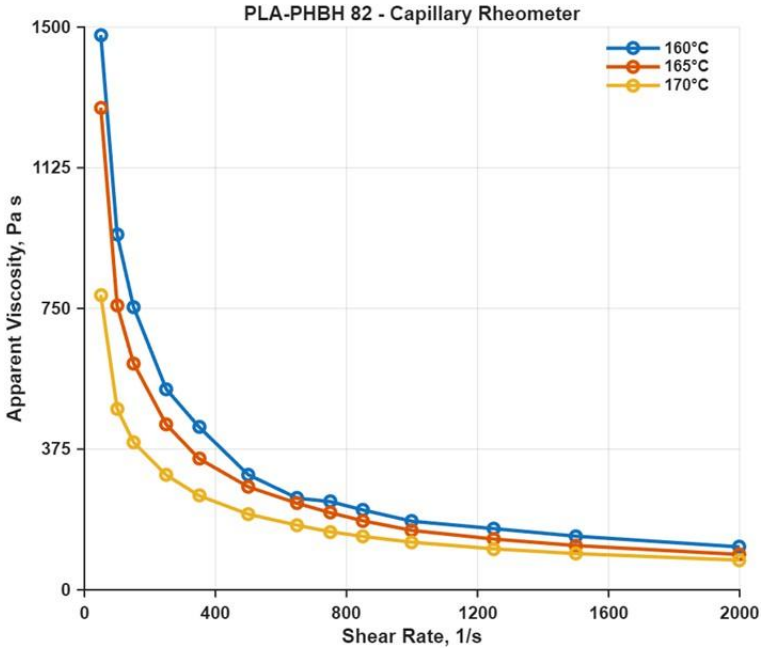

Figure 5.3 Apparent viscosity vs shear rate curves at different temperatures – PLA-PHBH 82

PLA-PHBH 82 showed the highest viscosity at 160°C, followed by PLA-PHBH and PLA-PHBH 28. As the test temperature increased from 160°C to 165°C, the viscosity of

the compound decreased, with this effect being more pronounced for PLA-PHBH 82. At 170°C, all three formulations exhibited similar behavior, with viscosity slightly below 800 Pa·s at 50 s^{-1}, suggesting the occurrence of degradation. In fact, the producer of the PHBH grade used indicates 170°C as the maximum working temperature. The obtained viscosity values are strongly influenced by the presence of PLA in the formulation. Compounds of PHBH and PBSA, in fact, exhibit viscosity values lower than 1100 Pa·s at 155°C [138].

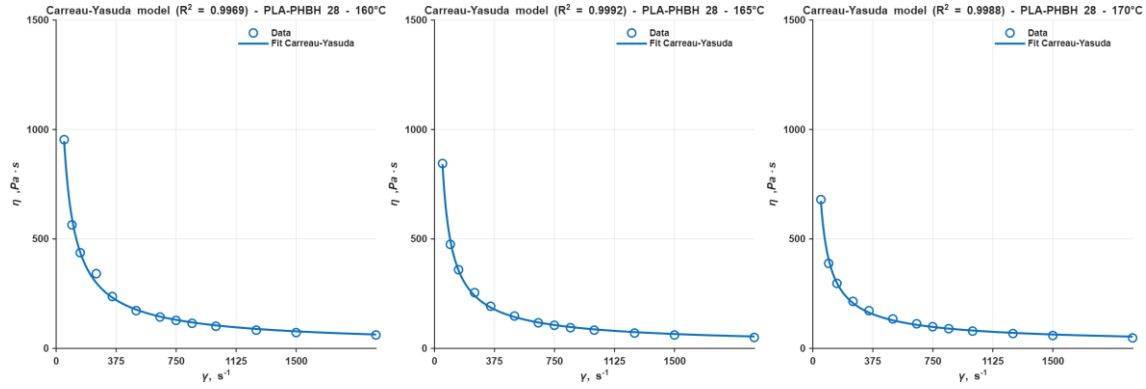

Figure 5.4 Carrau-Yasuda fitting for PLA-PHBH 28

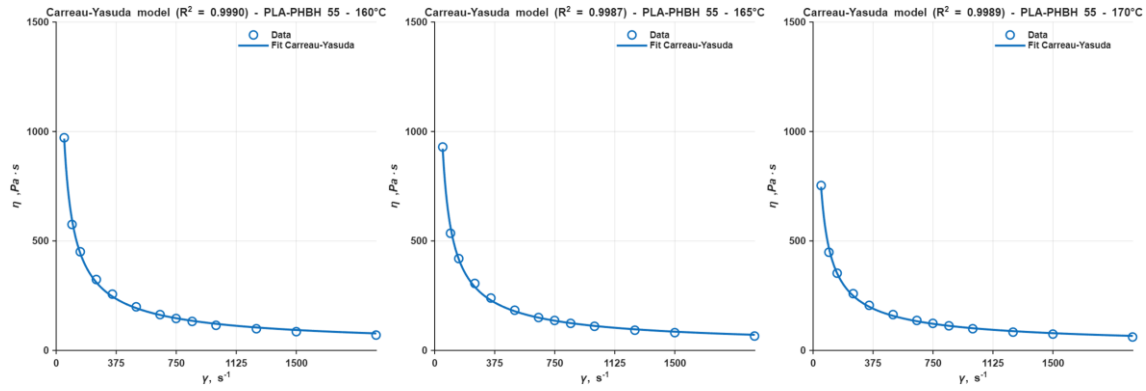

Figure 5.5 Carrau-Yasuda fitting for PLA-PHBH 55

The Carreau-Yasuda fitting of the PLA-PHBH compounds is depicted in Figure 5.4, Figure 5.5, and Figure 5.6. The fitting parameters are detailed in Table 5.3. The relaxation time λ is indicative of the point at which the polymer melt begins to deviate from

Newtonian behavior at low shear rates. A higher λ value suggests that the material exhibits greater elasticity or sensitivity to shear rate, implying that shear thinning initiates at lower shear rates. The power-law index n characterizes the slope of the viscosity curve within the shear-thinning regime. For polymer melts, n typically ranges between 0 and 1. A lower n value signifies a more pronounced degree of shear thinning, indicating that viscosity decreases more rapidly as shear rate increases. At a specified temperature, the value of λ demonstrates minimal fluctuations, indicating that the initiation point of shear-thinning remains relatively stable despite an increase in PHBH content, or that the influence of temperature predominantly governs the behavior. Additionally, an upward trend in the power-law index n is noted as the proportion of PHBH increases.

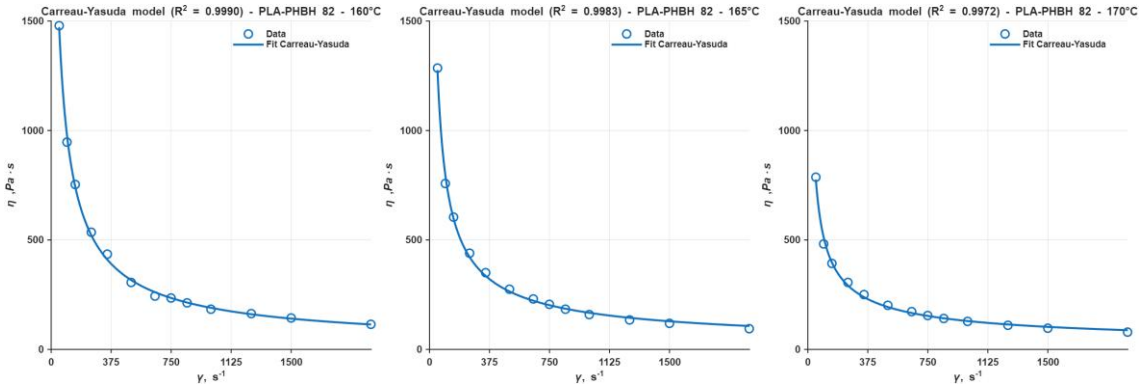

Figure 5.6 Carrau-Yasuda fitting for PLA-PHBH 82

Table 5.3 Carreau-Yasuda fitting paramters for PLA-PHBH compounds

Material	Temperature	λ	n
PLA-PHBH 28	160	0.1029	0.1524
PLA-PHBH 55	160	0.1592	0.2820
PLA-PHBH 82	160	0.0551	0.1828
PLA-PHBH 28	165	0.1850	0.2057
PLA-PHBH 55	165	0.1952	0.2682
PLA-PHBH 82	165	0.1433	0.3035
PLA-PHBH 28	170	0.2011	0.2372
PLA-PHBH 55	170	0.1964	0.3028
PLA-PHBH 82	170	0.1976	0.3798

An increase in the value of n indicates a reduction in shear-thinning behavior, suggesting a shift towards more Newtonian characteristics. This implies that augmenting the PHBH content diminishes the extent of shear thinning in the high-shear-rate regime, thereby making the melt less responsive to variations in shear rate. For the same material, λ exhibits a significant increase with rising temperature. This observation is atypical for a pure polymer melt, where an increase in temperature generally results in a reduction of the relaxation time, leading to decreased elasticity and overall viscosity. A plausible explanation for this phenomenon within this compound system (a blend) is that the temperature elevation may enhance miscibility or phase interaction between PLA and PHBH, or it may induce degradation followed by branching or gelation, thereby augmenting the melt elasticity and, consequently, λ. The power-law index n increases with temperature, signifying a diminished degree of shear-thinning, thereby indicating a more Newtonian behavior. This observation aligns with general theoretical expectations, as an elevation in temperature leads to a reduction in chain entanglement, subsequently decreasing the chains' ability to orient efficiently under shear stress.

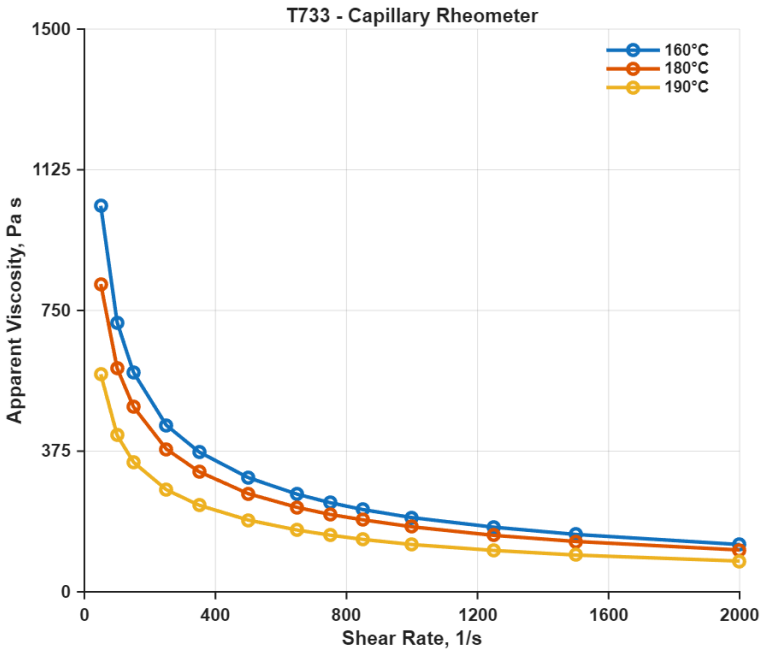

Figure 5.7 Apparent viscosity vs shear rate curves at different temperatures – T733

Figure 5.7 and Figure 5.8 show the capillary rheometer curves. Consistent with the MFR values, T734 exhibited a lower viscosity than T733. At 160 °C and 50 s^{-1}, T734 exhibited a viscosity exceeding 1400 Pa·s, whereas T733 exhibited a viscosity exceeding 1000 Pa·s. As the temperature increased, the measured viscosity decreased. For T734, the viscosity at 50 s^{-1} decreased to 1050 Pa·s at 180 °C and 725 Pa·s at 190 °C, respectively. For T733, it decreased to 820 Pa·s at 180 °C and 580 Pa·s at 190 °C, respectively. Both compounds demonstrated characteristic shear-thinning behavior, as evidenced by the reduction in viscosity observed at increasing shear rates.

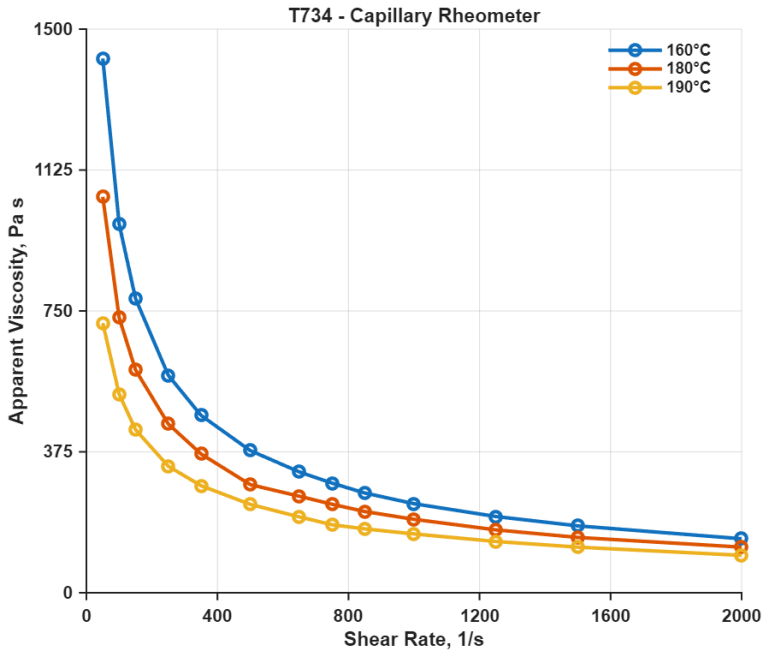

Figure 5.8 Apparent viscosity vs shear rate curves at different temperatures – T734

The Carreau-Yasuda fitting for the PBAT-PBS compounds are presented in Figure 5.9 and Figure 5.10. The fitting parameters are presented in Table 5.4. Sample T734 (λ = 0.1399 s) demonstrates a substantially higher λ value compared to sample T733 (λ = 0.0543 s). This observation aligns with the increased filler loading. The 40% talc content in T734 establishes a more robust particle-particle interaction network within the melt than the 30% talc in T733. This network confers greater elasticity to the material in its molten state and induces deviation from Newtonian behavior at lower shear rates, thereby resulting in a higher λ. The n values for T733 and T734 are nearly identical (0.3267 versus

0.3282). This observation indicates that while the concentration of talc significantly affects the initial viscoelastic response and melt elasticity (λ), a 10% increase in talc concentration (from 30% to 40%) does not markedly influence the slope of the viscosity curve in the high shear rate regime. Both materials demonstrate a comparable degree of shear thinning in this region.

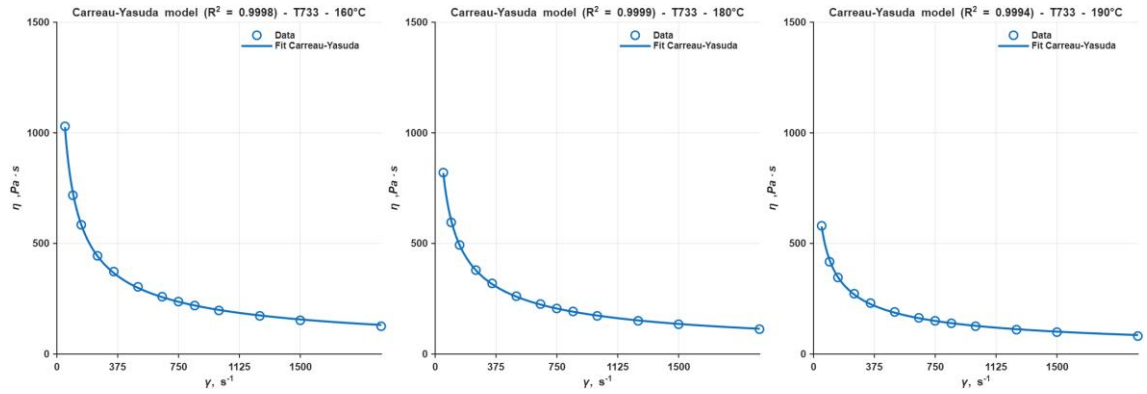

Figure 5.9 Carrau-Yasuda fitting for T733

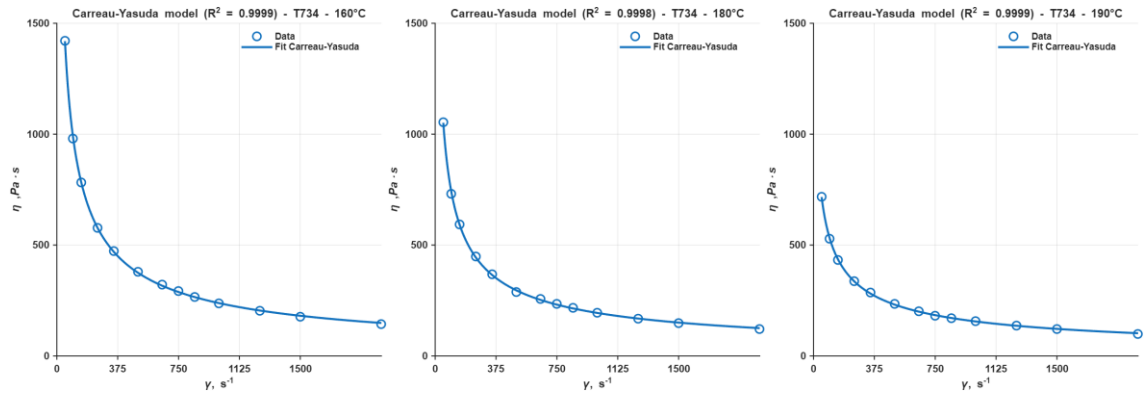

Figure 5.10 Carrau-Yasuda fitting for T734

An increase in λ is observed from 160°C to 180°C, indicating that the melt becomes more elastic, followed by a sharp decline at 190°C. This observation suggests that 180°C represents a critical temperature within this system. At this temperature, the PBAT/PBS matrix is sufficiently softened to facilitate the self-assembly or more effective interaction of talc particles. This may occur through mechanisms such as improved surface wetting

of the filler or enhanced Brownian motion, resulting in the temporary formation of a more robust particle network that increases elasticity, as evidenced by the rise in λ. At 190°C, the melt exhibits such fluidity that the shear forces generated within the rheometer more readily disrupt this network, with the fluidification of the polymer matrix predominating, thereby leading to the anticipated reduction in λ. A notable increase in n is observed from 160°C to 180°C (from 0.2594 to 0.3282), followed by stabilization at 190°C. This increase in n signifies that the material exhibits reduced shear-thinning behavior at elevated temperatures. The rise in temperature diminishes chain entanglement and flow resistance within the PBAT/PBS polymer matrix. Consequently, the melt demonstrates more Newtonian behavior (characterized by a shallower slope and higher n) within the high-shear-rate regime.

Table 5.4 Carreau-Yasuda fitting paramters for PBAT-PBS compounds

Material	Temperature	λ	n
T733	160	0.1912	0.3638
T734	160	0.0850	0.2594
T733	180	0.0543	0.3267
T734	180	0.1399	0.3282
T733	190	0.0936	0.3793
T734	190	0.0475	0.3259

5.2 Mechanical properties

5.2.1 Tensile properties of the cast extruded films

The stress-strain curves of the PLA-PHBH films are presented in Figure 5.11, and the results of the mechanical characterization are summarized in Table 5.5 and in Table 5.6. Both PLA and PHBH exhibited predominantly brittle behavior, as no yielding was observed. As the PLA content increased, both the elastic modulus and tensile strength increased. Without compatibilization, the introduction of 25% PLA into a PHBH matrix tends to increase the stiffness of the resulting compound [139]. Compared to the PLA-PHBH blends found in the literature, the introduction of talc caused an increase in the maximum stress, whereas it had a small influence on the rigidity and elongation at break.

Li et al. reported that PLA-PHBH (30/70 wt. %/wt.%) hot pressed specimens exhibited a tensile strength of around 32 MPa, an elongation at break of 2.6% and an Elastic Modulus of 1.2 GPa [140]. Zhou et al. studied the properties of compatibilized PLA-PHBH (20/80 wt.%/wt.%) blends, recording a tensile strength of approximately 19 MPa and a modulus of 1000 – 1200 MPa. The reactive compatibilizer allowed the elongation at break to increase by more than 10% [23]. In the present study, the injection-molded PLA–PHBH 28 specimens exhibited an elastic modulus of approximately 620 MPa, whereas the cast films exhibited a modulus of approximately 1000 MPa. The stress at break was approximately 30 – 35 MPa. The stress at break ranged from 30 to 35 MPa. The elongation at break values obtained in this study were slightly lower, primarily because of the presence of talc. Indeed, when high talc loadings are introduced into PLA, the resulting compounds exhibit markedly brittle behavior [55].

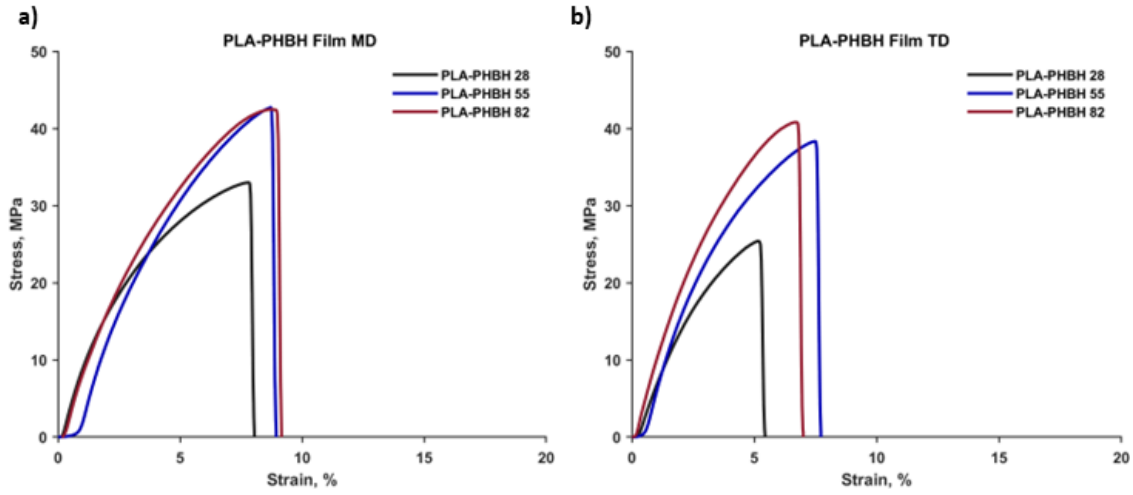

Figure 5.11 Stress – strain curves obtained for PLA - PHBH – Talc Cast extruded films a) in MD (Machine Direction) and b) in TD (Transverse Direction)

Table 5.5 Results of the mechanical characterization of the PLA - PHBH – Talc Cast extruded films in MD (Machine Direction)

	Max Stress, MPa	**Max Strain, %**	**Elastic Modulus, MPa**	**Yielding Stress, MPa**
PLA-PHBH 28	33.8 ± 1.4	8.2 ± 0.4	1069 ± 38	28.1 ± 1.3
PLA-PHBH 55	43.8 ± 1.2	9.4 ± 0.6	1117 ± 102	34.8 ± 5.4
PLA-PHBH 82	41.8 ± 3.5	9.3 ± 1.1	1187 ± 187	33.4 ± 4.5

The stress-strain curves derived from the mechanical characterization of the films are shown in Figure 5.12, and Table 5.7 presents the corresponding results. Both the T733 and T734 films exhibited a higher elastic modulus in the machine direction (380 MPa and 428 MPa, respectively) than in the transverse direction (314 MPa and 348 MPa, respectively), which can be attributed to molecular orientation [141]. The same trend was observed for cast-extruded PBAT/PBS 60/40 wt%/wt% blends [45]. The superior elastic modulus of T734 relative to that of T733 is ascribed to its higher talc content. Although talc may function as a nucleating agent [142], and crystalline polymers generally possess a higher modulus than amorphous ones [143], no significant differences were observed in the melt enthalpies from the DSC analysis. Therefore, the variation in the modulus is primarily attributed to the higher stiffness of the talc compared to that of the polymeric phase [144].

Table 5.6 Results of the mechanical characterization of the PLA - PHBH – Talc Cast extruded films in TD (Machine Direction)

	Max Stress, MPa	**Max Strain, %**	**Elastic Modulus, MPa**	**Yielding Stress, MPa**
PLA-PHBH 28	28.2 ± 1.6	5.7 ± 0.3	970 ± 83	27.1 ± 1.3
PLA-PHBH 55	36.9 ± 0.9	7.3 ± 0.5	1145 ± 94	33.6 ± 3.6
PLA-PHBH 82	39.1 ± 4.6	8.1 ± 1.3	1139 ± 69	33.2 ± 5.4

The film T733 exhibited significant ductility in both the machine and transverse directions, with an elongation at break of approximately 750%. In contrast, T734 demonstrated an elongation at break of approximately 550% in the machine direction, whereas in the transverse direction, breakage occurred at a deformation of less than 100%. The film extrusion process significantly influences the orientation of the polymer chains within the film and the distribution of the filler within the polymeric matrix. This orientation affects the interaction between the filler and the matrix, consequently reducing both the tensile strength and elongation at break [145]. In the case of the compatibilized PBS/PBAT matrix, this phenomenon was observed only when the talc loading reached 40%. The elongation at break in the machine direction was comparable to that of neat PBAT and significantly higher than that of neat PBS [39]. The maximum stress for both T733 and T734 was approximately 26 MPa, which is consistent with the values observed

for the PBS/talc composites. Similarly, no significant variation in tensile strength was detected when the talc content was increased from 30% to 40% within the PBS matrix [146].

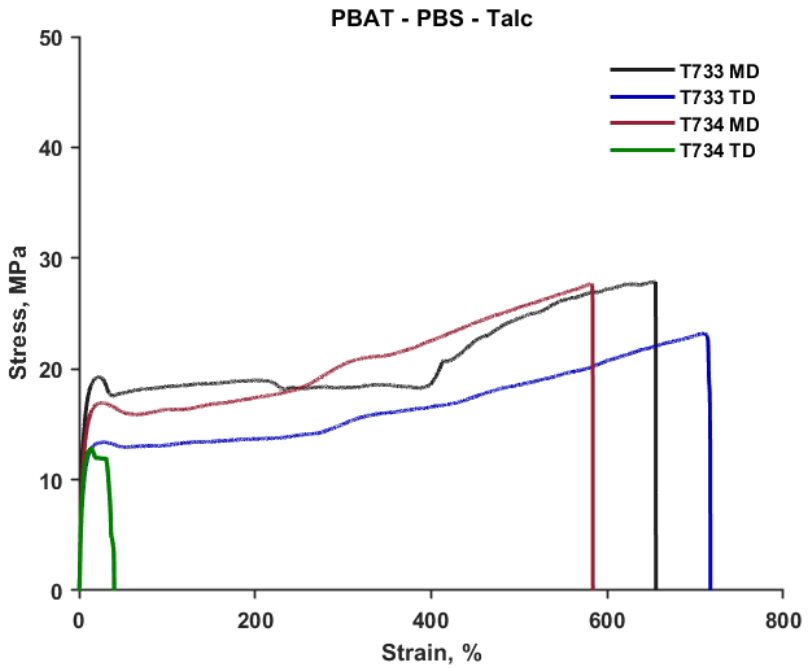

Figure 5.12 Stress – strain curves obtained for PBAT – PBS – Talc Cast extruded films in MD (Machine Direction) and in TD (Transverse Direction)

Table 5.7 Results of the mechanical characterization of the PBAT – PBS – Talc Cast extruded films in MD (Machine Direction) and in TD (Transverse Direction)

	Max Stress, MPa	**Max Strain, %**	**Elastic Modulus, MPa**	**Yielding Stress, MPa**
T733 MD	26.7 ± 2.9	712 ± 112	380 ± 33	12.2 ± 1.3
T733 TD	25.0 ± 1.2	747 ± 30	314 ± 34	10.1 ± 0.4
T734 MD	25.6 ± 3.0	549 ± 63	428 ± 43	12.0 ± 0.5
T734 TD	12.6 ± 1.0	65.3 ± 30.1	348 ± 16	9.4 ± 0.7

In comparison to neat polymers, the tensile strength of the resulting compound was lower than that of pure PBS, which exhibited a tensile strength exceeding 37 MPa, yet it was higher than that of pure PBAT, which had a tensile strength below 16 MPa [147]. Blends of PBAT and PBS in a 70/30 ratio exhibited a tensile strength of up to 35 MPa, an

elongation at break exceeding 1000%, and an elastic modulus of approximately 200 MPa [148]. These mechanical properties are consistent with the strain-hardening behavior observed in both the T733 and T734 curves and with the increased stiffness and brittleness caused by talc [55, 144].

5.2.2 Compression of the thermoformed trays

The force – displacement test curves along with pictures taken during the test are presented of the compression test of PLA-PHBH blends are presented in Figure 5.13, Figure 5.14 and Figure 5.15. The maximum force values are listed in Table 5.8.

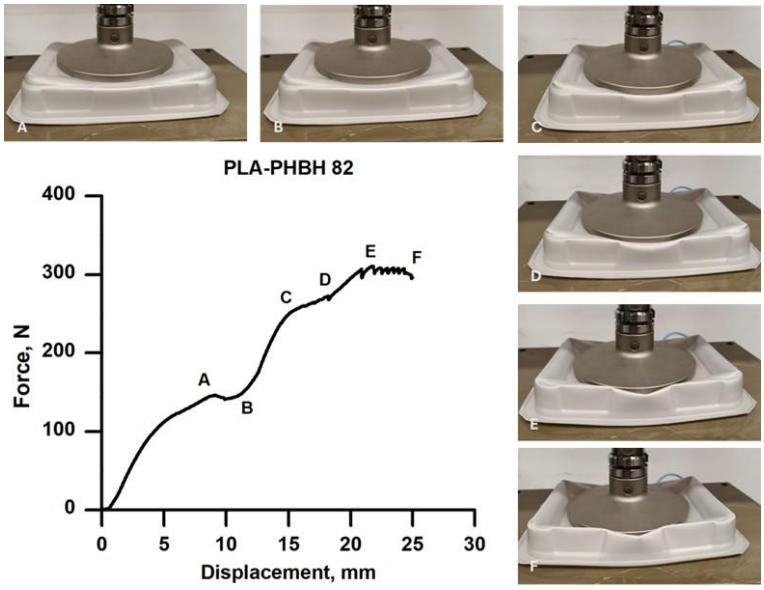

Figure 5.13 Force – displacement curve obtained during the compression of PLA-PHBH 82 thermoformed trays

As the PLA content in the formulation increased, both the maximum force and ductility of the trays increased. PLA-PHBH 28 trays, in which PHBH is the predominant polymeric phase, reached a maximum force of approximately 150 N and began to fracture at a displacement of approximately 12 mm (point B of Figure 5.13), corresponding to 40% of the total tray height. In contrast, the PLA–PHBH 55 and PLA–PHBH 82 trays exhibited maximum forces exceeding 200 N.

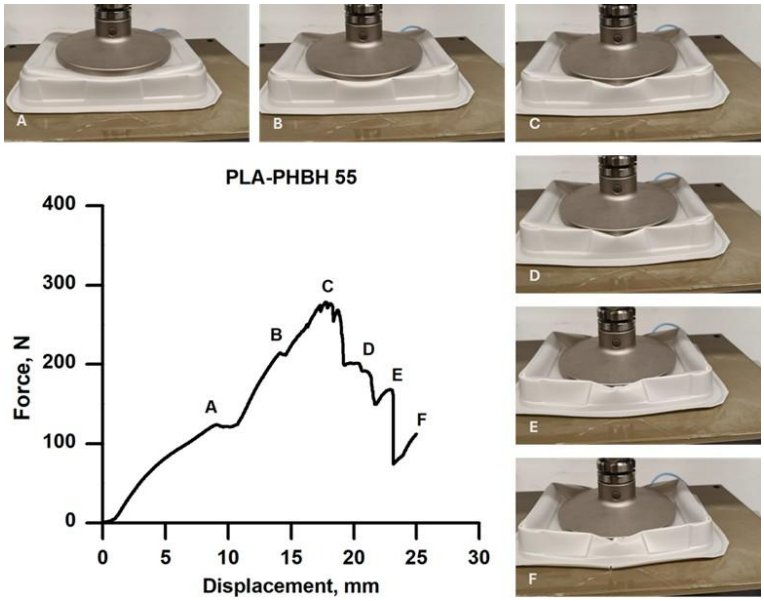

Figure 5.14 Force – displacement curve obtained during the compression of PLA-PHBH 55 thermoformed trays

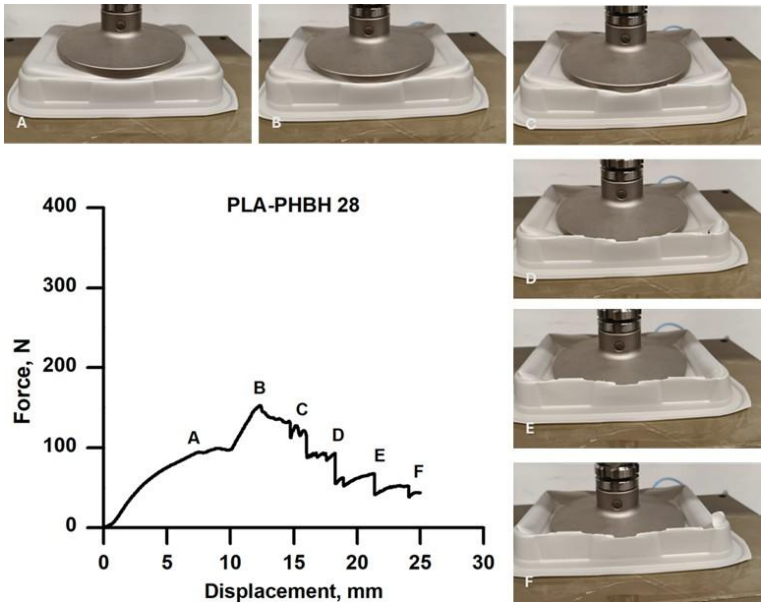

Figure 5.15 Force – displacement curve obtained during the compression of PLA-PHBH 28 thermoformed trays

The PLA–PHBH 55 tray began to fracture at approximately 17 mm of displacement (point C of Figure 5.14), at over 55% of the total height of the tray. PLA-PHBH 82, whose main polymeric phase is PLA, does not break, and only some vibrations associated with

yielding can be observed in the force – displacement curve (points E – F of Figure 5.15). The behavior of all the trays was good overall, as the breakage started for deformations higher than 40% of the total height in all cases.

Table 5.8 Results of the compression test for PLA - PHBH based thermoformed trays

	Max Force, N	**Sidewalls thickness, mm**
PLA-PHBH 28	156.4 ± 5.7	0.51 ± 0.01
PLA-PHBH 55	252.9 ± 36.0	0.42 ± 0.01
PLA-PHBH 82	282.6 ± 39.6	0.50 ± 0.02

The force-displacement curves derived from the compression test of the trays, accompanied by relevant images of the test, are presented in Figure 5.16 and Figure 5.17. Table 5.9 lists the maximum force values and sidewall thicknesses of the manufactured trays, which affect the mechanical resistance during the compression test. Although both T733 and T734 exhibit similar thicknesses, the maximum force recorded in the compression test for T734 is significantly higher, corroborating the stiffening effect of talc [144].

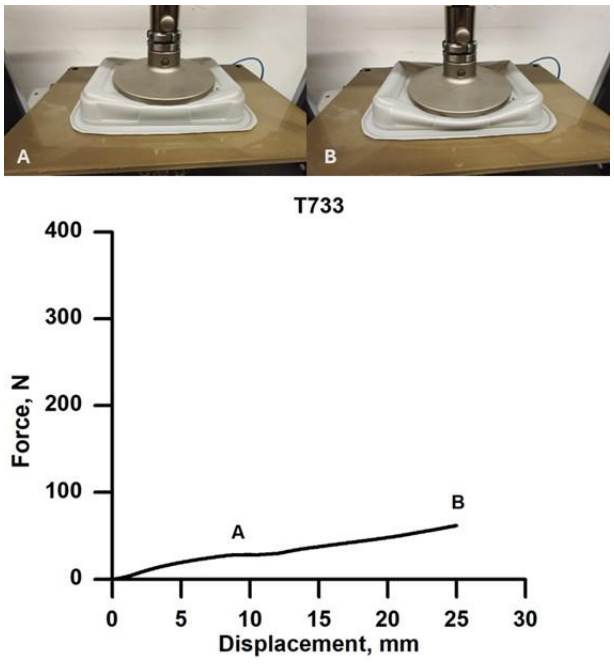

Figure 5.16 Force – displacement curve obtained during the compression of T733 thermoformed trays

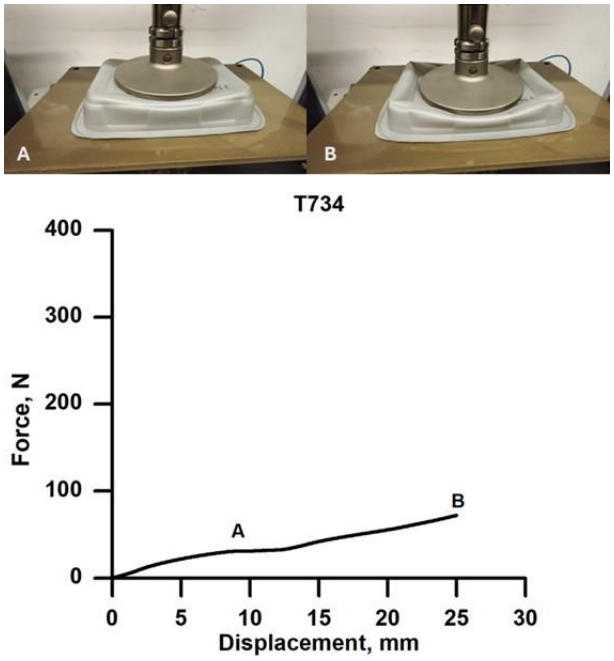

Figure 5.17 Force – displacement curve obtained during the compression of T734 thermoformed trays

Table 5.9 Results of the compression test for PBAT – PBS based thermoformed trays

	Max Force, N	**Sidewall thickness, mm**
T733	61.1 ± 1.1	0.50 ± 11
T734	71.2 ± 1.3	0.51 ± 27

5.3 FTIR Analysis

The FTIR spectra of the pellets, of the films and of the trays are shown in Figure 5.18. The peaks at approximately 2920 and 2870 cm^{-1} can be attributed to asymmetric stretching vibrations of the $–CH_3$, $–CH_2$, and –CH bonds of PHBH [149] and to CH stretching [150]. In the 3050 – 2850 cm^{-1} region, the CH_3, CH_2, and CH vibrations characteristic of PLA are also present [151]. PLA exhibits a C=O stretching vibration at approximately 1750 cm^{-1} [152], whose changes can also be associated with chain scission caused by thermo-oxidative and thermo-mechanical degradation [153]. The sharp peak observed at about 1715 cm^{-1} can be attributed to the C=O stretching vibration associated with the highly ordered crystalline structure of PHBH [150], confirming the predominantly crystalline nature of this polymer. An overlap of the signals of the two

carbonyl peaks can be identified in PLA-PHBH 82 and in PLA-PHBH 55. PHBH may also exhibit a C=O stretching vibration peak corresponding to its amorphous regions at approximately 1740 cm^{-1} [154], which, in this case, cannot be detected due to the superimposition of other more intense peaks. The position of the main C=O peak suggests the effectiveness of the compatibilization process achieved by an epoxy chain extender [23]. In the films and trays, the C=O peaks show shifts and changes in intensity, suggesting that reprocessing allows the complete reaction of the chain extender. In PLA-PHBH 82 tray, a third peak appears at 1732 cm^{-1}. Y. Zhou et al. observed a change in intensity and shifts of the C=O stretching vibration to lower wavenumbers after the introduction of a reactive epoxy chain extender due to an increase in the degree of association [23]. At around 1660 cm^{-1}, a small absorption band assigned to the stretching vibrations of the carbon–carbon double bond appears in the FTIR spectra of the films and trays. This band is associated with thermal degradation and is generated by the incorporation of vinyl ester and carboxyl groups into the PHB structure [155]. The peak at 1277 cm^{-1} can be attributed to the vibration of –C–O–C– groups in PHBH [155].

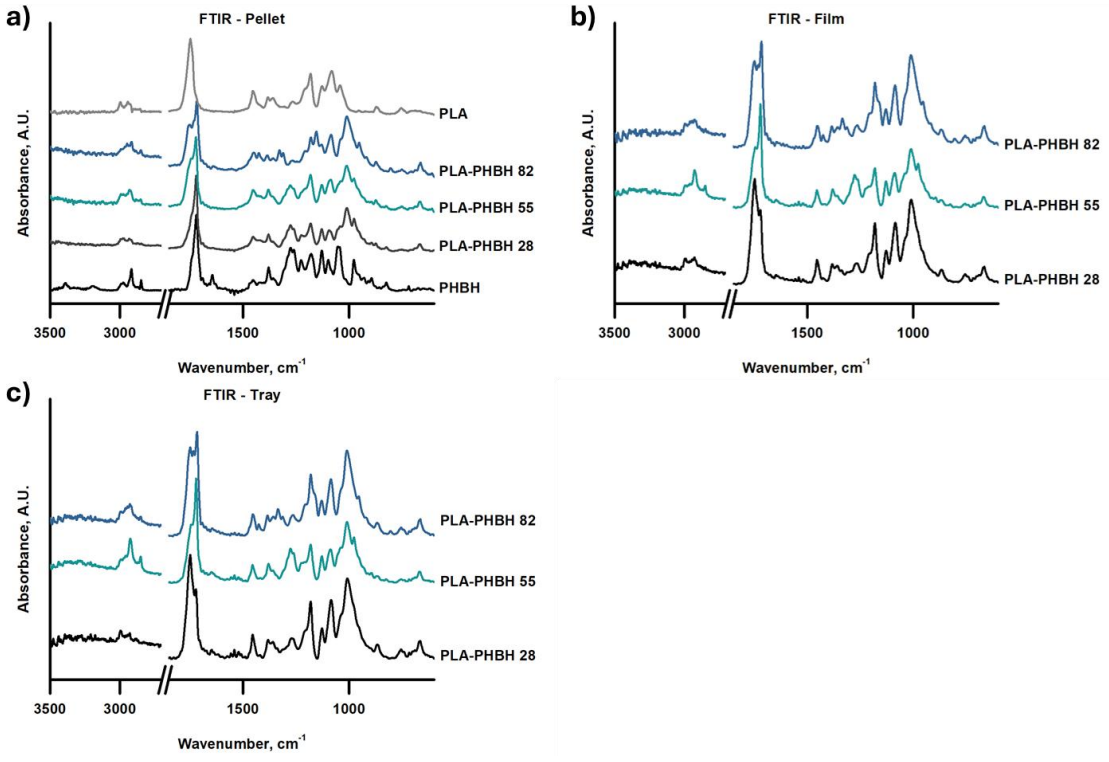

Figure 5.18 FTIR analysis of the PLA-PHBH blends. a) FTIR Spectra of the pellets; b) FTIR Spectra of the films; c) FTIR Spectra of the trays.

The peaks at 1265 and 1208 cm^{-1} are typical of PLA polymers formed by L-lactic units. The former corresponds to the bending vibration of CH and the stretching vibration of C–O–C, while the latter is associated with the asymmetrical stretching of C–O–C and CH_3 groups [156]. The peak at 1180 cm^{-1} arises from the ester groups in the polymer structure of PHB [150]. These peaks are characteristic of PHBH and become less pronounced as the PLA content increases. In the PLA-PHBH 82 spectrum, a sharp peak at 1150 cm-1 appears, which can be attributed to the C-O-C ether asymmetric stretching of PLA [151]. This peak is absent in the two formulations with lower PLA content. The presence of talc is evidenced by the peaks at 1010 cm^{-1}, attributed to the stretching vibration of Si-O bonds and at 665 cm^{-1} associated with OH bending [157].

The FTIR spectra of the compounds, trays, and films of PBAT – PBS based blends are presented in Figure 5.19. The peaks observed at 2955 and 2874 cm^{-1} correspond to the symmetric and asymmetric stretching vibrations of PBAT, respectively. Within the same spectral region (3000 – 2800 cm^{-1}), the asymmetric stretching of the PBS – CH – groups is discernible. The symmetrical vibration of the– CH – groups in PBS was identified at 1325 cm^{-1} [47]. The peak observed in the 1750–1700 cm^{-1} region is indicative of stretching of the C=O group. For pure PBS, this peak is located at 1715 cm^{-1} and attributed to the stretching vibration within the crystalline regions. Additionally, this peak exhibited a shoulder at 1728 cm^{-1}, which is associated with the vibration of carbonyl groups in the amorphous region of the polymer [158]. The carbonyl stretching of pure PBAT is located at 1713 cm^{-1} with a shoulder at 1730 cm^{-1}, generated by the amorphous and crystalline regions, respectively [159]. These peaks were superimposed, rendering it impossible to differentiate between the two in both T733 and T734. The peak observed at 1455 cm^{-1} is ascribed to the in-plane bending vibration of the phenylene group in PBAT [160]. The peaks at 1473, 1448, and 1390 cm^{-1} are attributed to the stretching vibration of CH_2, to the asymmetric stretching vibration of CH_3, and to the symmetric stretching vibration of CH_3 groups in PBS, respectively [161]. The peak observed at 1150 cm^{-1} is ascribed to the C-O-C stretching vibration within -OCH_2CH_2 of PBS [162]. The peak observed at 1042 cm^{-1} in the PBS spectrum and the peak at 1016 cm^{-1} in the PBAT spectrum are attributed to the C-OH linkage [163]. These peaks are not discernible in the blends because of their superimposition on the 1007 cm^{-1} peak, which is associated with the Si-O stretching vibration of talc. The presence of talc is further corroborated by the peak at 664 cm^{-1},

which is generated by the bending of OH [157]. In the 1080 – 1300 cm-1 region, PBAT presents multiple peaks related to the asymmetric and symmetric vibration modes of aliphatic and aromatic ester bonds [46]. The external bending vibration of the -C-H groups in the PBAT benzene rings was observed at 727 cm^{-1} in both T733 and T734 [164].

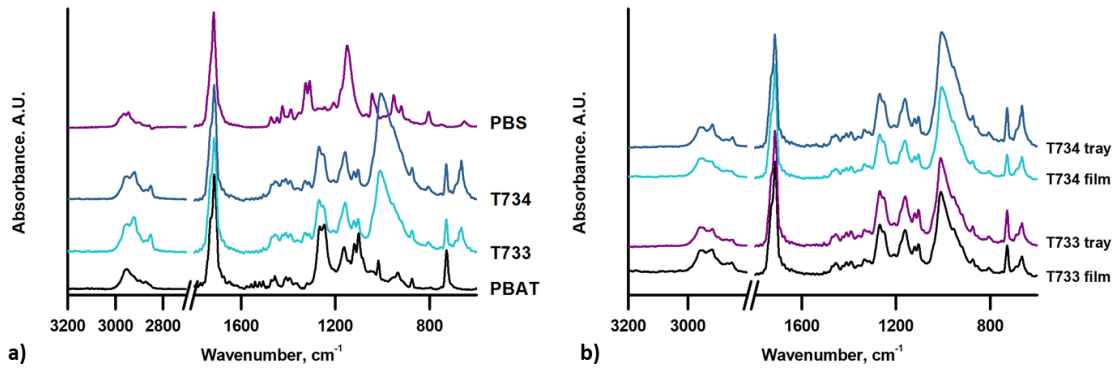

Figure 5.19 FTIR spectra of PBAT-PBS based a) pellets, and b) films and trays.

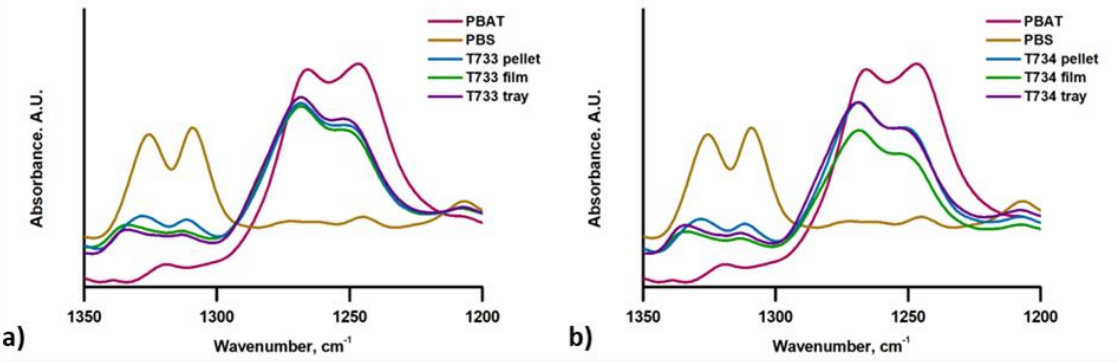

Figure 5.20 FTIR spectra in the 1350 – 1200 cm^{-1} region for pellets, films, and trays. a) T733 and b) T734.

The peaks within the 1300–1500 cm-1 range decreased in intensity as a result of subsequent reprocessing. This variation in peak intensity can be attributed to the interactions between carboxylic acid groups and epoxy or hydrogen-bond interactions [165]. The peaks at 1311 and 1328 cm^{-1} shifted to higher wavenumbers, specifically to

1313 and 1334 cm^{-1} (Figure 5.20), confirming a mutual interaction between PBAT and PBS, facilitated by the epoxy chain extender, following subsequent reprocessing [166]. In the T733 and T734 spectra, distinct peaks at 1265 and 1246 cm^{-1} emerged, indicating a reaction between the COOH groups of PBS and PBAT and the epoxy groups of the chain extender [167].

5.4 X-ray Diffraction

The results of the XRD analysis of the PLA-PHBH cast-extruded films are presented in Figure 5.21. The main peaks in each spectrum were generated by the presence of talc. Talc is characterized by two intense peaks at 9.5° and 29°, and a smaller one at approximately 19° [168], all of which are clearly visible in all blends.

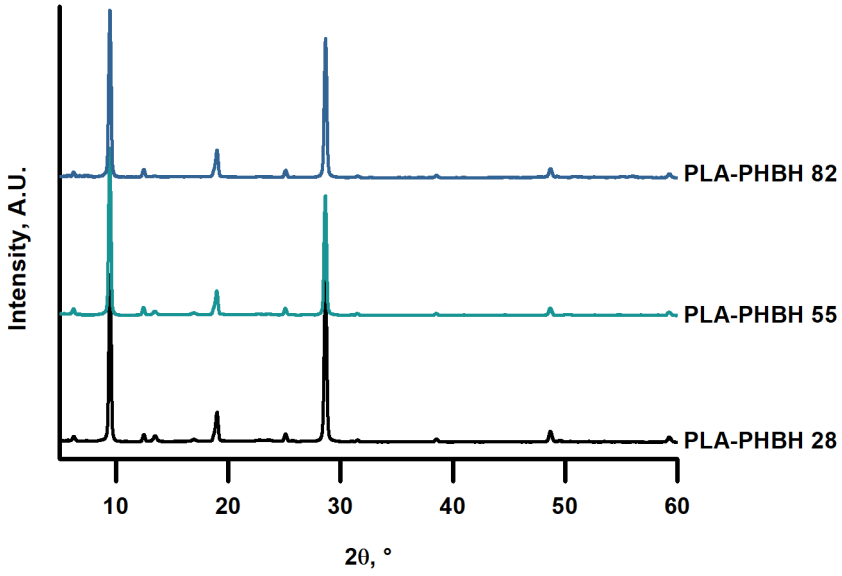

Figure 5.21 XRD Spectra of the PLA-PHBH films

The other less intense peaks can be attributed to PLA or PHBH. In particular, the peak at 16.8° is characteristic of α-phase PLA [169]. PHBH forms an orthorhombic lattice system [170] composed solely of HB units [150]. The peak at 13.5° corresponds to the (020) plane of PHBH [171], whereas the peak at 25° corresponds to the (121) plane of PHBH

[172]. PHBH is typically a semicrystalline polymer [173], whereas PLA is amorphous [174]. The identification of a peak in the crystalline structure of PLA suggests that talc acts as a nucleating agent for PLA [175]. The XRD spectra of the pellets are shown in Figure 5.22. Both T733 and T34 exhibited distinct peaks at 29.5° and 49.3°, corresponding to the (003) and (005) planes of talc, respectively [176]. PBAT is characterized by a semicrystalline structure with low crystallinity, resulting in weak diffraction peak intensities [164].The characteristic peaks of PBAT were primarily observed in the 16°–26° range. In this instance, the sole discernible peak was located at 23.6°, corresponding to the (011) plane [177]. The peaks observed at 19.8° and 27.8° are attributable to the (020) and (111) planes of the α-crystals of PBS, respectively [178].

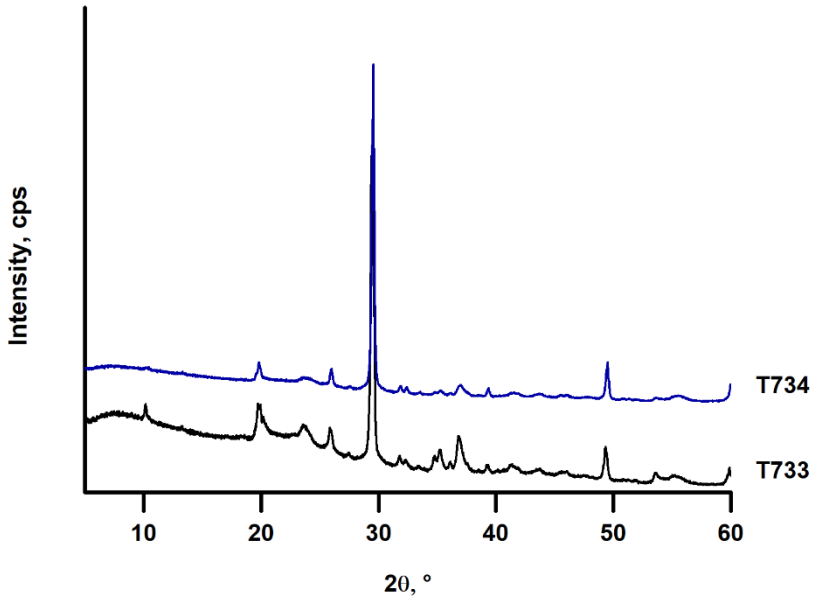

Figure 5.22 XRD Spectra of PBAT – PBS based compounds

5.5 Thermal characterization

5.5.1 DSC Analysis

The results of the thermal characterization of the PLA-PHBH blends are presented in Figure 5.23 and Table 5.10. The PLA and PHBH grades used exhibited melting peaks

within the same temperature range; therefore, only one endothermic event associated with fusion was observed in each thermogram. PLA–PHBH 28 exhibited a double melting peak, which was associated with the recrystallization of PHBH [179]. In the second heating scan, this double peak appeared more distinct, possibly due to the formation of imperfect crystals during the cooling ramp. These imperfect crystals melt at lower temperatures and subsequently rearrange into more stable crystalline structures, which are characterized by higher melting temperatures [180]. In PLA–PHBH 55 and PLA–PHBH 82, cold crystallization was observed in both the first and second heating scans. The temperature and enthalpy of cold crystallization increased with PLA content, indicating that PHBH restricted the chain mobility of PLA. In PLA-PHBH 28, the cold crystallization of PLA was not observed. As the PHBH content increased, the melting enthalpy of the compound also increased. This is consistent with the fact that PLA is substantially an amorphous polymer, whereas the PHBH grade used has a high crystallinity. In PLA–PHBH 55, PLA exhibited the lowest glass transition temperature.

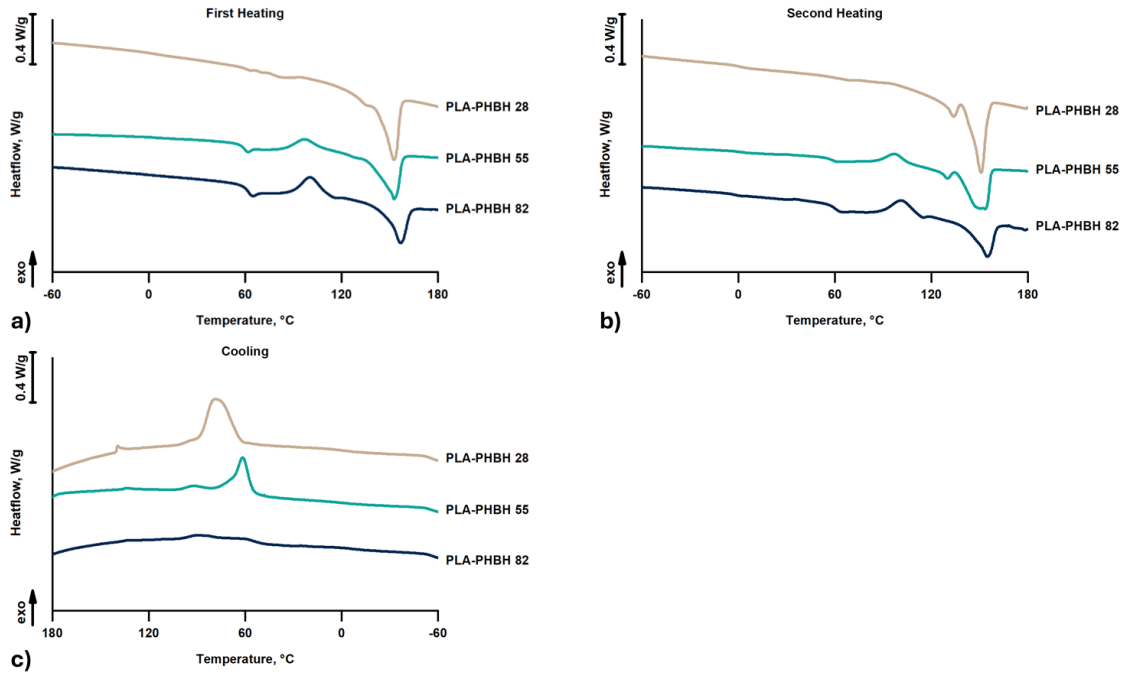

Figure 5.23 DSC thermograms of the PLA-PHBH compounds: a) First Heating; b) Second Heating; c) Cooling.

In the cooling curves, the crystallization peaks can be attributed to both PHBH and PLA. PLA typically does not exhibit crystallization peaks when cooled at high rates, such as those used in the present study. However, the presence of PHBH and talc may have acted as nucleating agents, resulting in the appearance of small peaks in the cooling thermograms. This effect was also observed in PLA/PBS blends, where PBS acted as a nucleating agent, even in the molten state [181]. Talc tends to increase the crystallization temperature of PHBH while simultaneously limiting its cold crystallization [28]. The melting temperature of PLA-PHBH 28 obtained from the second heating scan is about 3 °C lower than that of PLA-PHBH 55 and PLA-PHBH 82. This may be due to a reduction in the mobility of PLA segments associated with the PHBH polymeric phase, which leads to the formation of more defective PLA crystals [182]. In the cooling scan, the crystallization peaks of PLA and PHBH can be clearly identified. In PLA-PHBH 28, the peak at the higher temperature, which can be attributed to PLA [183], appears as a shoulder. The presence of distinct crystallization peaks indicates that both PHBH and PLA spherulites are present in the blends [184].

Table 5.10 Results of the DSC Analysis of the PLA-PHBH compounds

First Heating						
	T_g PHBH (°C)	T_g PLA (°C)	T_{cc} (°C)	ΔH_{cc} (J/g)	T_m (°C)	ΔH_m (J/g)
PLA-PHBH 82	/	64.9	100.5	12.1	156.0	-21.6
PLA-PHBH 55	4.4	59.8	97.1	7.6	152.2	-30.4
PLA-PHBH 28	3.8	67.7	/	/	152.1	-36.7
Second Heating						
	T_g PHBH (°C)	T_g PLA (°C)	T_{cc} (°C)	ΔH_{cc} (J/g)	T_m (°C)	ΔH_m (J/g)
PLA-PHBH 82	-3.3	59.3	101.1	10.6	154.0	-19.2
PLA-PHBH 55	1.6	57.4	97.1	6.7	153.2	-32.3
PLA-PHBH 28	0.8	59.2	/	/	150.4	-45.3
Cooling						
	T_c (°C)			ΔH_c (J/g)		
PLA-PHBH 82	88.6			11.4		
PLA-PHBH 55	61.7			25.1		
PLA-PHBH 28	78.7			41.2		

The DSC thermograms of PBAT-PBS blends are shown in Figure 5.24, and the data derived from these curves are presented in Table 5.11. In all the scans, a single glass

transition temperature was observed at approximately -30 °C, which can be attributed to the superimposition of T_g of PBS and PBAT [181, 185]. In the first heating curves, an endothermic event was detected within the 35–45 °C range, which was absent in subsequent heating curves. This minor endotherm is associated with the production process of the compounds and is generated by PBS. Specifically, when PBS crystallizes at low temperatures, a small endothermic event is observable at approximately 40–45 °C. This peak subsequently shifts towards higher temperatures as the crystallization temperature increases [186]. In the first heating curve, T733 exhibited a cold crystallization at approximately 94 °C. Cold crystallization phenomena were observed in both T733 and T734 during the second heating curve, occurring at approximately 89 °C and 90.5 °C, respectively. This cold crystallization is attributable to PBS, which exhibits a recrystallization peak following isothermal crystallization at temperatures up to 95 °C [187].

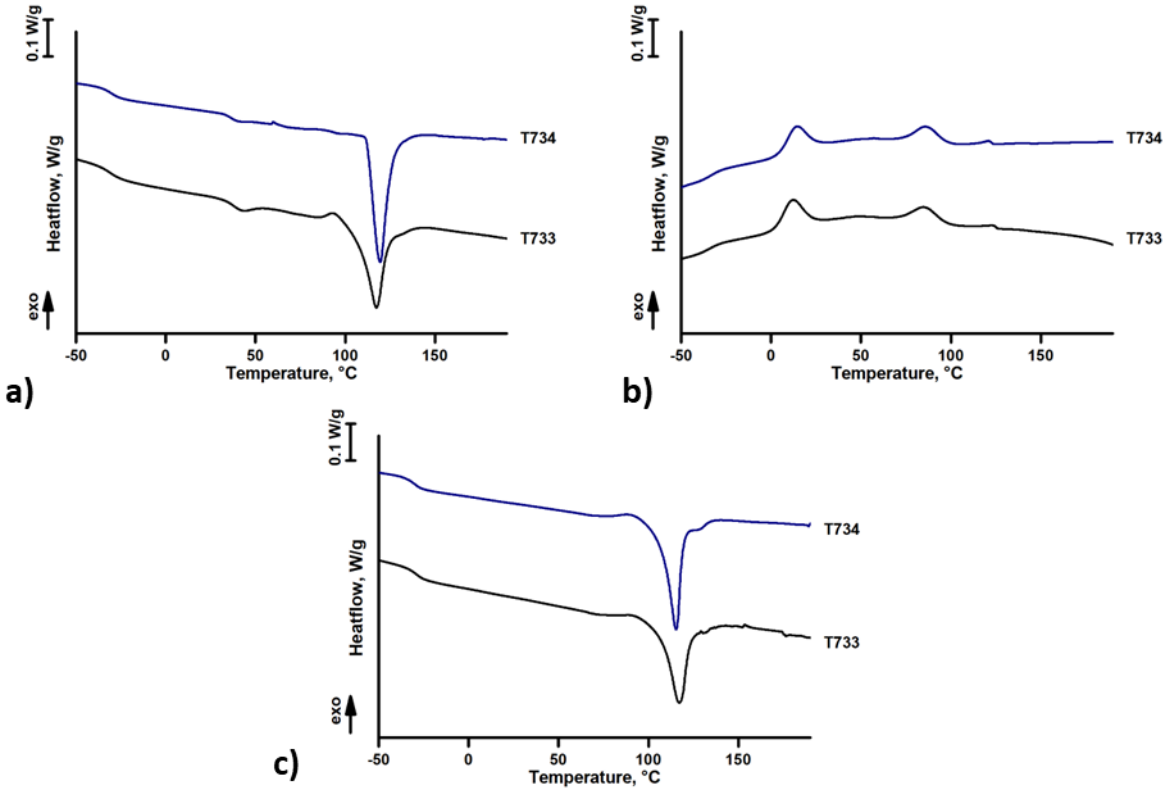

Figure 5.24 DSC thermograms: a) First heating, b) Cooling and c) Second Heating

Across all heating curves, a singular endothermic event was discernible, given that both PBAT and PBS exhibited melting temperatures within the 115–125 °C range. The melting peak temperature observed in the second heating curve was slightly lower for T734 than for T733. However, the endothermic melting peak of T734 is narrower and more concentrated around the melting temperature, suggesting the nucleating effect of talc in facilitating the formation of more uniform and homogenous crystalline regions.

In the cooling scan, two distinct crystallization peaks were discernible, indicating the formation of both PBS and PBAT crystalline structures. The crystallization temperature of pure PBS is approximately 85 °C [188]. However, a shift towards lower temperatures was observed in the PBAT/PBS blends, where PBS was the secondary phase. Notably, in PBAT/PBS blends, where PBAT is the predominant polymeric phase, the formation of PBS crystalline structures may vary. This phenomenon was corroborated by the emergence of broad crystallization peaks at lower temperatures [47]. Consequently, in this context, the crystallization peak at 12–15 °C is associated with PBS, whereas the peak at 85–87 °C is attributed to PBAT.

Table 5.11 Results of the DSC Analysis

First heating				
	T_g (°C)	**T_m (°C)**	**ΔH_m (J/g)**	
T733	-31.6	116.9	-20.0	
T734	-31.5	118.9	-18.6	
Cooling				
	T_c (°C)		**ΔH_c (J/g)**	
T733	85.2	12.2	3.9	5.5
T734	86.5	14.4	6.6	5.2
Second heating				
	T_g (°C)	**T_m (°C)**	**ΔH_m (J/g)**	
T733	-29.1	116.8	-17.5	
T734	-30.5	114.8	-19.6	

5.5.2 Thermal resistance

The results of the functional tests are displayed in Figure 5.25, Figure 5.26, Figure 5.27, Figure 5.28, and Figure 5.29. The objective of the test was to replicate the conditions

under which a tray might be used as a takeaway container, particularly when filled with hot food. The results indicated that the trays did not undergo significant deformation, and their geometry remained largely unchanged. This outcome aligns with the melting temperature determined through Differential Scanning Calorimetry (DSC) measurements. All trays demonstrated substantial thermal resistance, thereby confirming their appropriateness for use as single-use containers for takeaway hot food.

Figure 5.25 Thermal resistance test of PLA-PHBH 82 trays. From left to right: before, during and after the test.

Figure 5.26 Thermal resistance test of PLA-PHBH 55 trays. From left to right: before, during and after the test.

Figure 5.27 Thermal resistance test of PLA-PHBH 28 trays. From left to right: before, during and after the test.

Figure 5.28 Thermal resistance test of T733 trays. From left to right: before, during and after the test.

Figure 5.29 Thermal resistance test of T734 trays. From left to right: before, during and after the test.

5.6 Product cost evaluation

Currently, several alternative bioplastics are available in the market, with most being successfully commercialized and utilized for the production of high-consumption products. In 2024, bioplastics dominated the market for both rigid and flexible packaging, surpassing fossil-based production in most instances (Figure 5.30). The properties of bioplastics can match those of fossil-based plastics; therefore, cost becomes the determining factor in several specific applications.

In the realm of industrialization, the essential criteria for PLA-PHBH blends include a material cost capped at €0.03 per tray, matching that of polypropylene, a cycle time under 5 seconds, and the ability to retain over 90% of PHBH molecular weight after being processed at 150°C. Polypropylene (PP) is priced at €1.5 per kilogram, with a standard tray weighing 20 grams. To maintain an equivalent cost per tray, the mass of the bioplastic blend must be reduced to less than 13 grams, given a blend cost of approximately €2.3 per kilogram. A weight reduction of 30–35% is technically feasible, provided that the

processability of the sheet is verified at reduced thicknesses. This is because the inclusion of 20% talc effectively doubles the flexural modulus of the blend in comparison to pure PLA [55]. In the context of PBAT-PBS blends, cost requirements are more readily achievable. The cost of PBS ranges from $2900/MT to $3100/MT, while PBAT costs range from $1500/MT to $1800/MT. Incorporating 40% talc into the formulation results in a bio-based blend with a cost of 1.60 €/kg. To maintain the same cost per tray, a weight reduction of 5–10% per item is necessary, which is technically feasible when the compounds exhibit good processability.

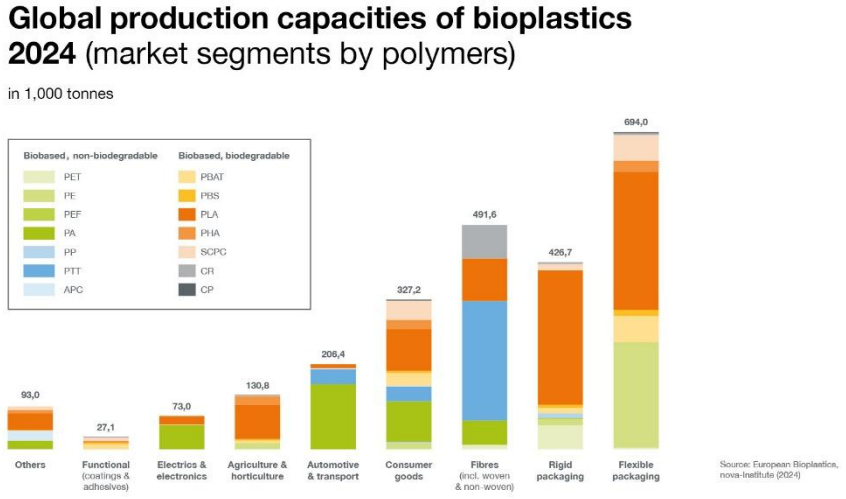

Figure 5.30 Global production capacities of bioplastics 2024 (market segments by polymers) [189]

The estimated costs of the compounds are detailed in Table 5.12. These costs pertain solely to the raw materials. The PBAT/PBS compounds are characterized by a low cost, primarily due to the recent price reduction of PBAT. In contrast, the PLA/PHBH formulation incurs higher material costs, largely attributable to the lower percentage of talc and the elevated cost of PHBH. Polyhydroxyalkanoates are associated with a high market price, ranging from 5 €/kg to 10 €/kg, contingent upon the producer. Consequently, the PLA-PHBH 28 formulation exhibits the highest material cost among all formulations.

Table 5.12 Cost of the defined materials per kg

	Cost of material per kg (€)
T733	1.71 €
T734	1.59 €
PLA-PHBH 28	4.26 €
PLA-PHBH 55	3.62 €
PLA-PHBH 82	2.98 €

Table 5.13 Cost of cast extruded sheets per kg

	Cost of cast extruded sheets per kg (€)
T733	2.21 €
T734	2.09 €
PLA-PHBH 28	4.76 €
PLA-PHBH 55	4.12 €
PLA-PHBH 82	3.48 €

Table 5.13 presents the cost associated of cast extruded sheets. This cost assessment incorporates an energy expenditure of 0.07 €/kg and a labor cost of 0.05 €/kg. Additionally, general costs amounting to 0.38 €/kg were considered, encompassing equipment depreciation, maintenance expenses, general overheads, and packaging costs related to the transportation of sheet rolls. Notably, the latter cost, estimated at 0.03 €/kg, can be eliminated if the thermoforming line is integrated continuously with the cast extrusion line.

The cost analysis of the final products was conducted, incorporating the thermoforming process. An industrial facility was considered for this evaluation, with an assumed theoretical annual production of 27,707,400 trays and an overall operational efficiency of 90%. Figure 5.31, Figure 5.32, and Figure 5.33 illustrate the cost per kilogram of the final product and the influence of material costs, the cast extrusion process, and the thermoforming process on the overall cost. In the cases of T734 and T733, the combined production costs account for approximately 50% of the total cost. The formulations PLA-PHBH 28 and PLA-PHBH 55 exhibit the highest total costs, primarily due to their elevated material costs. Conversely, PLA-PHBH 82 demonstrates lower overall

production costs compared to other PLA-PHBH-based formulations, which, when coupled with its slightly reduced material cost, results in a more competitive final price.

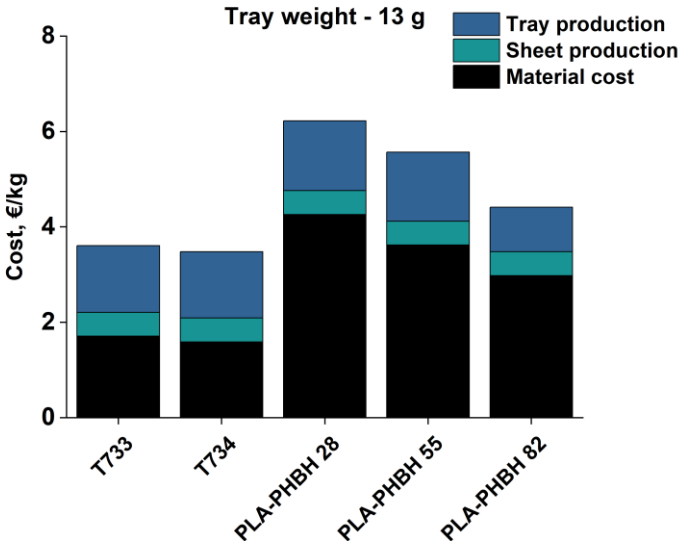

Figure 5.31 Cost per kg related to the production of 13 g - trays

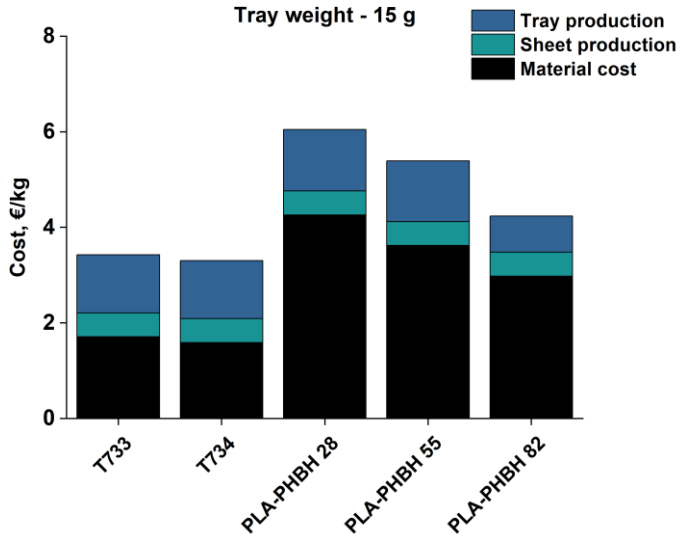

Figure 5.32 Cost per kg related to the production of 15 g - trays

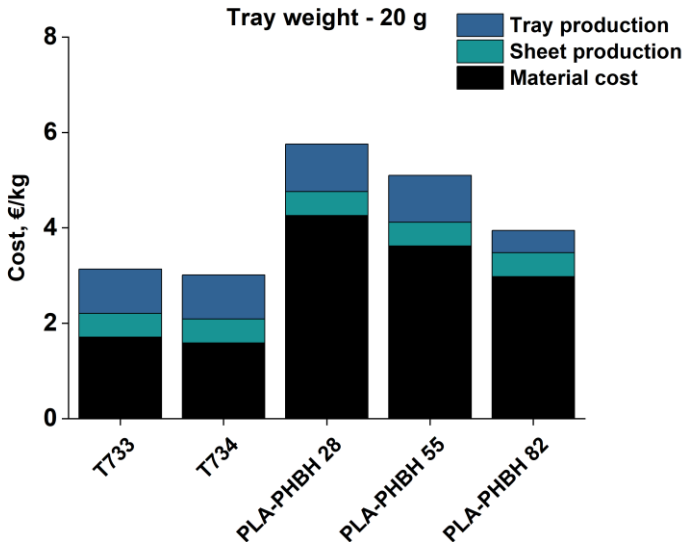

Figure 5.33 Cost per kg related to the production of 20 g - trays

For all materials, the total cost per kilogram (€/kg) remains largely unaffected by variations in tray weight. This observation indicates that the cost calculation is primarily influenced by fixed material pricing and relatively stable processing costs per unit mass of the polymer, rather than by the specific geometry or wall thickness variations necessitated by different tray weights.

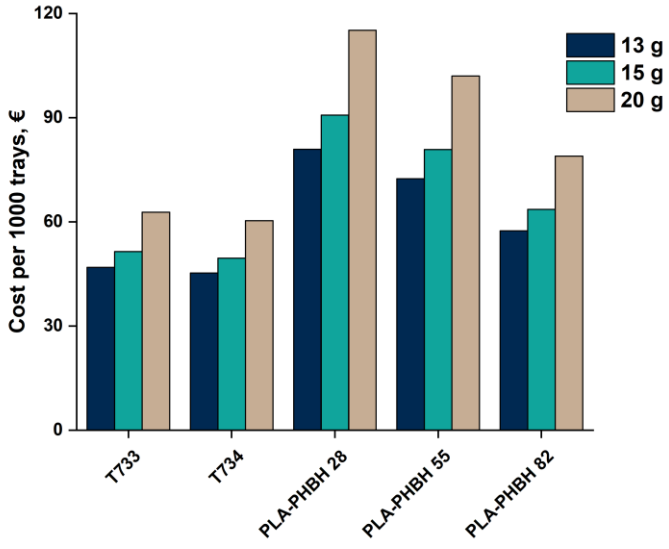

Figure 5.34 Material cost per 1000 trays

Figure 5.34 illustrates the final cost per 1000 trays as a function of material type and individual tray weight. As anticipated, the cost of the trays increases with the rising weight of the product, due to the greater amount of material required. T733 and T734 consistently maintain the lowest cost across all weights. Specifically, T733 and T734 exhibit a cost per tray of 0.06 € for 20 g trays. Both formulations can achieve cost parity with polypropylene by reducing the mass to 15 g. In this scenario, both T733 and T734 achieve a price per tray of approximately 0.05 €. In contrast, the PLA-PHBH blends incur a significantly higher cost, necessitating a reduction in weight to 13 g to reach 0.06 €/kg and approximate the cost of polypropylene trays. The previously mentioned increased cost is associated with PHBH, which is comparatively more expensive. Anticipated shifts in the production landscape of these polymers may alter the cost assessment, potentially leading to the development of new, low-cost compounds that are characterized by both reduced expenses and a diminished environmental impact.

6 Conclusions and future developments

This thesis aimed to define, investigate, and experimentally develop cost-effective bioplastic compounds suitable for thermoforming applications. Two distinct sets of materials were examined. The first set comprised compounds based on PLA and PHBH, while the second set included compounds based on PBAT and PBS. The PLA/PHBH compounds incorporated talc at a concentration of 20 wt%. The presence of PHBH, which tends to degrade during extrusion due to shear and thermal stress, limited the incorporation of higher percentages of mineral fillers. PHBH is a polyhydroxyalkanoate, a bioplastic derived from bacterial fermentation, characterized by its marine biodegradability and reduced environmental impact. This set of formulations demonstrated exceptional processability during compounding, cast-extrusion, and thermoforming processes. The properties of the compound were deemed appropriate for the production of food trays, as corroborated by subsequent evaluations of functional properties. Compression tests on trays composed of compounds with high PHBH content demonstrated failure only under conditions of significant deformation, thereby confirming their suitability for standard applications. Trays with a high concentration of PLA did not exhibit breakage. Thermal resistance assessments conducted with boiling water did not indicate any significant dimensional alterations in the trays.

The second set of analyzed formulations pertains to the investigation of compounds based on PBAT and PBS, with PBAT serving as the primary phase. PBAT is a bioplastic noted for its superior mechanical properties. Although initially synthesized from fossil sources, grades of PBAT derived entirely from renewable feedstocks have recently become commercially available. Concurrently, the cost of PBAT has decreased significantly, rendering this bioplastic appealing for single-use applications. The polymers' excellent processability and resistance to degradation have facilitated the incorporation of mineral filler at levels up to 40 wt%, thereby enabling a substantial reduction in compound cost. The studied compounds demonstrate exceptional processability in extrusion, cast-extrusion, and thermoforming. The properties of the compounds are suitable for the production of trays, as confirmed by subsequent evaluations of functional properties. None of the trays experienced failure during compression testing, and the thermal stability test did not result in significant deformation of the trays.

The formulations analyzed in this study achieve an optimal balance between cost, stiffness, and environmental sustainability. When prioritizing reduced environmental impact, the PLA/PHBH formulations stand out as the most suitable choice, although with higher production costs. Conversely, PBAT/PBS-based formulations are ideal when minimizing cost is the primary concern.

Future research endeavors will primarily focus on the development of injection molding compounds and the evaluation of their environmental impact. Injection molding technology is used to produce numerous single-use tableware items, such as forks, spoons, and knives. This process necessitates materials with adequate fluidity to fill the mold expeditiously and with minimal energy consumption. In comparison to the formulations developed in the present thesis, rheological modifications will be essential to achieve compounds with high Melt Flow Index values, ideally exceeding 20 g/10 min at processing temperatures. This can be achieved through the application of rheological modifiers and by the proper selection of the polymer grades utilized in the formulations. The presence of talc, especially in large quantities, tends to reduce the fluidity of compounds, a factor that must be taken into account during the formulation design process.

To facilitate a comprehensive evaluation of products, it is essential to conduct Life Cycle Assessment (LCA) studies. Environmental impact analyses are generally executed using well-established commercial databases, such as Ecoinvent. However, these databases predominantly encompass long-established production processes and materials. The modeling of synthesis processes for bioplastics necessitates further development and in-depth investigation, particularly within the proposed framework. In the scientific literature, LCA studies on polyhydroxyalkanoates frequently pertain to laboratory-scale production, which is considerably more impactful per kilogram of material produced compared to industrial-scale processes, where economies of scale can be leveraged across various stages. Similarly, it is imperative to refine the impact profiles for PBAT, especially in light of the novel renewable feedstocks from which it can now be synthesized.

The evaluation of production costs and competitiveness in comparison to conventional plastics was performed within the context of the current techno-economic environment

(years 2024–2026). The chemical industry is actively engaged in developing innovative systems to produce cost-effective bioplastics with a diminished environmental impact. Emerging economic equilibria may result in price reductions for other bioplastics in the forthcoming years, as observed with PBAT. Additionally, significant efforts are being made by polyhydroxyalkanoate manufacturers to decrease their costs and identify more efficient production methodologies. These dynamics have the potential to facilitate the emergence and commercialization of new materials in the near future, thereby creating opportunities for the development of novel low-cost compounds.

References

1. European Commission (2019) Directive (EU) 2019/904 of the European Parliament and of the Council of 5 June 2019 on the reduction of the impact of certain plastic products on the environment

2. Presidenza del Consiglio dei Ministri (2021) DECRETO LEGISLATIVO 8 novembre 2021, n. 196 - Normativa

3. Coiai S, Di Lorenzo ML, Cinelli P, et al (2021) Binary Green Blends of Poly(lactic acid) with Poly(butylene adipate-co-butylene terephthalate) and Poly(butylene succinate-co-butylene adipate) and Their Nanocomposites. Polymers 13:2489. https://doi.org/10.3390/polym13152489

4. Schyns ZOG, Shaver MP (2021) Mechanical Recycling of Packaging Plastics: A Review. Macromolecular Rapid Communications 42:2000415. https://doi.org/10.1002/marc.202000415

5. Cosate de Andrade MF, Fonseca G, Morales AR, Mei LHI (2018) Mechanical recycling simulation of polylactide using a chain extender. Advances in Polymer Technology 37:2053–2060. https://doi.org/10.1002/adv.21863

6. Agüero A, Morcillo MDC, Quiles-Carrillo L, et al (2019) Study of the Influence of the Reprocessing Cycles on the Final Properties of Polylactide Pieces Obtained by Injection Molding. Polymers 11:1908. https://doi.org/10.3390/polym11121908

7. Åkesson D, Vrignaud T, Tissot C, Skrifvars M (2016) Mechanical Recycling of PLA Filled with a High Level of Cellulose Fibres. J Polym Environ 24:185–195. https://doi.org/10.1007/s10924-016-0760-0

8. Żenkiewicz M, Richert J, Rytlewski P, et al (2009) Characterisation of multi-extruded poly(lactic acid). Polymer Testing 28:412–418. https://doi.org/10.1016/j.polymertesting.2009.01.012

9. Lendvai L, Bódi V, Danko M, et al (2025) Successive Mechanical Recycling of Poly(lactic Acid) by Injection Molding: Evolution of Molecular, Thermal, and Mechanical Properties. Macromolecular Materials and Engineering. https://doi.org/10.1002/mame.202500349

10. Koca N, Aversa C, Barletta M (2023) Recycling of poly(lactic acid)/poly(butylene succinate) (PLA/PBS) blends with high amounts of secondary raw material. Journal of Applied Polymer Science 140:e54659. https://doi.org/10.1002/app.54659

11. Milo di Villagrazia M, Caggiano A, Genovesi A, Barletta M (2025) Development of low environmental impact technological solutions based on PLA, PBS, PBAT and Talc blends for multilayer food packaging manufacturing

12. Dybka-Stępień K, Antolak H, Kmiotek M, et al (2021) Disposable Food Packaging and Serving Materials—Trends and Biodegradability. Polymers 13:3606. https://doi.org/10.3390/polym13203606

13. Mohareb E, Mittal GS (2007) Formulation and process conditions for biodegradable/edible soy-based packaging trays. Packaging Technology and Science 20:1–15. https://doi.org/10.1002/pts.736

14. Troya MDC, Power O-P, Kopke K (2022) Is It All About the Data? How Extruded Polystyrene Escaped Single-Use Plastic Directive Market Restrictions. Front Mar Sci 8:. https://doi.org/10.3389/fmars.2021.817707

15. Kale G, Kijchavengkul T, Auras R, et al (2007) Compostability of Bioplastic Packaging Materials: An Overview. Macromolecular Bioscience 7:255–277. https://doi.org/10.1002/mabi.200600168

16. Atiwesh G, Mikhael A, Parrish CC, et al (2021) Environmental impact of bioplastic use: A review. Heliyon 7:. https://doi.org/10.1016/j.heliyon.2021.e07918

17. Cheng H-Y, Yang Y-J, Li S-C, et al (2015) Modification and extrusion coating of polylactic acid films. Journal of Applied Polymer Science 132:. https://doi.org/10.1002/app.42472

18. Eraslan K, Aversa C, Nofar M, et al (2022) Poly(3-hydroxybutyrate-co-3-hydroxyhexanoate) (PHBH): Synthesis, properties, and applications - A review. European Polymer Journal 167:111044. https://doi.org/10.1016/j.eurpolymj.2022.111044

19. Soleymani Eil Bakhtiari S, Salehiyan R, Sasi A, et al (2025) The Critical Role of Processing Sequence on the Mechanical Properties of Reactively Compatibilized PLA/PBAT Blends: Effect of Manufacturing Method. Macromolecular Materials and Engineering n/a:e00108. https://doi.org/10.1002/mame.202500108

20. Michaeli W, Greefenstein A, Berghaus U (1995) Twin-Screw extruders for reactive extrusion. Polymer Engineering & Science 35:1485–1504. https://doi.org/10.1002/pen.760351902

21. Martin C (2016) Twin Screw Extruders as Continuous Mixers for Thermal Processing: a Technical and Historical Perspective. AAPS PharmSciTech 17:3–19. https://doi.org/10.1208/s12249-016-0485-3

22. Treece MA, Oberhauser JP (2007) Processing of polypropylene–clay nanocomposites: Single-screw extrusion with in-line supercritical carbon dioxide feed versus twin-screw extrusion. Journal of Applied Polymer Science 103:884–892. https://doi.org/10.1002/app.25226

23. Zhou Y, Huang Z, Diao X, et al (2015) Characterization of the effect of REC on the compatibility of PHBH and PLA. Polymer Testing 42:17–25. https://doi.org/10.1016/j.polymertesting.2014.12.014

24. Post W, Kuijpers LJ, Zijlstra M, et al (2021) Effect of Mineral Fillers on the Mechanical Properties of Commercially Available Biodegradable Polymers. Polymers 13:394. https://doi.org/10.3390/polym13030394

25. Alias NH, Abdullah N, Othman NH, et al (2022) Sustainability Challenges and Future Perspectives of Biopolymer. In: Nadda AK, Sharma S, Bhat R (eds) Biopolymers: Recent Updates, Challenges and Opportunities. Springer International Publishing, Cham, pp 373–389

26. Genovesi A, Aversa C, Barletta M, et al (2023) Role of wood flour on processability of marine biodegradable poly (3-hydroxybutyrate-co-3-hydroxyhexanoate) (PHBH)/poly(butylene succinate-co-butylene adipate) (PBSA) blends in cast extrusion and thermoforming of take-away food containers. Journal of Applied Polymer Science n/a:e54346. https://doi.org/10.1002/app.54346

27. Ahmad Fauzi AA, Osman AF, Alrashdi AA, et al (2022) On the Use of Dolomite as a Mineral Filler and Co-Filler in the Field of Polymer Composites: A Review. Polymers 14:2843. https://doi.org/10.3390/polym14142843

28. Vandewijngaarden J, Murariu M, Dubois P, et al (2016) Effect of ultrafine talc on crystallization and end-use properties of poly(3-hydroxybutyrate-co-3-hydroxyhexanoate). Journal of Applied Polymer Science 133:. https://doi.org/10.1002/app.43808

29. Xu P, Wang Q, Yu M, et al (2021) Enhanced crystallization and storage stability of mechanical properties of biosynthesized poly (3-hydroxybutyrate-*co*-3-hydroxyhexanate) induced by self-nucleation. International Journal of Biological Macromolecules 184:797–803. https://doi.org/10.1016/j.ijbiomac.2021.06.120

30. Xiang H, Wen X, Miu X, et al (2016) Thermal depolymerization mechanisms of poly(3-hydroxybutyrate-co-3-hydroxyvalerate). Progress in Natural Science: Materials International 26:58–64. https://doi.org/10.1016/j.pnsc.2016.01.007

31. Feijoo P, Samaniego-Aguilar K, Sánchez-Safont E, et al (2022) Development and Characterization of Fully Renewable and Biodegradable Polyhydroxyalkanoate Blends with Improved Thermoformability. Polymers 14:2527. https://doi.org/10.3390/polym14132527

32. Thellen C, Coyne M, Froio D, et al (2008) A Processing, Characterization and Marine Biodegradation Study of Melt-Extruded Polyhydroxyalkanoate (PHA) Films. J Polym Environ 16:1–11. https://doi.org/10.1007/s10924-008-0079-6

33. Ramos-Hernández T, Robledo-Ortíz JR, González-López ME, et al (2023) Mechanical recycling of PLA: Effect of weathering, extrusion cycles, and chain extender. Journal of Applied Polymer Science 140:e53759. https://doi.org/10.1002/app.53759

34. Duangphet S, Szegda D, Song J, Tarverdi K (2014) The Effect of Chain Extender on Poly(3-hydroxybutyrate-co-3-hydroxyvalerate): Thermal Degradation, Crystallization, and Rheological Behaviours. J Polym Environ 22:1–8. https://doi.org/10.1007/s10924-012-0568-5

35. Gupta A, Chudasama B, Chang BP, Mekonnen T (2021) Robust and sustainable PBAT – Hemp residue biocomposites: Reactive extrusion compatibilization and

fabrication. Composites Science and Technology 215:109014. https://doi.org/10.1016/j.compscitech.2021.109014

36. Ferreira FV, Cividanes LS, Gouveia RF, Lona LMF (2019) An overview on properties and applications of poly(butylene adipate-co-terephthalate)–PBAT based composites. Polymer Engineering & Science 59:E7–E15. https://doi.org/10.1002/pen.24770

37. Luo C, Zhou Y, Chen Z, et al (2024) Comparative life cycle assessment of PBAT from fossil-based and second-generation generation bio-based feedstocks. Science of The Total Environment 954:176421. https://doi.org/10.1016/j.scitotenv.2024.176421

38. Barletta M, Genovesi A, Desole MP, Gisario A (2025) Melt processing of biodegradable poly(butylene succinate) (PBS)—a critical review. Clean Techn Environ Policy. https://doi.org/10.1007/s10098-024-03005-8

39. Muthuraj R, Misra M, Mohanty AK (2014) Biodegradable Poly(butylene succinate) and Poly(butylene adipate-co-terephthalate) Blends: Reactive Extrusion and Performance Evaluation. J Polym Environ 22:336–349. https://doi.org/10.1007/s10924-013-0636-5

40. Muthuraj R, Misra M, Kumar Mohanty A (2017) Biocomposite consisting of miscanthus fiber and biodegradable binary blend matrix: compatibilization and performance evaluation. RSC Advances 7:27538–27548. https://doi.org/10.1039/C6RA27987B

41. Chieng BW, Ibrahim NA, Wan Yunus WMZ (2010) Effect of organo-modified montmorillonite on poly(butylene succinate)/poly(butylene adipate-co-terephthalate) nanocomposites. Express Polym Lett 4:404–414. https://doi.org/10.3144/expresspolymlett.2010.51

42. Boonprasertpoh A, Pentrakoon D, Junkasem J (2017) Investigating rheological, morphological and mechanical properties of PBS/PBAT blends. Journal of Metals, Materials and Minerals 27:1–11

43. Lopes HSM, de Oliveira GHM, Maia THS, et al (2023) Transesterification of poly(butylene adipate-co-terephthalate) (PBAT) and poly(butylene succinate) (PBS) blends: variations in some processing parameters. Iran Polym J 32:313–324. https://doi.org/10.1007/s13726-022-01133-w

44. Conceição PCG, Lemos PVF, Santana JS, et al (2024) Characterization of extruded films based on poly (butylene succinate) blends to utilize a partially degraded poly (butylene adipate-co-terephthalate). Journal of Applied Polymer Science 141:e55289. https://doi.org/10.1002/app.55289

45. Promhuad K, Phothisarattana D, Laorenza Y, et al (2023) Zinc oxide enhanced the antibacterial efficacy of biodegradable PBAT/PBS nanocomposite films: Morphology and food packaging properties. Food Bioscience 55:103077. https://doi.org/10.1016/j.fbio.2023.103077

46. Bumbudsanpharoke N, Wongphan P, Promhuad K, et al (2022) Morphology and permeability of bio-based poly(butylene adipate-co-terephthalate) (PBAT), poly(butylene succinate) (PBS) and linear low-density polyethylene (LLDPE) blend films control shelf-life of packaged bread. Food Control 132:108541. https://doi.org/10.1016/j.foodcont.2021.108541

47. de Matos Costa AR, Crocitti A, Hecker de Carvalho L, et al (2020) Properties of Biodegradable Films Based on Poly(butylene Succinate) (PBS) and Poly(butylene Adipate-co-Terephthalate) (PBAT) Blends. Polymers 12:2317. https://doi.org/10.3390/polym12102317

48. Threepopnatkul P, Charoendee N, Wiriyamontree N, Phodaeng A (2022) Effect of essential oil on properties of PBAT/PBS for bio-packaging films. J Phys: Conf Ser 2175:012023. https://doi.org/10.1088/1742-6596/2175/1/012023

49. Civancik-Uslu D, Ferrer L, Puig R, Fullana-i-Palmer P (2018) Are functional fillers improving environmental behavior of plastics? A review on LCA studies. Science of The Total Environment 626:927–940. https://doi.org/10.1016/j.scitotenv.2018.01.149

50. Saw LT, Zainuddin F, Cao XV, Lan DNU (2021) The thermal-mechanical degradation of mineral-filled polypropylene-ethylene copolymer composites during extrusion process. Polymer Composites 42:83–97. https://doi.org/10.1002/pc.25809

51. Barletta M, Aversa C, Pizzi E, Puopolo M (2020) Advance on processing of compostable and thermally stable biodegradable polyester blends. Journal of Applied Polymer Science 137:48722. https://doi.org/10.1002/app.48722

52. Hassan M, Mohanty AK, Dhakal HN, Misra M (2025) Design, Optimization, and Mechanical Properties Evaluation of 3D-Printed Auxetic Structures from a Talc-Filled PLA/BioPBS/PBAT Composite for Advanced Engineering Applications. ACS Appl Eng Mater. https://doi.org/10.1021/acsaenm.5c00697

53. Weidenfeller B, Höfer M, Schilling FR (2004) Thermal conductivity, thermal diffusivity, and specific heat capacity of particle filled polypropylene. Composites Part A: Applied Science and Manufacturing 35:423–429. https://doi.org/10.1016/j.compositesa.2003.11.005

54. Hinterberger K, Main P, Waly C, Lucyshyn T (2025) Effect of Epoxy Chain Extender and Multiple Processing on Poly-(R)-3-Hydroxybutyrate's Properties. J Polym Environ 33:112–124. https://doi.org/10.1007/s10924-024-03425-z

55. Yu F, Liu T, Zhao X, et al (2012) Effects of talc on the mechanical and thermal properties of polylactide. Journal of Applied Polymer Science 125:E99–E109. https://doi.org/10.1002/app.36260

56. Lackner M, Mukherjee A, Koller M (2023) What Are "Bioplastics"? Defining Renewability, Biosynthesis, Biodegradability, and Biocompatibility. Polymers (Basel) 15:4695. https://doi.org/10.3390/polym15244695

57. EUBIO_Admin Bioplastics. In: European Bioplastics e.V. https://www.european-bioplastics.org/bioplastics/. Accessed 5 Aug 2025

58. European Bioplastics (2022) What are bioplastics? https://docs.european-bioplastics.org/publications/fs/EuBP_FS_What_are_bioplastics.pdf

59. Samuel H, Ekpan F-DM, Ori MO (2024) Biodegradable, Recyclable, and Renewable Polymers as Alternatives to Traditional Petroleum-based Plastics. Asian Journal of Environmental Research 1:152–165. https://doi.org/10.69930/ajer.v1i3.86

60. Moreno Raja M, Lim PQ, Wong YS, et al (2019) Chapter 18 - Polymeric Nanomaterials: Methods of Preparation and Characterization. In: Mohapatra SS, Ranjan S, Dasgupta N, et al (eds) Nanocarriers for Drug Delivery. Elsevier, pp 557–653

61. Taib N-AAB, Rahman MR, Huda D, et al (2023) A review on poly lactic acid (PLA) as a biodegradable polymer. Polym Bull 80:1179–1213. https://doi.org/10.1007/s00289-022-04160-y

62. Ashby MF (2013) Chapter 15 - Material profiles. In: Ashby MF (ed) Materials and the Environment (Second Edition). Butterworth-Heinemann, Boston, pp 459–595

63. Intellect MR Largest PLA producers curbing the edge of the non-biodegradable plastics. In: Market Research Intellect. https://www.marketresearchintellect.com/blog/largest-pla-producers/. Accessed 5 Aug 2025

64. NatureWorks | Home. https://www.natureworksllc.com/. Accessed 5 Aug 2025

65. Products. In: TotalEnergies Corbion. https://totalenergies-corbion.com/products/. Accessed 5 Aug 2025

66. Xu J, Manepalli PH, Zhu L, et al (2019) Morphological, barrier and mechanical properties of films from poly (butylene succinate) reinforced with nanocrystalline cellulose and chitin whiskers using melt extrusion. Journal of Polymer Research 26:. https://doi.org/10.1007/s10965-019-1783-8

67. Xu J, Guo B-H (2010) Poly(butylene succinate) and its copolymers: Research, development and industrialization. Biotechnology Journal 5:1149–1163. https://doi.org/10.1002/biot.201000136

68. Rafiqah SA, Khalina A, Harmaen AS, et al (2021) A Review on Properties and Application of Bio-Based Poly(Butylene Succinate). Polymers 13:1436. https://doi.org/10.3390/polym13091436

69. Barletta M, Aversa C, Ayyoob M, et al (2022) Poly(butylene succinate) (PBS): Materials, processing, and industrial applications. Progress in Polymer Science 132:101579. https://doi.org/10.1016/j.progpolymsci.2022.101579

70. Home | PTT MCC BIOCHEM CO., LTD. https://pttmcc.com/. Accessed 6 Aug 2025

71. XINJIANG BLUE RIDGE TUNHE POLYESTER CO. LTD. https://www.pbat-resin.com/. Accessed 6 Aug 2025

72. Bartolucci L, Cordiner S, De Maina E, et al (2023) Sustainable Valorization of Bioplastic Waste: A Review on Effective Recycling Routes for the Most Widely Used Biopolymers. International Journal of Molecular Sciences 24:7696. https://doi.org/10.3390/ijms24097696

73. Roy S, Ghosh T, Zhang W, Rhim J-W (2024) Recent progress in PBAT-based films and food packaging applications: A mini-review. Food Chemistry 437:137822. https://doi.org/10.1016/j.foodchem.2023.137822

74. Küster AN, Paula C, Azevedo J, et al (2025) Formulations, Processing, and Application of Poly(butylene adipate-co-terephthalate)/Thermoplastic Starch Blends: A Review. Polymers 17:1457. https://doi.org/10.3390/polym17111457

75. Raquez JM, Nabar Y, Narayan R, Dubois P (2008) Novel High-Performance Talc/Poly[(butylene adipate)-co-terephthalate] Hybrid Materials. Macromolecular Materials and Engineering 293:310–320. https://doi.org/10.1002/mame.200700352

76. Jian J, Xiangbin Z, Xianbo H (2020) An Overview on Synthesis, Propertiesand Applications of Poly(butylene-adipate-co-terephthalate)–PBAT. Advanced Industrial and Engineering Polymer Research 3:. https://doi.org/10.1016/j.aiepr.2020.01.001

77. Bordes P, Pollet E, Avérous L (2009) Nano-biocomposites: Biodegradable polyester/nanoclay systems. Progress in Polymer Science 34:125–155. https://doi.org/10.1016/j.progpolymsci.2008.10.002

78. Lule ZC, Kim J (2021) Properties of economical and eco-friendly polybutylene adipate terephthalate composites loaded with surface treated coffee husk. Composites Part A: Applied Science and Manufacturing 140:106154. https://doi.org/10.1016/j.compositesa.2020.106154

79. Zhang X, Ma P, Zhang Y (2016) Structure and properties of surface-acetylated cellulose nanocrystal/poly(butylene adipate-co-terephthalate) composites. Polym Bull 73:2073–2085. https://doi.org/10.1007/s00289-015-1594-y

80. Li X, Ai X, Pan H, et al (2018) The morphological, mechanical, rheological, and thermal properties of PLA/PBAT blown films with chain extender. Polymers for Advanced Technologies 29:1706–1717. https://doi.org/10.1002/pat.4274

81. Khanna S, Srivastava AK (2005) Recent advances in microbial polyhydroxyalkanoates. Process Biochemistry 40:607–619. https://doi.org/10.1016/j.procbio.2004.01.053

82. Lee SY (1996) Bacterial polyhydroxyalkanoates. Biotechnology and Bioengineering 49:1–14. https://doi.org/10.1002/(SICI)1097-0290(19960105)49:1%253C1::AID-BIT1%253E3.0.CO;2-P

83. Możejko-Ciesielska J, Kiewisz R (2016) Bacterial polyhydroxyalkanoates: Still fabulous? Microbiological Research 192:271–282. https://doi.org/10.1016/j.micres.2016.07.010

84. Reddy CSK, Ghai R, Rashmi, Kalia VC (2003) Polyhydroxyalkanoates: an overview. Bioresource Technology 87:137–146. https://doi.org/10.1016/S0960-8524(02)00212-2

85. Höfer P, Choi YJ, Osborne MJ, et al (2010) Production of functionalized polyhydroxyalkanoates by genetically modified Methylobacterium extorquens strains. Microbial Cell Factories 9:70. https://doi.org/10.1186/1475-2859-9-70

86. Pederson EN, McChalicher CWJ, Srienc F (2006) Bacterial Synthesis of PHA Block Copolymers. Biomacromolecules 7:1904–1911. https://doi.org/10.1021/bm0510101

87. Zhou W, Bergsma S, Colpa DI, et al (2023) Polyhydroxyalkanoates (PHAs) synthesis and degradation by microbes and applications towards a circular economy. Journal of Environmental Management 341:118033. https://doi.org/10.1016/j.jenvman.2023.118033

88. Palmeiro-Sánchez T, O'Flaherty V, Lens PNL (2022) Polyhydroxyalkanoate bio-production and its rise as biomaterial of the future. Journal of Biotechnology 348:10–25. https://doi.org/10.1016/j.jbiotec.2022.03.001

89. Wang J, Liu S, Huang J, et al (2023) Genetic engineering strategies for sustainable polyhydroxyalkanoate (PHA) production from carbon-rich wastes. Environmental Technology & Innovation 30:103069. https://doi.org/10.1016/j.eti.2023.103069

90. Anbukarasu P, Sauvageau D, Elias A (2015) Tuning the properties of polyhydroxybutyrate films using acetic acid via solvent casting. Sci Rep 5:17884. https://doi.org/10.1038/srep17884

91. Hill RG (2005) 10 - Biomedical polymers. In: Hench LL, Jones JR (eds) Biomaterials, Artificial Organs and Tissue Engineering. Woodhead Publishing, pp 97–106

92. McAdam B, Brennan Fournet M, McDonald P, Mojicevic M (2020) Production of Polyhydroxybutyrate (PHB) and Factors Impacting Its Chemical and Mechanical Characteristics. Polymers (Basel) 12:2908. https://doi.org/10.3390/polym12122908

93. Wang Q, Xu Y, Xu P, et al (2022) Crystallization of microbial polyhydroxyalkanoates: A review. International Journal of Biological Macromolecules 209:330–343. https://doi.org/10.1016/j.ijbiomac.2022.04.018

94. Reusch R (2014) Biogenesis of Ion Channels. Journal of Biochemistry and Biophysics 1:

95. Policastro G, Panico A, Fabbricino M (2021) Improving biological production of poly(3-hydroxybutyrate-co-3-hydroxyvalerate) (PHBV) co-polymer: a critical review. Rev Environ Sci Biotechnol 20:479–513. https://doi.org/10.1007/s11157-021-09575-z

96. Van Nguyen T, Nagata T, Noso K, et al (2021) Effect of the 3-Hydroxyhexanoate Content on Melt-Isothermal Crystallization Behavior of Microbial Poly(3-hydroxybutyrate-co-3-hydroxyhexanoate). Macromolecules 54:8738–8750. https://doi.org/10.1021/acs.macromol.1c01177

97. Ivorra-Martinez J, Verdu I, Fenollar O, et al (2020) Manufacturing and Properties of Binary Blend from Bacterial Polyester Poly(3-hydroxybutyrate-co-3-hydroxyhexanoate) and Poly(caprolactone) with Improved Toughness. Polymers 12:1118. https://doi.org/10.3390/polym12051118

98. Giubilini A, Sciancalepore C, Messori M, Bondioli F (2020) New biocomposite obtained using poly(3-hydroxybutyrate-co-3-hydroxyhexanoate) (PHBH) and microfibrillated cellulose. Journal of Applied Polymer Science 137:48953. https://doi.org/10.1002/app.48953

99. Feijoo P, Samaniego-Aguilar K, Sánchez-Safont E, et al (2022) Development and Characterization of Fully Renewable and Biodegradable Polyhydroxyalkanoate Blends with Improved Thermoformability. Polymers 14:2527. https://doi.org/10.3390/polym14132527

100. Wang Y-W, Mo W, Yao H, et al (2004) Biodegradation studies of poly(3-hydroxybutyrate-co-3-hydroxyhexanoate). Polymer Degradation and Stability 85:815–821. https://doi.org/10.1016/j.polymdegradstab.2004.02.010

101. Lee J, Hikima Y, Sekiguchi T, Ohshima M (2022) Thermal, rheological, and mechanical properties of cellulose nanofiber (CNF) and poly(3-hydroxybutyrate-co-3-hydroxyhexanoate) (PHBH) biopolymer nanocomposites. Cellulose 29:3901–3913. https://doi.org/10.1007/s10570-022-04539-0

102. Qiu Y, Fu J, Sun B, Ma X (2021) Sustainable nanocomposite films based on SiO2 and biodegradable poly(3-hydroxybutyrate-co-3-hydroxyhexanoate) (PHBH) for food packaging. e-Polymers 21:072–081. https://doi.org/10.1515/epoly-2021-0009

103. Erdmann R, Rennert M, Meins T (2023) Influence of Epoxy Functional Chain-Extenders on the Thermal and Rheological Properties of Bio-Based Polyamide 10.10. Polymers 15:3571. https://doi.org/10.3390/polym15173571

104. Standau T, Nofar M, Dörr D, et al (2022) A Review on Multifunctional Epoxy-Based Joncryl® ADR Chain Extended Thermoplastics. Polymer Reviews 62:296–350. https://doi.org/10.1080/15583724.2021.1918710

105. Mallegni N, Cicogna F, Passaglia E, et al (2025) Natural Antioxidants: Advancing Stability and Performance in Sustainable Biobased and Biodegradable Plastics. Compounds 5:4. https://doi.org/10.3390/compounds5010004

106. Nagarajan S, Nagarajan R, Kumar J, et al (2020) Antioxidant Activity of Synthetic Polymers of Phenolic Compounds. Polymers 12:1646. https://doi.org/10.3390/polym12081646

107. Schwetlick K (1990) Mechanisms of Antioxidant Action of Phosphite and Phosphonite Esters. In: Scott G (ed) Mechanisms of Polymer Degradation and Stabilisation. Springer Netherlands, Dordrecht, pp 23–60

108. Antioxidants. https://plastics-rubber.basf.com/global/en/plastic_additives/products/antioxidants. Accessed 8 Oct 2025

109. Schwetlick K, Habicher WD (1996) Action Mechanisms of Phosphite and Phosphonite Stabilizers. In: Polymer Durability. American Chemical Society, pp 349–358

110. (2015) Additives for Polyolefins

111. Tolinski M (2009) Additives for Polyolefins: Getting the Most Out of Polypropylene, Polyethylene and TPO. William Andrew Publishing

112. Mastura MT, Noryani M (2022) Mineral-Filled Composite: A Review on Characteristics, Applications, and Potential Materials Selection Process. In: Mineral-Filled Polymer Composites. CRC Press

113. Yu F, Liu T, Zhao X, et al (2012) Effects of talc on the mechanical and thermal properties of polylactide. Journal of Applied Polymer Science 125:E99–E109. https://doi.org/10.1002/app.36260

114. Ege University, Faculty of Engineering, Altay L, Sarikanat M, et al (2021) The effect of various mineral fillers on thermal, mechanical, and rheological properties of polypropylene. Res Eng Struct Mater. https://doi.org/10.17515/resm2021.258ma0213

115. Branciforti MC, Oliveira CA, de Sousa JA (2010) Molecular orientation, crystallinity, and flexural modulus correlations in injection molded polypropylene/talc composites. Polymers for Advanced Technologies 21:322–330. https://doi.org/10.1002/pat.1431

116. Tolinski M (2015) Processing Aids for Extrusion. In: Additives for Polyolefins. Elsevier, pp 135–144

117. Introduction to Reactive Extrusion - Reactive Extrusion - Wiley Online Library. https://onlinelibrary.wiley.com/doi/10.1002/9783527801541.ch1. Accessed 22 Dec 2023

118. Home – Coperion. https://coperion.com/it/home-it. Accessed 24 July 2025

119. Delvar E, Oliveira I, Brito MSCA, et al (2025) Literature Review on Single and Twin-Screw Extruders Design for Polymerization Using CFD Simulation. Fluids 10:9. https://doi.org/10.3390/fluids10010009

120. Lechner F (2017) The Co-rotating Twin-Screw Extruder for Reactive Extrusion. In: Reactive Extrusion. John Wiley & Sons, Ltd, pp 11–35

121. Harold F. Jr Giles, Wagner JRJ, Mount EMI (2013) Extrusion: The Definitive Processing Guide and Handbook. William Andrew

122. Bostijn N, Dhondt J, Ryckaert A, et al (2019) A multivariate approach to predict the volumetric and gravimetric feeding behavior of a low feed rate feeder based on raw material properties. International Journal of Pharmaceutics 557:342–353. https://doi.org/10.1016/j.ijpharm.2018.12.066

123. Schöppner V, Resonnek V (2019) Investigation of the barrel temperature profile on the process behavior of single screw extruders and strategies to determine the optimal temperature control. AIP Conf Proc 2139:020003. https://doi.org/10.1063/1.5121650

124. Production Process and Printing Techniques for Plastic Bags. https://www.iqsdirectory.com/articles/plastic-bag/printed-plastic-bags.html. Accessed 4 Dec 2025

125. Lafleur PG, Vergnes B (2014) Polymer Extrusion. John Wiley & Sons

126. De Filippi AM (2004) Fabbricazione di componenti in materiali polimerici. HOEPLI EDITORE

127. Injection Moulders' website. http://pcbolur.freeservers.com/extrusion0.html. Accessed 4 Dec 2025

128. Vlachopoulos J, Polychronopoulos N, Nakamura T (2008) CHALLENGES IN COMPUTER AIDED POLYMER EXTRUSION DIE DESIGN

129. Harper CA (2006) Handbook of Plastic Processes. John Wiley & Sons

130. Subramanian MN (2024) Thermoforming: Processing and Technology. John Wiley & Sons

131. ImpactSolutions Melt Flow Rate. In: Impact Solutions. https://www.impact-solutions.co.uk/plastic-testing/testing-capabilities-list/melt-flow-rate-plastic-rheology/. Accessed 18 June 2025

132. Qenos | Polyethylene | Technical Guides. https://qenos.com/internet/home.nsf/web/PolyethyleneTechGuides. Accessed 18 June 2025

133. Macosko CW (1994) Rheology: principles, measurements, and applications. VCH, New York

134. Mahmood R, Bilal S, Khan I, et al (2020) A comprehensive finite element examination of Carreau Yasuda fluid model in a lid driven cavity and channel with obstacle by way of kinetic energy and drag and lift coefficient measurements. Journal of Materials Research and Technology 9:1785–1800. https://doi.org/10.1016/j.jmrt.2019.12.010

135. Sun H, Jiang Y, Zhang Y, Jiang L (2024) A review of constitutive models for non-Newtonian fluids. Fract Calc Appl Anal 27:1483–1526. https://doi.org/10.1007/s13540-024-00294-0

136. ISO 527-1:2019. In: ISO. https://www.iso.org/standard/75824.html. Accessed 17 June 2025

137. Matveenko VN, Kirsanov EA (2023) Structural Causes of the Non-Newtonian Behavior of Fluid Systems. Russ J Phys Chem 97:1708–1724. https://doi.org/10.1134/S0036024423080162

138. Genovesi A, Koca N, Barletta M, Aversa C (2024) Extrusion and thermoforming of poly(butylene succinate–co-butylene adipate)/poly(3–hydroxybutyrate–co–3–hydroxyhexanoate) bio-based blends for the fabrication of disposable packaging. Journal of Applied Polymer Science n/a:e55464. https://doi.org/10.1002/app.55464

139. Nofar M, Salehiyan R, Barletta M (2024) Tuning the Structure–Property Relationships in Binary and Ternary Blends of PLA/PBAT/PHBH. Polymers 16:1699. https://doi.org/10.3390/polym16121699

140. Li Y, Guo J, Wang H, et al (2025) Tuning the rheological and mechanical properties of biodegradable PHBH/PLA/PVAc ternary blends via PVAc content control. Polym Bull 82:1949–1972. https://doi.org/10.1007/s00289-024-05594-2

141. Billham M, Clarke A h., Garrett G, et al (2003) The Effect of Extrusion Processing Conditions on the Properties of Blown and Cast Polyolefin Packaging Films. Developments in Chemical Engineering and Mineral Processing 11:137–146. https://doi.org/10.1002/apj.5500110214

142. Somsunan R, Mainoiy N (2020) Isothermal and non-isothermal crystallization kinetics of PLA/PBS blends with talc as nucleating agent. J Therm Anal Calorim 139:1941–1948. https://doi.org/10.1007/s10973-019-08631-9

143. Humbert S, Lame O, Séguéla R, Vigier G (2011) A re-examination of the elastic modulus dependence on crystallinity in semi-crystalline polymers. Polymer 52:4899–4909. https://doi.org/10.1016/j.polymer.2011.07.060

144. Castillo LA, Barbosa SE, Capiati NJ (2013) Influence of talc morphology on the mechanical properties of talc filled polypropylene. J Polym Res 20:152. https://doi.org/10.1007/s10965-013-0152-2

145. Helanto K, Talja R, Rojas OJ (2021) Talc reinforcement of polylactide and biodegradable polyester blends via injection-molding and pilot-scale film extrusion. Journal of Applied Polymer Science 138:51225. https://doi.org/10.1002/app.51225

146. Zhou Y, Xia X, Liu X, et al (2019) Preparation and Rheological and Mechanical Properties of Poly(butylene succinate)/Talc Composites for Material Extrusion Additive Manufacturing. Macromolecular Materials and Engineering 304:1900021. https://doi.org/10.1002/mame.201900021

147. Dmitruk A, Ludwiczak J, Skwarski M, et al (2023) Influence of PBS, PBAT and TPS content on tensile and processing properties of PLA-based polymeric blends at different temperatures. J Mater Sci 58:1991–2004. https://doi.org/10.1007/s10853-022-08081-z

148. Pothinuch P, Promsorn J, Sablani SS, Harnkarnsujarit N (2024) Antioxidant release, morphology and packaging properties of gallic acid incorporated biodegradable PBAT blended PBS active packaging. Food Packaging and Shelf Life 43:101304. https://doi.org/10.1016/j.fpsl.2024.101304

149. Xu X, Ma X, Li D, Dong J (2021) Toward sustainable biocomposites based on MMT and PHBH reinforced with acetylated cellulose nanocrystals. Cellulose 28:2981–2993. https://doi.org/10.1007/s10570-021-03735-8

150. Rebia RA, Rozet S, Tamada Y, Tanaka T (2018) Biodegradable PHBH/PVA blend nanofibers: Fabrication, characterization, in vitro degradation, and in vitro biocompatibility. Polymer Degradation and Stability 154:124–136. https://doi.org/10.1016/j.polymdegradstab.2018.05.018

151. Wang DK, Varanasi S, Fredericks PM, et al (2013) FT-IR characterization and hydrolysis of PLA-PEG-PLA based copolyester hydrogels with short PLA segments and a cytocompatibility study. Journal of Polymer Science Part A: Polymer Chemistry 51:5163–5176. https://doi.org/10.1002/pola.26930

152. Szuman K, Krucińska I, Boguń M, Draczyński Z (2016) PLA/PHA-Biodegradable Blends for Pneumothermic Fabrication of Nonwovens. Autex Research Journal 16:119–127. https://doi.org/10.1515/aut-2015-0047

153. Cuadri AA, Martín-Alfonso JE (2018) Thermal, thermo-oxidative and thermomechanical degradation of PLA: A comparative study based on rheological, chemical and thermal properties. Polymer Degradation and Stability 150:37–45. https://doi.org/10.1016/j.polymdegradstab.2018.02.011

154. Lu H, Kazarian SG, Sato H (2020) Simultaneous Visualization of Phase Separation and Crystallization in PHB/PLLA Blends with In Situ ATR-FTIR Spectroscopic Imaging. Macromolecules 53:9074–9085. https://doi.org/10.1021/acs.macromol.0c00713

155. Rivas LF, Casarin SA, Nepomuceno NC, et al (2017) Reprocessability of PHB in extrusion: ATR-FTIR, tensile tests and thermal studies. Polímeros 27:122–128. https://doi.org/10.1590/0104-1428.2406

156. Leroy A, Ribeiro S, Grossiord C, et al (2017) FTIR microscopy contribution for comprehension of degradation mechanisms in PLA-based implantable medical devices. J Mater Sci: Mater Med 28:87. https://doi.org/10.1007/s10856-017-5894-7

157. Wiewióra A, Sánchez-Soto PJ, Avilés MA, et al (1997) Talc from Puebla de Lillo, Spain. I. XRD study. Applied Clay Science 12:233–245. https://doi.org/10.1016/S0169-1317(97)00009-4

158. Dong T, He Y, Shin K, Inoue Y (2004) Formation and Characterization of Inclusion Complexes of Poly(butylene succinate) with α- and γ-Cyclodextrins. Macromolecular Bioscience 4:1084–1091. https://doi.org/10.1002/mabi.200400054

159. Phothisarattana D, Wongphan P, Promhuad K, et al (2021) Biodegradable Poly(Butylene Adipate-Co-Terephthalate) and Thermoplastic Starch-Blended TiO2 Nanocomposite Blown Films as Functional Active Packaging of Fresh Fruit. Polymers 13:4192. https://doi.org/10.3390/polym13234192

160. Ruggero F, Carretti E, Gori R, et al (2020) Monitoring of degradation of starch-based biopolymer film under different composting conditions, using TGA, FTIR and SEM analysis. Chemosphere 246:125770. https://doi.org/10.1016/j.chemosphere.2019.125770

161. Siracusa V, Lotti N, Munari A, Dalla Rosa M (2015) Poly(butylene succinate) and poly(butylene succinate-co-adipate) for food packaging applications: Gas barrier properties after stressed treatments. Polymer Degradation and Stability 119:35–45. https://doi.org/10.1016/j.polymdegradstab.2015.04.026

162. Abderrahim B, Abderrahman E, Mohamed A, et al (2015) Kinetic Thermal Degradation of Cellulose, Polybutylene Succinate and a Green Composite: Comparative Study. World Journal of Environmental Engineering

163. Radhakrishnan S, Thorat S, Desale A, et al (2022) Structure and Properties of PBS/PBAT blends and nanocomposites. IOP Conf Ser: Mater Sci Eng 1248:012013. https://doi.org/10.1088/1757-899X/1248/1/012013

164. Kanwal A, Zhang M, Sharaf F, Li C (2022) Enzymatic degradation of poly (butylene adipate co-terephthalate) (PBAT) copolymer using lipase B from Candida antarctica (CALB) and effect of PBAT on plant growth. Polym Bull 79:9059–9073. https://doi.org/10.1007/s00289-021-03946-w

165. Ullah MS, Yildirim R, Kodal M, Ozkoc G (2023) Reactive compatibilization of PLA/PBS bio-blends via a new generation of hybrid nanoparticles. Journal of Vinyl and Additive Technology 29:737–757. https://doi.org/10.1002/vnl.21969

166. Ge Q, Dou Q (2023) Preparation of Supertough Polylactide/Polybutylene Succinate/Epoxidized Soybean Oil Bio-Blends by Chain Extension. ACS Sustainable Chem Eng 11:9620–9629. https://doi.org/10.1021/acssuschemeng.3c01042

167. Rachtanapun P, Suhr J, Oh E, et al (2025) Flame Retardance and Antistatic Polybutylene Succinate/Polybutylene Adipate-Co-Terephthalate/Magnesium Composite. Polymers 17:1675. https://doi.org/10.3390/polym17121675

168. Vela E, Peiteado M, García F, et al (2007) Sintering behaviour of steatite materials with barium carbonate flux. Ceramics International 33:1325–1329. https://doi.org/10.1016/j.ceramint.2006.04.015

169. Nanaki S, Barmpalexis P, Iatrou A, et al (2018) Risperidone Controlled Release Microspheres Based on Poly(Lactic Acid)-Poly(Propylene Adipate) Novel Polymer

Blends Appropriate for Long Acting Injectable Formulations. Pharmaceutics 10:130. https://doi.org/10.3390/pharmaceutics10030130

170. Farrag Y, Barral L, Gualillo O, et al (2022) Effect of Different Plasticizers on Thermal, Crystalline, and Permeability Properties of Poly(3–hydroxybutyrate–co−3–hydroxyhexanoate) Films. Polymers 14:3503. https://doi.org/10.3390/polym14173503

171. Abdelwahab MA, Flynn A, Chiou B-S, et al (2012) Thermal, mechanical and morphological characterization of plasticized PLA–PHB blends. Polymer Degradation and Stability 97:1822–1828. https://doi.org/10.1016/j.polymdegradstab.2012.05.036

172. Florez JP, Fazeli M, Simão RA (2019) Preparation and characterization of thermoplastic starch composite reinforced by plasma-treated poly (hydroxybutyrate) PHB. International Journal of Biological Macromolecules 123:609–621. https://doi.org/10.1016/j.ijbiomac.2018.11.070

173. Koike T, Muranaka Y, Hikima Y, et al (2025) Evaluation of the Relationship between Crystal Orientation and Enzymatic Degradation Rate of Poly[(R)-3-hydroxybutyrate-co-(R)-3-hydroxyhexanoate] Banded Spherulites via FT-IR Imaging. Macromolecules. https://doi.org/10.1021/acs.macromol.5c01352

174. Hopmann C, Schippers S, Höfs C (2015) Influence of recycling of poly(lactic acid) on packaging relevant properties. Journal of Applied Polymer Science 132:. https://doi.org/10.1002/app.41532

175. Kovalcik A, Pérez-Camargo RA, Fürst C, et al (2017) Nucleating efficiency and thermal stability of industrial non-purified lignins and ultrafine talc in poly(lactic acid) (PLA). Polymer Degradation and Stability 142:244–254. https://doi.org/10.1016/j.polymdegradstab.2017.07.009

176. Pivsa-Art W, Pivsa-Art S (2019) Effect of Talc on Mechanical Characteristics and Fracture Toughness of Poly(lactic acid)/Poly(butylene succinate) Blend. J Polym Environ 27:1821–1827. https://doi.org/10.1007/s10924-019-01478-z

177. Dhali K, Daver F, Cass P, et al (2023) Development and Characterisation of Poly(butylene adipate-co-terephthalate)- Silane Modified Cellulose Nanocrystals Composite Materials and Films. J Polym Environ 31:4506–4521. https://doi.org/10.1007/s10924-023-02896-w

178. Wang K, Jiao T, Wang Y, et al (2013) The microstructures of extrusion cast biodegradable poly(butylene succinate) films investigated by X-ray diffraction. Materials Letters 92:334–337. https://doi.org/10.1016/j.matlet.2012.10.121

179. Xu X, Li Y, Ma X, Li J (2020) Synergistic reinforcing effect of nano-montmorillonite and cellulose nanocrystals on poly(3-hydroxybutyrate-co-3-hydroxyhexanoate). Cellulose 27:6249–6261. https://doi.org/10.1007/s10570-020-03252-0

180. Zhou J, Ma X, Li J, Zhu L (2019) Preparation and characterization of a bionanocomposite from poly (3-hydroxybutyrate-co-3-hydroxyhexanoate) and cellulose nanocrystals. Cellulose 26:979–990. https://doi.org/10.1007/s10570-018-2136-1

181. Yokohara T, Yamaguchi M (2008) Structure and properties for biomass-based polyester blends of PLA and PBS. European Polymer Journal 44:677–685. https://doi.org/10.1016/j.eurpolymj.2008.01.008

182. Jin Y, Guo J, Cheng H, et al (2024) Supertoughened biodegradable poly(L-lactic acid) by multiphase blends system: Crystallization, rheological and mechanical properties. Thermochimica Acta 739:179810. https://doi.org/10.1016/j.tca.2024.179810

183. Běhálek L, Maršálková M, Lenfeld P, et al (2013) STUDY OF CRYSTALLIZATION OF POLYLACTIC ACID COMPOSITES AND NANOCOMPOSITES WITH NATURAL FIBRES BY DSC METHOD

184. Zhang M, Diao X, Jin Y, Weng Y (2016) Preparation and characterization of biodegradable blends of poly(3-hydroxybutyrate-co-3-hydroxyhexanoate) and poly(butylene adipate-co-terephthalate). Journal of Polymer Engineering 36:473–480. https://doi.org/10.1515/polyeng-2015-0076

185. Ding Y, Zhang C, Luo C, et al (2021) Effect of talc and diatomite on compatible, morphological, and mechanical behavior of PLA/PBAT blends. e-Polymers 21:234–243. https://doi.org/10.1515/epoly-2021-0022

186. Yoo ES, Im SS (1999) Melting behavior of poly(butylene succinate) during heating scan by DSC. Journal of Polymer Science Part B: Polymer Physics 37:1357–1366. https://doi.org/10.1002/(SICI)1099-0488(19990701)37:13%253C1357::AID-POLB2%253E3.0.CO;2-Q

187. Wang X, Zhou J, Li L (2007) Multiple melting behavior of poly(butylene succinate). European Polymer Journal 43:3163–3170. https://doi.org/10.1016/j.eurpolymj.2007.05.013

188. Zhao T, Yu J, Zhang X, et al (2024) Thermal, crystallization, and mechanical properties of polylactic acid (PLA)/poly(butylene succinate) (PBS) blends. Polym Bull 81:2481–2504. https://doi.org/10.1007/s00289-023-04848-9

189. Ishimwe S (2024) BIOPLASTICS MARKET DEVELOPMENT UPDATE 2024. In: European Bioplastics e.V. https://www.european-bioplastics.org/bioplastics-market-development-update-2024/. Accessed 5 Dec 2025